Frequency Analysis of Non-Stationary Signals with Harmonic Components

Yaron Doweck

Frequency Analysis of Non-Stationary Signals with Harmonic Components

Research Thesis

Submitted in partial fulfillment of the requirements
for the degree of Master of Science in Electrical Engineering

Yaron Doweck

Submitted to the Senate of the
Technion — Israel Institute of Technology
Kislev 5776 Haifa November 2015

Acknowledgments

The research thesis was done under the supervision of Dr. Alon Amar and Prof. Israel Cohen in the Department of Electrical Engineering. I would like to express my gratitude to both of them for the supervision, guidance and support throughout all the stages of this research.

I would like to express my deep gratitude to my wife Yael, for the constant love, encouragement and support.

List of Publications

The following papers have been published or submitted for publication based on the results of the work described in this thesis:

- Y. Doweck, A. Amar, and I. Cohen, "Joint model order selection and parameter estimation of chirps with harmonic components," *IEEE Trans. Signal Process.*, vol. 63, no. 7, pp. 1765-1778, Apr. 2015.
- Y. Doweck, A. Amar, and I. Cohen, "Fundamental initial frequency and frequency rate estimation of random amplitude harmonic chirps," *IEEE Trans. Signal Process.*, vol. 63, no. 23, pp. 6213-6228, Dec. 2015.
- Y. Doweck, A. Amar, and I. Cohen, "Parameter estimation of harmonic Linear chirps," in *The 23rd European Signal Processing Conference (EUSIPCO)*, Nice, France, Sept. 2015, pp 1491-1495.

Contents

List of Figures

Abstract

In this work we consider the case of chirps with harmonic components. That is, the frequency of each component is an integer multiple of the time-varying frequency of a fundamental signal. Harmonic signals appear in various applications. Such signals occur due to propagation through nonlinear media, for example in systems such as radar, sonar and communication systems and also in speech and music signals and vibrational analysis. Harmonics can also be used deliberately, to increase detectability, for example in tissue ultrasound or echolocations calls of bats, whales and dolphins.

The problem of estimating the fundamental frequency of harmonic signals has received much attention in literature. In all estimation methods, the frequency is assumed to be constant during the observation time. This assumption limits the possible observation time to be very short since constant frequency signals are not common. However, by assuming a model of time-varying frequency, the observation time can be increased and consequently the estimation accuracy is improved. In this work we assume that in each observation time, the signals can be modeled as a sum of harmonic linear chirps where the number of harmonic components is unknown. Under this assumption, we propose estimation methods for the parameters of such signals, i.e. the initial frequency and frequency rate of the fundamental chirp. As opposed to parameter estimation of multi-component chirp signals, in this case the problem involves only the two parameters of the fundamental chirp. Estimation methods of these two parameters for such model have not been presented in literature to date.

We consider two types of signal model. In the first part, we assume that the amplitude of each component is constant during the observation time. We start by presenting statistical model order selection criteria, based on the maximum likelihood estimator, which requires a high resolution two-dimensional search. To overcome this problem, we propose a low-complexity estimator, which we term the harmonic separate-estimate method. We

show that the proposed method achieves the performance of the maximum likelihood estimator in moderate to high signal-to-noise ratio, and can successfully replace it in the model order selection criteria.

The second signal model is a more general case of time-varying amplitudes. In this case, each amplitude can be either independent random process, or varying according to some unknown dynamic. We show that the model order selection criteria and the maximum likelihood estimator cannot be applied to this model. We develop a computationally intensive iterative estimator, based on the nonlinear least squares estimator for mono-component chirp signals with random amplitudes, and show that the number of harmonic components can be selected using concentration measures of the spectrum of the signal. We then show how the harmonic separate-estimate method can be extended for random amplitude harmonic chirps. Simulation results show that the proposed low complexity method performs well in high signal-to-noise ratio.

Abbreviations

AIC	Akaike information criterion
CRLB	Cramer-Rao lower bound
DFT	Discrete Fourier transform
DTFT	Discrete time Fourier transform
FFT	Fast Fourier transform
FIM	Fisher information matrix
FrFT	Fractional Fourier transform
HAF	High order ambiguity function
Harmonic-SEES	Harmonic separate-estimate
HRA-SEES	Harmonic random separate-estimate
IDFT	Inverse DFT
IHNLSE	Iterative harmonic-NLSE
IHNLSE-MO	Iterative harmonic-NLSE with model order selection
LFM	Linear frequency modulated
LS	Least-squares
MAP	Maximum *a posteriori* probability
MDL	Minimum description length
MLE	Maximum likelihood estimator
NLS	Nonlinear least-squares
NLSE	Nonlinear least-squares estimator
pdf	Probability density function
PHAF	Product high order ambiguity function
PPS	Polynomial phase signals
RMSE	Root mean square error

SEES	Separate-estimate
SNR	Signal-to-noise ratio
w.r.t.	With respect to

List of Notations

$\mathrm{diag}(\mathbf{x})$	A diagonal matrix whose main diagonal is $\mathbf{x}$
$E(\cdot)$	Expectation operator
$\mathcal{F}(\cdot)$	The Fourier transform
$(\cdot)^H$	The Hermitian operator
$\Im(\cdot)$	Imaginary part of a complex number
$\mathbf{I}_N$	The $N \times N$ identity matrix
$\mathbf{J}$	Fisher information matrix
j	The imaginary unit
M	Number of harmonic components
N	Number of samples
$\mathbf{P_S}$	Projection matrix to the space of the columns of $\mathbf{S}$
$\mathbf{P}_{\mathbf{S}}^{\perp}$	Projection matrix to the null space of the columns of $\mathbf{S}$
$\Re(\cdot)$	Real part of a complex number
$(\cdot)^T$	The transpose operator
$\mathrm{tr}(\mathbf{A})$	The trace of matrix $\mathbf{A}$
Δx	The discrete derivative of x
θ_1	The initial frequency of the fundamental component
θ_1	The frequency rate of the fundamental component
θ	The parameters vector
$\hat{\theta}$	The estimated parameters vector
$\mathbf{0}_n$	A $n \times 1$ vector with all elements equal to 0

$\mathbf{1}_n$	A $n \times 1$ vector with all elements equal to 1
$\mathbb{1}_{a=b}$	An indicator function that equals 1 when $a = b$ and 0 otherwise
$(\cdot)^*$	The complex conjugate operator
$\circ$	Functions composition
$\odot$	Hadamard product

Chapter 1

Introduction

1.1 Motivation

The problem of estimating the fundamental frequency of harmonic time-stationary sinusoids has wide applications in speech processing, communication, radar and sonar, biomedical systems, electrical power, and semiconductor devices [1–11]. The fundamental frequency is assumed to be constant during the observation segment, and this assumption sets a constraint on the possible length of the observation segment. Short segments will ensure that the assumption is valid, but better estimation accuracy is achieved if long segments are used as the signal-to-noise ratio (SNR) is increased.

In some other applications the signal is more appropriately modeled as a sum of harmonic components of a non-stationary signal, i.e., a signal that its frequency content is varied with respect to (w.r.t.) time, also known as a chirp signal [12–14]. For example, in active transmission used in tissue harmonic imaging in ultrasound [15] or by mammals [13, 14] (e.g., bats, dolphins, whales) the signal is deliberately transmitted as a sum of harmonic linear frequency modulated (LFM) chirps to increase the detectability of the source of interest, e.g., an organ in ultrasound or a prey in case of mammals. Such harmonic signals also occur in other applications due to propagation through a nonlinear media including rotating machinery in vibrational analysis, music and formants in audio and speech processing, electrical power systems, and target localization [16, 17]. Harmonics of higher orders of frequency modulated chirps, known as polynomial phase signals (PPS) [18–20], or non-linear frequency modulated chirps (e.g., hyperbolic frequency modulated signals [13]), are also used in synthetic aperture radar [21], biomedical [22], radio communications, or marine mammals [13, 14].

Estimating the parameters of chirp signals has received much attention in literature and has a wide variety of applications. It is used, for example, in radar [23], vehicle tracking [24], sonar [16, 17, 20] and underwater communication. A common assumption in chirp analysis methods is that the amplitude of the signal is constant during each observation time.

Methods for estimating the parameters of a mono-component LFM with a constant amplitude include using maximum likelihood [25], rank reduction techniques [26, 27], ambiguity function [28], phase unwrapping [29] and the Wigner-Ville distribution [30]. Methods for estimating the parameters of a multi-component LFM are based on combining a time-frequency transform, such as the Wigner-Ville transform, with an image processing technique (e.g., the Hough transform) [31], Monte-Carlo methods such as importance sampling [32] or Markov chain Monte Carlo [33], using time-frequency representations such as the fractional Fourier transform (FrFT) [34], which is suited to LFM chirps, and the high-order phase function [35].

An LFM signal is a specific case of the PPS family. Estimating the parameters of a PPS with a constant amplitude can be done, for example, using the well-known high order ambiguity function (HAF) [36] based parameters estimation for mono-component PPS [18, 19] and for multi-component signals [23, 37–39]. The HAF based estimation is an iterative process. In each iteration, the highest remaining coefficient of the PPS is estimated and then subtracted. Therefore, estimation errors propagate to the lower order coefficients. The product high order ambiguity function (PHAF) method, based on multi-lag HAF, offers improved performance with a minor increase in computational complexity [23]. The HAF based estimation methods, and specifically the PHAF, are very popular as they are simple and relatively low complexity methods. Other methods for estimating the parameters of a mono-component PPS include the phase unwrapping [40, 41], multi-linear time-frequency representation [42], iterative methods [43], Wigner-Ville distribution [44], nonlinear least-squares (NLS) [45], high-order phase function [46–48] and subspace methods [49]. Solutions for multi-component PPS include the NLS method [50], separation of the signal components [20] and multi-linear methods [51].

In some applications such as radar, sonar and communication, distortions caused by scattering, fluctuations or multi-path phenomena result in a signal with time-varying amplitude [52–58]. Chirps with random amplitude are also used to model formants in speech processing applications [59,60], electric currents in induction motor fault analysis [61], and

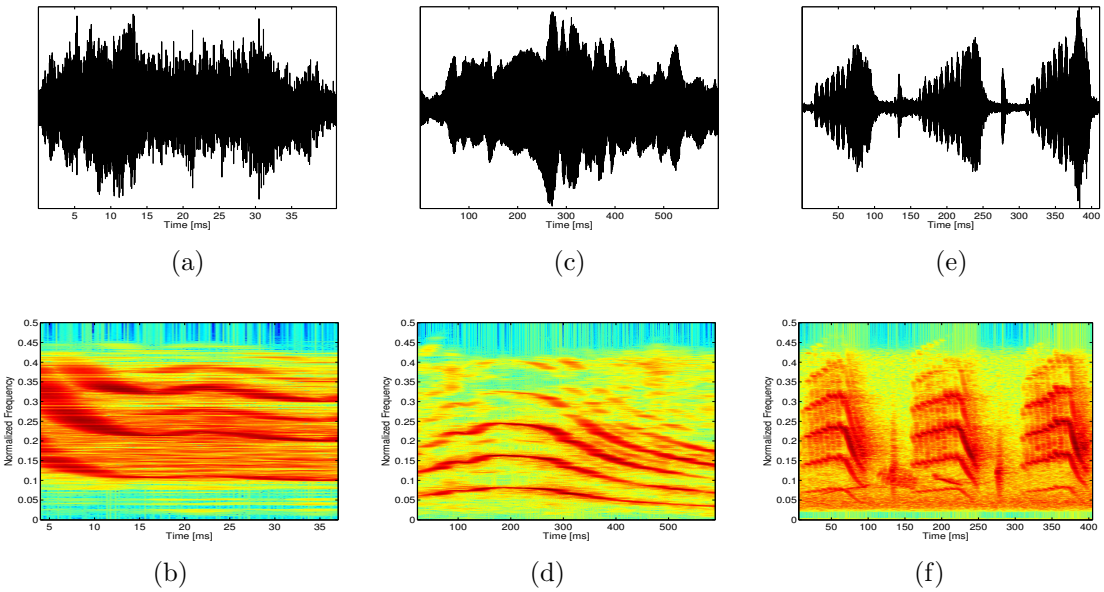

Figure 1.1: Examples of animal harmonic chirps. Time domain samples and spectrogram of (a,b) an echolocation call produced by an *E. Nilssonii* bat, (c,d) an echolocation call produced by a *G. melas* whale and (e,f) a call of a *Hippolais icterina* bird.

animals sounds (bats, whales, dolphins, birds etc.).

Previous work on the analysis of time-varying amplitude signals can be divided into two cases. The first case focuses on complex exponential signals (i.e. constant frequency). Frequency estimation for such signals can be achieved using cyclic moments [52], least-squares (LS) [53] and nonlinear least-squares estimator (NLSE) [62,63], subspace methods [64], high-order spectra [65, 66] and pulse-pair method [67]. The second case, which received significantly less attention, considers the model of a mono-component chirp with time-varying amplitude. Methods for parameter estimation of such signals include the cyclic moment approach [54,59], NLSE and HAF based estimation [58], high-order instantaneous moments [68] and the Wigner-Ville distribution based methods [69, 70].

It is noteworthy to mention that most parameter estimation algorithms for multi-component signals assume that the number of components, i.e. the model order, is known *a priori*. Otherwise, an order selection rule should be applied. Statistical selection criteria, such as the minimum description length (MDL), Akaike information criterion (AIC) or maximum *a posteriori* probability (MAP) [71], has been successfully applied to multi-components sinusoids [72, 73] and sinusoids with harmonic components [74], both assuming a constant amplitude model. The statistical criteria are not applicable for random-amplitudes. Therefore, a different approach is required. All multi-component methods

for time-varying amplitudes mentioned above, assume that the number of components is known.

Herein, we consider a class of multi-component chirps, where the components satisfy a harmonic relation. For example, Fig. 1.1 presents three types of calls, produced by *E. Nilssonii* bat [75], *G. melas* whale [76] and *Hippolais icterina* bird [77], showing harmonic chirp signals with time-varying amplitude. The frequency of each component is an integer multiple of the time-varying frequency of a fundamental chirp. We further assume that in each observation window, the components can be approximated as an LFM chirp signal and the number of harmonic components is unknown. As opposed to multi-component signal, the harmonic components problem only involves estimating the parameters of the fundamental chirp, as we only estimate the initial frequency and frequency rate of the fundamental chirp. Estimation methods of these two parameters for such model have not been presented in literature to date, and thus it is the motivation of the current work.

The model of harmonic components of a fundamental LFM chirp can be considered as a special case of the multi-component chirps estimation problem. Obviously, one can argue that the parameters of each harmonic component can be estimated using any of the multi-component estimation method mentioned above. The parameters of the fundamental LFM can then be determined, e.g. by properly averaging the previous estimates. However, as we later show, this yields a sub-optimal estimation that does not achieve the Cramer-Rao lower bound (CRLB), even in high SNR.

The work is divided into two parts. First, we consider the case of constant-amplitude signals. Then, in the second part we consider signals with time-varying amplitudes.

1.2 Constant Amplitudes

We start by presenting two model order selection criteria, the MDL and AIC. Both of them are based on the maximum likelihood estimator (MLE). We then derive the computationally intensive MLE and suggest a reduced complexity estimator. Both estimators require a two-dimensional high resolution search, in the order of N^3 points to achieve the CRLB, where N is the number of samples. We present two low complexity suboptimal estimation methods. The first is a modification of the well-known PHAF method for signals with harmonic components. We then propose a new estimation method, harmonic separate-estimate (Harmonic-SEES). It is based on the separate-estimate (SEES) approach, used

for estimating the coefficients of a constant modulus signals [20]. The Harmonic-SEES uses the fast Fourier transform (FFT) to obtain a coarse estimation of the parameters and separate the harmonic components. Once separated, the parameters are estimated using a joint LS given the phases of the components.

We show that asymptotically, given a large number of data samples, the Harmonic-SEES estimator is unbiased, and obtain a closed-form expression for its theoretical covariance matrix. We evaluate the computation load of all four estimation methods and show that the MLE involves an order of N^5 and N^4 multiplications per harmonic component for the exact and approximated solutions, respectively, and the Harmonic-SEES only involves an order of $N^2 \log N$ multiplications per harmonic component, which is substantially smaller computational load. We show through simulations that the proposed method achieves the CRLB in moderate to high SNR and can be used instead of the MLE in order to estimate the number of harmonic components.

1.3 Random Amplitudes

We first present an iterative process by extending the NLSE presented in [58] for mono-component chirp with random amplitude, to the current case of a harmonic LFM signal with a known number of components, which we term the iterative harmonic-NLSE (IHNLSE). We then suggest a framework to determine the number of harmonic components using peakedness measures evaluated for the spectrum of the residual signal. The IHNLSE requires exhaustive search in the initial frequency-frequency rate space. We show that, in order to achieve the optimal accuracy, a search resolution of N^3 and N^5 is required for the initial frequency and frequency rate, respectively, where N is the number of samples. We further propose two low-complexity estimators to avoid such search. The first is a modification of the HAF based estimation method [58]. The second is a modification of the Harmonic-SEES method for random amplitude harmonic chirps, which we term the harmonic random separate-estimate (HRA-SEES). Similarly to the NLSE and HAF based estimator, in order to use the Harmonic-SEES method on random amplitude chirp, we use the squared signal. We then modify the Harmonic-SEES steps to suit the transformed signal.

We show that both methods can be successfully modified for harmonic LFM signals with unknown number of harmonic components. We evaluate the computational load

for each method and show that the IHNLSE involves an order of N^4 multiplications per harmonic component while the HAF and the HRA-SEES methods involve an order of $N^{5/2}$ and $N^2 \log N$ multiplications per harmonic component, respectively. Simulations show that the IHNLSE achieves its analytic asymptotic accuracy in medium to high SNR and that both low-complexity methods yield good estimation results for high SNR. Two real-data examples demonstrate the application of the HRA-SEES method to echolocation calls.

1.4 Problem Statement and Model Assumptions

Consider a discrete-time signal composed of M attenuated harmonic components observed in the presence of noise,

$$x[n] = \sum_{m=1}^{M} a_m[n] s_m[n; \boldsymbol{\theta}] + v[n],\ n = 0, \ldots, N-1 \tag{1.1}$$

where M is unknown, $a_m[n]$ is the unknown amplitude of the mth harmonic, and $v[n]$ is a zero mean white circularly symmetric Gaussian discrete-time process representing the additive noise with an unknown variance σ_v^2, uncorrelated with the amplitudes. We assume that the amplitudes can be described as $a_m[n] = \alpha_m[n] e^{j\varphi_m}$, where φ_m is the constant phase of the m'th component. Generally, $\alpha_m[n]$ is a real time-varying process, where we do not assume any kind of model for the amplitudes. This is a generalization of the signal model presented in [58], for multi-component signal. In the constant amplitude model, $\alpha_m[n] = |a_m|$ is a real, constant and positive attenuation. The m'th harmonic component in discrete-time is

$$s_m[n; \theta] = e^{j\phi_m[n]}, \quad \begin{array}{l} n = 0, \ldots, N-1 \\ m = 1, \ldots, M \end{array} \tag{1.2}$$

where the phase is defined as $\phi_m[n] = 2\pi m(\theta_1 n + \frac{1}{2}\theta_2 n^2)$ where $\theta_1 = F_0/F_s$ and $\theta_2 = \beta_0/F_s^2$ are the normalized initial frequency and normalized frequency rate, where F_s is the sampling frequency, F_0 is the initial frequency of the fundamental harmonic, and $\beta_0 = B/T$ is the frequency rate of the fundamental harmonic, where B and T are the signal bandwidth and duration time of the fundamental harmonic, respectively. Also, $N = TF_s$ is the total number of data samples. We assume that the length of the observed signal equals the length of the chirp, which can be obtained by first detecting the presence of the signal and then determining its start and end times. We further assume that

$F_s \geq 2 \cdot \max\{MF_0, M(F_0 + \beta_0 T)\}$, where the first and second arguments correspond to the case of decreasing and increasing chirp harmonics, respectively. This implies that $|\theta_1| < 1/2$ and $|\theta_2| < 1/(2N)$. Finally, note that the differences between the initial (or final) frequencies of the chirps are F_0/F_s (or $(F_0 + \beta_0 T)/F_s$) in case of increasing (or decreasing) chirps. Thus, to ensure that the harmonic components are well separated, we assume that the $\min\{F_0/F_s, (F_0 + \beta_0 T)/F_s\} \geq \delta$, where δ is a pre-defined frequency interval. For simplicity, all frequencies mentioned hereafter are assumed to be normalized by the sampling rate, F_s, unless otherwise stated. Thus, the sampling rate is set to $F_s = 1$.

The problem herein is: Given N samples of the signal $x[n]$, estimate the unknown parameter vector, $\boldsymbol{\theta} = [\theta_1, \theta_2]^T$, and the model order, M.

1.5 Thesis Structure

This thesis is organized as follows. In Chapter 2 we briefly review methods for analyzing chirp signals that are used in this work. In Chapter 3 we consider the case of constant amplitudes model. We present statistical model order selection criteria, based on the computationally intensive MLE. We develop a novel low-complexity estimation method, discuss its strengths and limits, and show that it can successfully replace the MLE in medium to high SNR. The more general case, of time-varying amplitudes is considered in Chapter 4. We show that the MLE, and consequently the statistical model order selection criteria, cannot be applied in that case. We suggest a model order selection framework and develop the computationally intensive IHNLSE. Next, we extend the estimation method developed for the constant amplitudes to time-varying amplitudes. Finally, in Chapter 5 we conclude the work and suggest some future research directions.

Chapter 2

Background

2.1 Introduction

In this chapter we present a brief review of parameter estimation methods that can be applied to LFM signals. There are countless methods for analyzing chirp signals. Here, we focus on those who are related to this research and have been the foundation of our work. We start by presenting the phase unwrapping method for parameter estimation of mono-component LFM signals in Section 2.2. Next, we present the application of the HAF for parameter estimation of PPS in Section 2.3. The HAF based methods are perhaps the most popular when analyzing PPS. We show how the HAF can be used in order to estimate the parameters of mono-component and multi-component PPS.

2.2 Phase Unwrapping Method

The phase unwrapping method for parameter estimation of mono-component LFM was introduced by Djuric and Kay [29]. It uses the fact that, for mono-component chirp, the entire information about the frequency is hidden in the phase of the signal. Consider an LFM signal given by

$$x[n] = a \cdot e^{j2\pi(\theta_0+\theta_1 n+\frac{1}{2}\theta_2 n^2)} + v[n] \tag{2.1}$$

where $v[n]$ is a circularly symmetric Gaussian additive noise. For high SNR, we can assume that the signal can be approximated by

$$x[n] \cong a \cdot e^{j2\pi(\theta_0+\theta_1 n+\frac{1}{2}\theta_2 n^2)+j\varepsilon_v[n]}. \tag{2.2}$$

That is, the noise can be considered as a phase noise only. It can also be shown that $\varepsilon_v[n]$ is a real Gaussian process [29]. Therefore, the phase of the input signal is approximately

$$\phi[n] = \left(2\pi(\theta_0 + \theta_1 n + \frac{1}{2}\theta_2 n^2) + \varepsilon_v[n]\right) \textbf{ mod } 2\pi. \tag{2.3}$$

In order to estimate the parameters we need to consider the unwrapped phase, $\tilde{\phi}[n]$. The phase unwrapping method for LFM signals uses the fact that the second derivative of the unwrapped phase is constant. Thus, the phase of the signal is also constant, despite the modulo 2π operator, and therefore and can be easily extracted from the signal. The second derivative is given by

$$\begin{aligned} \Delta^2\tilde{\phi}[n] &= \tilde{\phi}[n] - 2\tilde{\phi}[n-1] + \tilde{\phi}[n+2] \\ &= \Delta^2\phi[n] \\ &= \arg\left(x[n](x^*[n-1])^2 x[n-2]\right) \\ &\cong 2\pi\theta_2 \end{aligned} \tag{2.4}$$

for $n = 2, \ldots, N-1$. Once $\Delta^2\tilde{\phi}[n]$ is extracted, the unwrapped phase can be obtained be integrating twice. The first derivative is obtained as follows

$$\Delta\tilde{\phi}[n] = \Delta^2\tilde{\phi}[n] + \Delta\tilde{\phi}[n-1]. \tag{2.5}$$

And finally, the unwrapped phase is given by

$$\tilde{\phi}[n] = \Delta\tilde{\phi}[n] + \tilde{\phi}[n-1]. \tag{2.6}$$

The procedure is initialized with

$$\tilde{\phi}[0] = \arg(x[0]) \tag{2.7}$$

$$\Delta\tilde{\phi}[1] = \arg(x[0]x^*[1]). \tag{2.8}$$

The unwrapped phase can be written as a linear model of the parameters

$$\tilde{\boldsymbol{\phi}} = 2\pi\mathbf{H}\boldsymbol{\theta} + \boldsymbol{\varepsilon}_v \tag{2.9}$$

where $\tilde{\boldsymbol{\phi}} = [\tilde{\phi}[0], \ldots, \tilde{\phi}[N-1]]^T$, $\boldsymbol{\varepsilon}_v = [\varepsilon_v[0], \ldots, \varepsilon_v[N-1]]^T$ and $\mathbf{H} = [\mathbf{1}_N, \mathbf{h}_1, \mathbf{h}_2]$ with $\mathbf{h}_1 = [0, 1, \ldots, N-1]^T$, $\mathbf{h}_2 = [0^2/2, 1^2/2, \ldots, (N-1)^2/2]^T$ and $\mathbf{1}_N$ is the $N \times 1$ vector with all elements equal to one. The parameters can then be estimated using LS approach

$$\hat{\boldsymbol{\theta}} = \frac{1}{2\pi} \left(\mathbf{H}^T \mathbf{H}\right)^{-1} \mathbf{H}^T \tilde{\boldsymbol{\phi}}. \tag{2.10}$$

The phase unwrapping method is very simple and perform well in high SNR [29]. However, it suffers from a few problems. It requires that the unwrapped phase difference between two consecutive samples should be less than π. In addition, large phase unwrapping errors occur if the phase difference, $\Delta\tilde{\phi}[n]$, is close to $\pm\pi$. It was extended for a general P'th order PPS [40] but is not suitable for multi-component signals. A recursive implementation of the phase unwrapping with a concurrent coefficients estimation was suggested in [41]. The integration of the parameter estimation into the phase unwrapping reduces the unwrapping errors and improve the performance of the method.

2.3 High Order Ambiguity Function

The HAF was first introduced for the parameter estimation of mono-component PPS with a constant amplitude by Peleg and Porat [18]. It was later extended for PPS with random or time-varying amplitudes [54,68], and to multi-component PPS [23,37–39]. Applying the HAF to a multi-component signal introduces polynomial-phase cross-terms. However, they are usually negligible relative to the auto-terms [39]. The simplicity and low-complexity of the HAF based estimation, along with its good performance, make it very popular and a standard method for parameter estimation of PPS.

We now present a short summary of the HAF based estimation for mono-component PPS. The high-order instantaneous moments of $x[n]$ are define as

$$\begin{aligned} x_1[n,\tau] &= x[n] \\ x_2[n,\tau] &= x_1[n] x_1^*[n-\tau;\tau] \\ &\vdots \\ x_K[n,\tau] &= x_{K-1}[n] x_{K-1}^*[n-\tau;\tau] \end{aligned} \tag{2.11}$$

where τ is a delay, in samples. The Kth order ambiguity function of $x[n]$ is define as the

discrete time Fourier transform (DTFT) of the Kth order instantaneous moment

$$X_K(\theta,\tau) = \sum_{n=0}^{N-1} x_K[n,\tau]e^{-j2\pi\theta n}. \tag{2.12}$$

Consider a Pth order PPS given by

$$x[n] = e^{j2\pi\phi[n]} \tag{2.13}$$

where $\phi[n] = \sum_{p=0}^{P} \theta_p n^p$. The second order instantaneous moment of $x[n]$ is given by

$$\begin{aligned} x_2[n,\tau] &= x[n]x^*[n-\tau] \\ &= e^{j2\pi\phi[n]}e^{-2\pi j\phi[n-\tau]} \\ &= e^{j2\pi(\phi[n]-\phi[n-\tau])}. \end{aligned} \tag{2.14}$$

The delayed phase, $\phi[n-\tau]$, is

$$\begin{aligned} \phi[n-\tau] &= \sum_{p=0}^{P} \theta_p (n-\tau)^p \\ &= \sum_{p=0}^{P} \theta_p \left[\sum_{k=0}^{p} \binom{p}{k} (-\tau)^{p-k} n^k \right] \\ &= \sum_{p=0}^{P} \tilde{\theta}_p n^p. \end{aligned} \tag{2.15}$$

where $\tilde{\theta}_p = \sum_{k=0}^{P-p} \binom{p+k}{p} (-\tau)^k \theta_{p+k}$. Note that $\tilde{\theta}_P = \theta_P$. Therefore, we get that

$$\phi[n] - \phi[n-\tau] = \sum_{p=0}^{P-1} (\theta_p - \tilde{\theta}_p) n^p. \tag{2.16}$$

That is, the second order instantaneous moment reduces the degree of the polynomial phase, which is the basis of all HAF based estimation methods. Furthermore, the highest remaining coefficient, given by $\theta_{P-1} - \tilde{\theta}_{P-1} = P\tau\theta_P$, depends only on θ_P and τ. By repeating the process $P-1$ times, it can be shown that the Pth order instantaneous moment is a complex exponential (i.e. constant frequency signal), with frequency that depends only on θ_P and τ. Therefore, θ_P can be estimated by maximizing the Pth order

HAF [23]

$$\hat{\theta}_P = \frac{1}{P!\tau^{P-1}} \arg\max_{\theta} \{|X_P(\theta,\tau)|\}. \tag{2.17}$$

Next, we obtain from $x[n]$ a $(P-1)$th order PPS as

$$x_2[n] = x[n]e^{-j\hat{\theta}_P n^p} \tag{2.18}$$

and repeat the process to obtain $\hat{\theta}_{P-1}$, and so on. The HAF based method transform a P-dimensional problem to P one-dimensional problems.

The HAF based method is an iterative process. Every time, the highest remaining coefficient is estimated and then subtracted from the signal. It therefore suffers from error propagation phenomenon. Estimation errors in any of the coefficients propagate to the lower order coefficients.

As mentioned above, the HAF of multi-component PPS contains cross-terms. That is, products of each component with delayed replicas of all the other components. The peaks corresponding to the cross terms are negligible relative to the peaks of the auto-terms in the HAF [39]. Therefore, the HAF can be considered almost additive, which allows the extension of HAF based estimation to multi-component PPS, under the assumption that the highest order coefficients do not coincide [23]. Consider a multi-component Pth order PPS given by

$$x[n] = \sum_{m=1}^{M} A_m e^{j2\pi\phi^{(m)}[n]} \tag{2.19}$$

where $\phi[n] = \sum_{p=0}^{P} \theta_p^{(m)} n^p$, and A_m is the amplitude of the mth component and M is the number of components. The highest order coefficients of each component, $\{\theta_P^{(m)}\}_{m=1}^{M}$, are estimated by selecting the M highest peaks in

$$\frac{1}{P!\tau^{P-1}} |X_P(\theta,\tau)|. \tag{2.20}$$

Then, a set of M demodulated signals is obtained as

$$x_2^{(m)}[n] = x[n]e^{-j\hat{\theta}_P^{(m)} n^p}, \; m = 1, \ldots, M. \tag{2.21}$$

Each signal $x_2^{(m)}[n]$ contains a $(P-1)$th order PPS, which is the mth component, and $M-1$ other components that are transformed by (2.21) to a different Pth order PPS. Therefore, the rest of the coefficients of the mth component can be estimated using the

HAF based method of order $(P-1)$ on $x_2^{(m)}[n]$ [23].

2.4 Discussion

In this chapter, we reviewed two methods for parameter estimation of LFM signals that are relevant to this research. Both methods are very simple, have low computational complexity and perform well in good SNR conditions. The first is the phase unwrapping method, which is suitable only for mono-component signals. The phase unwrapping method offers simple and closed form estimator but suffers from high sensitivity when the phase of the signal approaches $\pm\pi$. The second is the HAF based estimation method, perhaps the most popular method for estimating the parameters of PPS. This is an order-recursive method where each time the highest remaining coefficient is estimated and eliminated. Therefore it suffers from error propagation, where estimation errors in high order coefficients propagates to the lower order ones. The HAF based estimator was first introduced for mono-component signals but was successfully applied also to multi-component signals.

Chapter 3

Constant Amplitude Model

3.1 Introduction

In this chapter, we consider the case of harmonic LFM with constant amplitudes. Common model order criteria select the number of harmonics based on the MLE. In Section 3.3, we develop exact and approximated MLE of these parameters and the CRLB of the estimator. To avoid an exhaustive search in the initial frequency-frequency rate space involved by those estimators, we propose two alternative low-complexity estimation methods. First we present an extension of the PHAF estimation method developed originally for multi-component PPS in Section 3.4. Next we propose a novel two-step estimation method in Section 3.5, which we term the Harmonic-SEES. The first step separates the signal to its harmonic components. Then, in the second step, the parameters of interest are estimated using least squares method given the phases of the harmonic components. The method is compared to the exact and approximated MLE and to the well-known HAF based method. Finally, in Section 3.6 we present numerical simulations and real data examples that demonstrate that the proposed low-complexity method can successfully replace the MLE in the model order criteria at moderate to high SNR. Since the estimates obtained by the proposed method achieve the CRLB at these SNR values.

3.1.1 Notation

In this chapter we use the following vector form notations. By collecting the N samples of the received signal in (1.1) we obtain a compact vector-form model given as,

$$\mathbf{x} = \mathbf{S}_M \mathbf{a}_M + \mathbf{v} \tag{3.1}$$

where we define $\mathbf{x} = [x[0], \ldots, x[N-1]]^T$, $\mathbf{S}_M = [\mathbf{s}_1(\theta), \cdots, \mathbf{s}_M(\theta)]$, $\mathbf{s}_m(\theta) = [s_m[0;\theta], \ldots, s_m[N-1;\theta]]^T$, $\mathbf{a}_M = [a_1, \ldots, a_M]^T$, and $\mathbf{v} = [v[0], \ldots, v[N-1]]^T$. The unknown parameter vector of the model is $\boldsymbol{\psi} = [\boldsymbol{\theta}^T, \mathbf{a}_M^T, \sigma_v^2]^T$, where $\boldsymbol{\theta} = [\theta_1, \theta_2]^T$ is the parameter vector of interest.

3.2 Model Order Selection

When the number of harmonics is unknown, a model order selection criterion should be used to choose the correct order, M. Two commonly used criteria are the MDL and AIC [71]. Both have the same form, which includes two terms: 1) the minimum of the negative log-likelihood function, $\ell(\hat{\boldsymbol{\psi}}|m)$, where $\hat{\boldsymbol{\psi}}$ is the MLE of $\boldsymbol{\psi}$ and 2) a penalty term, a monotonically increasing function w.r.t. the model order designed to prevent over estimation, $p(m)$. That is

$$\begin{aligned} \hat{M} &= \underset{m=1,\ldots,D}{\operatorname{argmin}} \left\{ \underset{\boldsymbol{\psi}}{min}\ \ell(\boldsymbol{\psi}|m) + p(m) \right\}. \\ &= \underset{m=1,\ldots,D}{\operatorname{argmin}} \left\{ \ell(\hat{\boldsymbol{\psi}}|m) + p(m) \right\} \end{aligned} \tag{3.2}$$

where D is the highest possible model order.

In the current case, the observation vector in (3.1) is distributed as a complex multivariate circularly Gaussian random vector, $\mathbf{x} \sim \mathcal{N}_C(\mathbf{S}_m\mathbf{a}_m, \sigma_v^2\mathbf{I}_N)$, where $\mathbf{I}_N$ is the $N \times N$ identity matrix. The negative log likelihood function of the signal in (3.1) is obtained by taking the natural logarithm of its probability density function (pdf) conditioned on both the parameter vector, $\boldsymbol{\psi}$, and an assumed model order m. The minimum of the negative log likelihood is given by

$$\ell(\hat{\boldsymbol{\psi}}|m) = \frac{1}{2\sigma_v^2} \left\| \mathbf{x} - \hat{\mathbf{S}}_m \hat{\mathbf{a}}_m \right\|^2 + \frac{N}{2}\log(\sigma_v^2) + \log(K) \tag{3.3}$$

where K is a constant and $\hat{(\cdot)}$ denotes the MLE estimate given a number of harmonics. The penalty terms for each criterion are given by [78]

$$p(m) = \begin{cases} \frac{1}{2}(2m+2)\log(N), & \text{MDL} \\ 2m+2, & \text{AIC} \end{cases} \tag{3.4}$$

where $2m+2$ is the number of unknown parameters. A Bayesian approach can also be

used to derive a MAP selection criterion. However, the result, for this case, is equivalent to the MDL criterion [24].

3.3 Maximum Likelihood Estimation

We present an exact MLE for a given number of harmonics, which requires an exhaustive search in the normalized initial frequency - frequency rate space, and involves a large number of computations at each candidate point in this space. It is known that chirps with different time varying frequencies are almost orthogonal. Based on this result and in order to reduce the computations, we further derive the approximated MLE. We term this estimator as the Harmochirp-gram since it extends the idea of the Harmogram [7] used for estimating harmonic sinusoids (see Appendix A). This estimator still requires a search in the normalized initial frequency-frequency rate space. However, the cost function obtained requires less computations at each point in this space. Simulation results show that the orthogonality approximation is reasonable as the estimation performances of both estimators are similar.

3.3.1 The Exact MLE

As noted above, the MLE of $\boldsymbol{\psi}$ is found by minimizing (3.3). Assuming some model order, m, the MLE of $\mathbf{a}_m$, denoted by $\hat{\mathbf{a}}_m$, is obtained by taking the derivative of (3.3) w.r.t. $\mathbf{a}_m^H$, and equating the derivative to zero. This results in $\hat{\mathbf{a}}_m = (\mathbf{S}_m^H\mathbf{S}_m)^{-1}\mathbf{S}_m^H\mathbf{x}$. Substituting this estimate in (3.3) yields the MLE of $\boldsymbol{\theta}$, denoted by $\hat{\boldsymbol{\theta}}_m^{(\mathrm{MLE})}$,

$$\hat{\boldsymbol{\theta}}_m^{(\mathrm{MLE})} = \underset{\boldsymbol{\theta}}{\operatorname{argmax}} \left\{Q_e(\boldsymbol{\theta}) = \mathbf{x}^H\mathbf{P}_{\mathbf{S}_m}\mathbf{x}\right\} \tag{3.5}$$

where $\mathbf{P}_{\mathbf{S}_m} = \mathbf{S}_m(\mathbf{S}_m^H\mathbf{S}_m)^{-1}\mathbf{S}_m^H$ is the projection matrix of $\mathbf{S}_m$.

In Fig. 3.1 we present an illustration of the cost function, $Q_e(\boldsymbol{\theta})$, in the (θ_1, θ_2) space. The cost function is composed from a narrow ridge, centered around the location of the true parameters and several local maximums at normalized initial frequency and normalized frequency rates that are half, twice, four times etc. the true fundamental normalized initial frequency and normalized frequency rate, where in high noise scenario, the estimator may yield false estimates.

Unfortunately, there is no closed-form expression for this estimator. Therefore, a two-dimensional exhaustive search in the initial frequency-frequency rate is required. Finally,

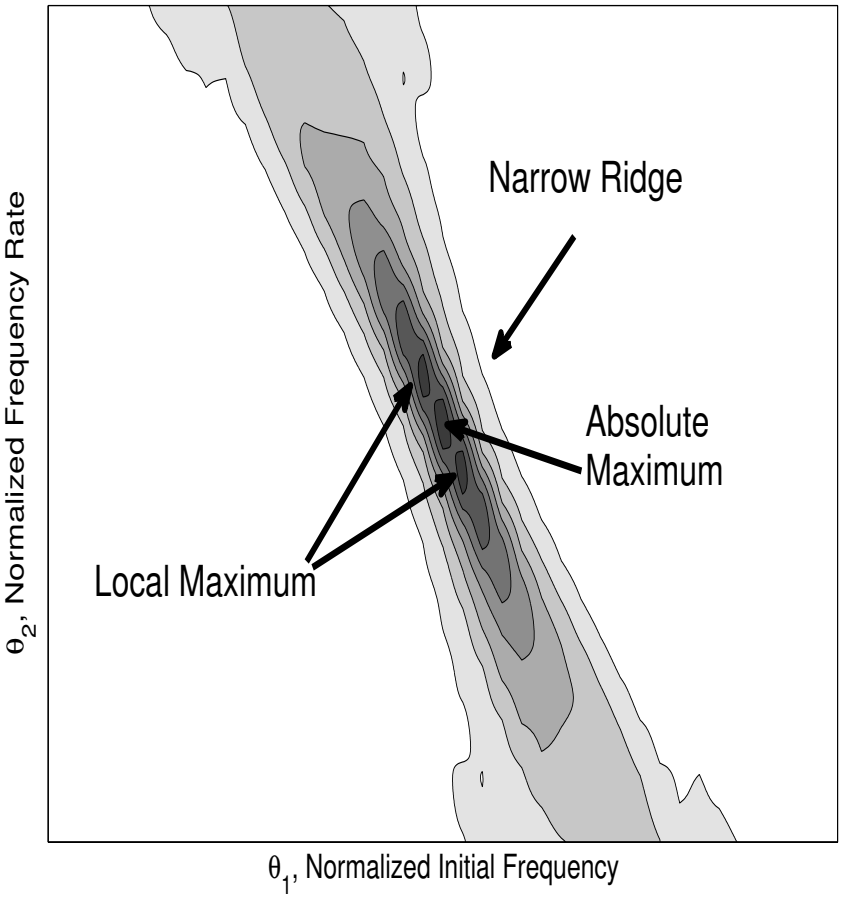

Figure 3.1: Illustration of the cost function of the exact MLE.

taking the derivative w.r.t. σ_v^2 and equating to zero yields

$$\hat{\sigma}_{v,m}^2 = \frac{1}{N}\mathbf{x}^H \hat{\mathbf{P}}_{\mathbf{S}_m}^{\perp}\mathbf{x} \tag{3.6}$$

where $\hat{\mathbf{P}}_{\mathbf{S}_m}^{\perp} = \mathbf{I}_N - \hat{\mathbf{P}}_{\mathbf{S}_m}$. Substituting (3.6) into (3.3) results in

$$\ell(\hat{\boldsymbol{\psi}}|m) = \frac{N}{2} + \frac{N}{2}\log(\hat{\sigma}_{v,m}^2) + \log(K) \tag{3.7}$$

Substituting (3.7) into (3.2) and discarding all constants yields

$$\hat{M} = \underset{m=1,\ldots,D}{\operatorname{argmin}} \left\{ \log(\hat{\sigma}_{v,m}^2) + \frac{2}{N}p(m) \right\}. \tag{3.8}$$

3.3.2 The Approximated MLE

The basic assumption of the approximated MLE is that for large number of samples, the cross-product between the ℓth and kth harmonic components ($\ell \neq k$) is negligible w.r.t. N, i.e., $\sum_{n=0}^{N-1} s_\ell^*[n]s_k[n] \ll N$. We thus obtain that, for large number of samples, $\mathbf{S}^H\mathbf{S} \cong N\mathbf{I}_M$. We can then replace the cost function $Q_e(\boldsymbol{\theta})$ in (3.5) by $Q_a(\boldsymbol{\theta}) = \|\mathbf{S}^H\mathbf{x}\|^2 = \sum_{m=1}^{M} |\mathbf{s}_m(\boldsymbol{\theta})^H\mathbf{x}|^2$. We further note that

$$\begin{aligned} Q_a(\boldsymbol{\theta}) &= \sum_{m=1}^{M} |\sum_{n=0}^{N-1} x_m^{(\theta_2)}[n]e^{-j2\pi m\theta_1 n}|^2 \\ &= \sum_{m=1}^{M} |\bar{x}_m^{(\theta_2)}(m\theta_1)|^2 \end{aligned} \tag{3.9}$$

where

$$x_m^{(\theta_2)}[n] = x[n]e^{-j2\pi\frac{1}{2}m\theta_2 n^2} \tag{3.10}$$

and $\bar{x}_m^{(\theta_2)}(m\theta_1) = \sum_{n=0}^{N-1} x_m^{(\theta_2)}[n]e^{-j2\pi\cdot m\theta_1\cdot n}$ is the DTFT of $x_m^{(\theta_2)}[n]$ computed at the normalized frequency $m\theta_1$. We term the cost function in (3.9) as the Harmochirp-gram. In addition, (3.10) is termed the de-chirping of $x[n]$ since it transforms a chirp with frequency rate of $m\theta_2$ into a constant frequency signal.

The estimated parameters using (3.9) are not the exact MLE for finite data lengths, but are asymptotically efficient when the number of samples is large. To obtain these estimates we actually perform the following steps for each candidate point (θ_1, θ_2): 1) given θ_2, we de-chirp the observed signal with a set of normalized frequency rates $\{m\theta_2\}_{m=1}^{M}$ which

yields the signals $\{x_m^{(\theta_2)}[n]\}_{m=1}^M$; 2) Taking the DTFT of each de-chirped signal, $x_m^{(\theta_2)}[n]$, at normalized frequency, $\{m\theta_1\}_{m=1}^M$, and combining the absolute values of the M DTFT at these frequencies (the second step is similar to the Harmogram technique [7] which is used to estimate the fundamental frequency of harmonic sinusoids).

Observe that by substituting (1.1) into (3.10) and assuming that θ_2 equals the true normalized frequency rate, $\theta_{2,0}$, we get that

$$x_m^{(\theta_2)}[n] = a_m e^{j2\pi m\theta_{1,0}n} + r_{\theta_{2,0}}[n] + v_{\theta_{2,0}}[n] \tag{3.11}$$

where $\theta_{1,0}$ is the true normalized initial frequency , $v_{\theta_{2,0}}[n] = v[n]e^{-j2\pi\frac{1}{2}m\theta_{2,0}n^2}$, and $r_{\theta_{2,0}}[n] = \sum_{\substack{k=1\\k\neq m}}^M a_k e^{j2\pi\frac{1}{2}(k-m)\theta_{2,0}n^2} e^{j2\pi k\theta_1 n}$ are the de-chirped noise and the residual term due to de-chriping the other harmonic components. That is,

$$\bar{x}_m^{(\theta_2)}[n](m\theta_1) \cong a_m D(m(\theta_{1,0}-\theta_1)) + \bar{r}_{\theta_{2,0}}(m\theta_1) + \bar{v}_{\theta_{2,0}}(m\theta_1) \tag{3.12}$$

where $D(\theta) = \sum_{n=0}^{N-1} e^{-j2\pi\theta n}$ is the Dirichlet kernel which equals N at $\theta = 0$. Assume that the noise term in (3.12) is negligible and consider the case where $\theta_1 = \theta_{1,0}$. The first term then equals $a_m N$ while the second term is approximately zero according to the analysis in [79]. Approximately, the value of $Q_a(\boldsymbol{\theta})$ in (3.9) at the true point is then $Q_a(\theta_{1,0}, \theta_{2,0}) \cong N^2 \sum_{m=1}^M |a_m|^2$ which means that the Harmochirp-gram combines the energies of all the harmonic components together.

In order to understand how large the number of samples is required to be in order for the orthogonality assumption to hold, we wish to examine the ratio between the main and first diagonals of $\mathbf{S}^H\mathbf{S}$

$$r(\boldsymbol{\theta}, N) = \left|\frac{\mathbf{s}_m^H(\boldsymbol{\theta})\mathbf{s}_{m+1}(\boldsymbol{\theta})}{\mathbf{s}_m^H(\boldsymbol{\theta})\mathbf{s}_m(\boldsymbol{\theta})}\right|^2 = \left|\frac{1}{N}\sum_{n=0}^{N-1} e^{-j2\pi(\theta_1 n + \frac{1}{2}\theta_2 n^2)}\right|^2. \tag{3.13}$$

Note that (3.13) is independent of m and thus holds for each $m = 1, \ldots, M$. For $\theta_2 = 0$, we get that $r(\boldsymbol{\theta}, N)$ is the magnitude of the DTFT of a rectangular window with length N. Fig. 3.2 present $r(\boldsymbol{\theta}, N)$ versus $N \cdot \delta$ for three different values of θ_2. As it can be seen, θ_2 has a scaling effect on $r(\boldsymbol{\theta}, N)$. Again, considering the case of $\theta_2 = 0$, then $r(\boldsymbol{\theta}, N)$ has a local minimum at $N \cdot \delta = k,\ k = 1, 2, ...$, a side-lobe level of -13dB and side-lobes fall rate of -6dB/octave [80]. Hence, in order to assure more than 20dB attenuation, we

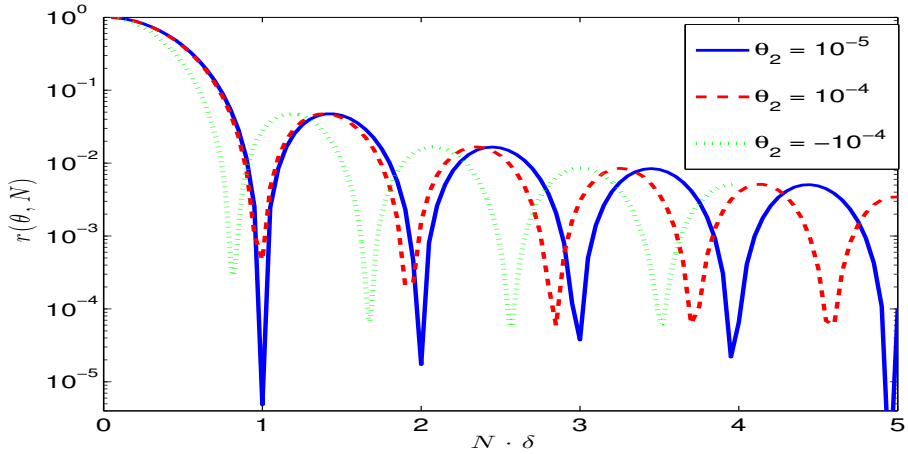

Figure 3.2: The ratio between the main and first diagonals of $\mathbf{S}^H\mathbf{S}$

require that

$$N > \frac{3}{\delta}. \tag{3.14}$$

Note that the scaling, caused by θ_2, means that (3.14) ensures that the cross product between two components is sufficiently small for each θ_2.

3.3.3 The Cramer-Rao Lower Bound

The covariance matrix of any unbiased estimate of $\boldsymbol{\psi}$, denoted by $\text{cov}(\hat{\boldsymbol{\psi}}) = E[(\hat{\boldsymbol{\psi}} - \boldsymbol{\psi})(\hat{\boldsymbol{\psi}} - \boldsymbol{\psi})^T]$, is lower bounded by the inverse of the Fisher information matrix (FIM), denoted by $\mathbf{J}_{\boldsymbol{\psi},\boldsymbol{\psi}}$, that is, $\text{cov}(\hat{\boldsymbol{\psi}}) \geq \mathbf{J}^{-1}_{\boldsymbol{\psi},\boldsymbol{\psi}}$, where

$$\mathbf{J}_{\boldsymbol{\psi},\boldsymbol{\psi}} = \begin{bmatrix} \mathbf{J}_{\boldsymbol{\theta},\boldsymbol{\theta}} & \mathbf{J}_{\boldsymbol{\theta},\mathbf{a}} & \mathbf{0} \\ \mathbf{J}^T_{\boldsymbol{\theta},\mathbf{a}} & \mathbf{J}_{\mathbf{a},\mathbf{a}} & \mathbf{0} \\ \mathbf{0}^T & \mathbf{0}^T & \boldsymbol{J}_{\sigma_v^2,\sigma_v^2} \end{bmatrix} \tag{3.15}$$

where the sub-matrices of $\mathbf{J}_{\boldsymbol{\psi},\boldsymbol{\psi}}$ are shown to be given by (see Appendix C)

$$\mathbf{J}_{\boldsymbol{\theta},\boldsymbol{\theta}} = \frac{4\pi^2}{\sigma_v^2}\begin{bmatrix} 2\mathbf{W}_1 & \mathbf{W}_2 \\ \mathbf{W}_2 & \mathbf{W}_3 \end{bmatrix} \tag{3.16}$$

$$\mathbf{J}_{\mathbf{a},\mathbf{a}} = \frac{2}{\sigma_v^2}\begin{bmatrix} (\mathbf{S}^H\mathbf{S})_r & (\mathbf{S}^H\mathbf{S})_i \\ -(\mathbf{S}^H\mathbf{S})_i & (\mathbf{S}^H\mathbf{S})_r \end{bmatrix} \tag{3.17}$$

$$\mathbf{J}_{\boldsymbol{\theta},\mathbf{a}} = \frac{2\pi}{\sigma_v^2}\begin{bmatrix} 2(\mathbf{U}_1)_i & 2(\mathbf{U}_1)_r \\ (\mathbf{U}_2)_i & (\mathbf{U}_2)_r \end{bmatrix} \tag{3.18}$$

where $\mathbf{x}_r = \Re\{\mathbf{x}\}$ and $\mathbf{x}_i = \Im\{\mathbf{x}\}$ denote the real and imaginary parts of $\mathbf{x}$, respectively. Also, $\mathbf{W}_i = \|\mathbf{Q}^{(i+1)/2}\mathbf{S}\mathbf{D}\mathbf{a}\|^2$, $i = 1,2,3$, $\mathbf{U}_i = \mathbf{a}^H\mathbf{D}^T\mathbf{S}^H\mathbf{Q}^i\mathbf{S}$, $i = 1,2$ with $\mathbf{D} = \mathrm{diag}(1,2,\ldots,M)$ and $\mathbf{Q} = \mathrm{diag}(0,1,\ldots,N-1)$, where we defined $\mathbf{A}^k = \mathrm{diag}(a_1^k,\ldots,a_L^k)$ for real k. Using the matrix inversion lemma [78, App. A] we get that the CRLB on $\boldsymbol{\theta}$ is then given by

$$\mathrm{cov}(\hat{\boldsymbol{\theta}}) \geq (\mathbf{J}_{\boldsymbol{\theta},\boldsymbol{\theta}} - \mathbf{J}_{\boldsymbol{\theta},\mathbf{a}}\mathbf{J}_{\mathbf{a},\mathbf{a}}^{-1}\mathbf{J}_{\boldsymbol{\theta},\mathbf{a}}^T)^{-1} \tag{3.19}$$

where $\mathrm{cov}(\hat{\boldsymbol{\theta}}) = E[(\hat{\boldsymbol{\theta}} - \boldsymbol{\theta})(\hat{\boldsymbol{\theta}} - \boldsymbol{\theta})^T]$ is the covariance of $\hat{\boldsymbol{\theta}}$.

The Large-Samples Approximation of the CRLB

Observe that the terms $\{\mathbf{S}^H\mathbf{Q}^u\mathbf{S}\}_{u=0}^4$ appears in the expressions of $\mathbf{J}_{\boldsymbol{\theta},\boldsymbol{\theta}}$ and $\mathbf{J}_{\boldsymbol{\theta},\mathbf{a}}$ via the matrices $\{\mathbf{W}_i\}_{i=1}^3$, and $\{\mathbf{U}_i\}_{i=1}^2$. The (ℓ,k)th element of $\{\mathbf{S}^H\mathbf{Q}^u\mathbf{S}\}_{u=0}^4$ is given by,

$$\mathbf{s}_\ell^H(\boldsymbol{\theta})\mathbf{Q}^u\mathbf{s}_k(\boldsymbol{\theta}) = \sum_{n=0}^{N-1} n^u e^{-j2\pi(\ell-k)\frac{1}{2}\theta_{2,0}n^2} e^{-j2\pi(\ell-k)\theta_{1,0}n} \tag{3.20}$$

The value of $\mathbf{S}^H\mathbf{Q}^u\mathbf{S}$ along the main diagonal is $\sum_{n=0}^{N-1} n^u$, which for $N \gg 1$, is approximately $N^{u+1}/(u+1)$. We assume that for $N \gg 1$, $\mathbf{S}^H\mathbf{Q}^u\mathbf{S} \cong \frac{N^{u+1}}{u+1}\mathbf{I}_M$, i.e., we neglect the off-diagonal terms of the matrix. We thus obtain after few simple mathematical steps

that the different FIM in (3.16)-(3.18) are approximately given as

$$\mathbf{J}_{\boldsymbol{\theta},\boldsymbol{\theta}} \cong \frac{\pi^2 N^3}{\sigma_v^2} \begin{bmatrix} \frac{8}{3}\mathbf{a}^H\mathbf{D}^2\mathbf{a} & N\mathbf{a}^H\mathbf{D}^2\mathbf{a} \\ N\mathbf{a}^H\mathbf{D}^2\mathbf{a} & \frac{2N^2}{5}\mathbf{a}^H\mathbf{D}^2\mathbf{a} \end{bmatrix} \tag{3.21}$$

$$\mathbf{J}_{\mathbf{a},\mathbf{a}} \cong \frac{2N}{\sigma_v^2}\mathbf{I}_M \tag{3.22}$$

$$\mathbf{J}_{\boldsymbol{\theta},\mathbf{a}} \cong \frac{2\pi N^2}{\sigma_v^2} \begin{bmatrix} -\mathbf{a}_i^T\mathbf{D} & \mathbf{a}_r^T\mathbf{D} \\ -\frac{N}{3}\mathbf{a}_i^T\mathbf{D} & \frac{N}{3}\mathbf{a}_r^T\mathbf{D} \end{bmatrix} \tag{3.23}$$

Substituting (3.21)-(3.23) in (3.19) yields that the large-samples CRLB on the parameter vector $\boldsymbol{\theta}$ is given by,

$$\mathrm{cov}(\hat{\boldsymbol{\theta}}) \geq \frac{1}{\mathbf{a}_M^H\mathbf{D}^2\mathbf{a}_M}\frac{\sigma_v^2}{\pi^2 N^3} \begin{bmatrix} 24 & -\frac{45}{N} \\ -\frac{45}{N} & \frac{90}{N^2} \end{bmatrix}. \tag{3.24}$$

The large-samples CRLB on the estimation error of the normalized initial frequency and frequency rate are,

$$E[\theta_1^2] \geq \frac{24\sigma_v^2}{\pi^2 N^3}\frac{1}{\mathbf{a}^H\mathbf{D}^2\mathbf{a}}\ , E[\theta_2^2] \geq \frac{90\sigma_v^2}{\pi^2 N^5}\frac{1}{\mathbf{a}^H\mathbf{D}^2\mathbf{a}}. \tag{3.25}$$

Observe that $\mathbf{a}^H\mathbf{D}^2\mathbf{a} = \sum_{m=1}^{M} m^2|a_m|^2 < \sum_{m=1}^{M} m^2 = (M+1)M(2M+1)/6$, where the inequality holds for $|a_m| \leq 1$. By estimating the normalized initial frequency and frequency rate using all the M harmonic components, we improve the estimation error w.r.t. M^3. Furthermore, the estimation accuracy of θ_1 and θ_2 decrease as $1/N^{3/2}$ and $1/N^{5/2}$, respectively, which can be obtained using the DTFT as is being used by the Harmochirp-gram.

3.3.4 Computational Load

We evaluate the computational complexity of the Harmochirp-gram and the MLE method by calculating the number of on-line real multiplications involved in each method. Consider first the Harmochirp-gram in (3.9). Assume that the number of possible values of θ_1 and θ_2 are n_1 and n_2, respectively. At each point, we perform M times de-chirping and DTFT at a single frequency. The de-chirping and the squared magnitude of the DTFT requires $\mathcal{O}(N)$ multiplications. The total number of real multiplications is $\mathcal{O}(n_1 n_2 M N)$. Using the fact that $|\theta_1| < 1/2$ and $|\theta_2| < 1/(2N)$ and the CRLB, n_1 and n_2 should be in the order

of $N^{3/2}$ in order to achieve the CRLB. Therefore the complexity of the Harmochirp-gram is $\mathcal{O}\left(N^4 M\right)$. The exact MLE involves the calculation of (3.5) at each point. This requires inversion of an $M \times M$ matrix and multiplication of an $N \times M$ matrix by $M \times N$ matrix. Assuming $N \gg M$, the total complexity of the exact MLE is $\mathcal{O}\left(N^5 M\right)$.

3.4 Product High Order Ambiguity Function

The PHAF method for estimating parameters of a multi component PPS was introduced in [23]. It is a low complexity sub-optimal estimation method that uses multi-lag HAF [18] to reduce the dimension of the problem to one dimensional search. We now wish to present the methods and its application to the estimation of the parameters of harmonic LFM signals.

The second order ambiguity function is defined as [23]

$$X_2(\theta;\tau) = \sum_{n=0}^{N-1} x_2[n;\tau] e^{-j2\pi\theta n} \tag{3.26}$$

where $x_2[n;\tau] = x[n]x^*[n-\tau]$ and τ is a delay, in samples. The ambiguity function, when applied to LFM, transform the signal into a complex sinusoids [23]. That is, $x_2[n;\tau]$ will be a sum of M complex sinusoids at the frequencies $\theta_m = \tau m \theta_2$. Therefore, $X_2(\theta;\tau)$ should have M strong peaks at the expected frequencies. Given a set of L lags, $\boldsymbol{\tau} = [\tau_1, \ldots, \tau_L]$, the PHAF is defined as a product of L scaled second order ambiguity functions

$$X_2(\theta;\boldsymbol{\tau}) = \prod_{\ell=1}^{L} X_2(\theta\tau_\ell/\tau_1;\tau_\ell). \tag{3.27}$$

The scaling procedure aligns the sinusoids to the same frequency. Hence, $X_2(\theta;\boldsymbol{\tau})$ will have very strong peaks at $\theta = \tau_1\theta_2, \ldots, \tau_1 M\theta_2$. Note that (3.26) is constructed using a DTFT. Thus, a high resolution search is still required. However, as opposed to the MLE, the problem is now reduced to a one dimensional search. As we showed, the required resolution in order to achieve the CRLB is $1/N^{5/2}$.

Following the estimation procedure for a multi-component signals from [23], the parameters are estimated as follows. First, the frequency rates of each component ,$\hat{\theta}_2^{(1)}, \ldots, \hat{\theta}_2^{(M)}$, are estimated separately by picking the M highest peaks in (3.27). Then, M de-chirped signals are defined as

$$x_m[n] = x[n]e^{-j2\pi\frac{1}{2}\hat{\theta}_2^{(m)}n^2}. \tag{3.28}$$

Each de-chirped signal should be composed of a complex sinusoid in presence of interfering harmonics. The initial frequency of each component ,$\hat{\theta}_1^{(1)}, \ldots, \hat{\theta}_1^{(M)}$, are thus estimated as

$$\hat{\theta}_1^{(m)} = \arg\max_{\theta_1} x_m[n] e^{-j2\pi\theta_1 n}. \tag{3.29}$$

We define the estimated parameters vectors $\hat{\boldsymbol{\theta}}^{(m)} = [\hat{\theta}_1^{(m)}, \hat{\theta}_2^{(m)}]^T$, $m = 1, \ldots, M$. We define a mapping of the components numbers, $f : [1, M] \to [1, M]$, such that $\hat{\theta}_1^{(f(1))} < \hat{\theta}_1^{(f(2))} < \ldots < \hat{\theta}_1^{(f(M))}$. Then, the parameters can be estimated by solving the following LS problem

$$\hat{\boldsymbol{\theta}}^{(\mathrm{PHAF})} = \arg\min_{\boldsymbol{\theta}} \|\mathbf{A}_M \boldsymbol{\theta} - \boldsymbol{\theta}_M\|^2 \tag{3.30}$$

where

$$\mathbf{A}_M = \begin{bmatrix} \mathbf{g}_M & \mathbf{0}_M \\ \mathbf{0}_M & \mathbf{g}_M \end{bmatrix}, \tag{3.31}$$

$\mathbf{0}_n$ is the $n \times 1$ vector with all elements equal to zero, $\mathbf{g}_M = [1, \ldots, M]^T$ and $\boldsymbol{\theta}_M = [\hat{\theta}_1^{(f(1))}, \ldots, \hat{\theta}_1^{(f(M))}, \hat{\theta}_2^{(f(1))}, \ldots, \hat{\theta}_2^{(f(M))}]^T$. Solving the above problem yields

$$\hat{\boldsymbol{\theta}}^{(\mathrm{PHAF})} = (\mathbf{A}_M^T \mathbf{A}_M)^{-1} \mathbf{A}_M^T \boldsymbol{\theta}_M = \frac{1}{C_M} \sum_{m=1}^{M} m \hat{\boldsymbol{\theta}}^{(f(m))} \tag{3.32}$$

where $C_M = \sum_{m=1}^{M} m^2 = \frac{1}{6}(M+1)M(2M+1)$.

Once θ is estimated, $\hat{\boldsymbol{\theta}}^{(\mathrm{PHAF})}$ can be substituted in (3.6) instead of the $\hat{\boldsymbol{\theta}}^{(\mathrm{MLE})}$ in order to estimate the conditional negative log-likelihood and select the number of harmonics according to (3.8).

A major problem with the PHAF based estimation is that the parameters are estimated separately. Therefore, the estimation error of the frequency rate will propagate to the estimation of the initial frequency [23].

3.4.1 Accuracy Analysis

For a single LFM component at high SNR, the PHAF method is known to achieve the CRLB [23]. That is, we assume that the estimated parameters of each component, $\hat{\boldsymbol{\theta}}^{(f(m))}$, is given by $\hat{\boldsymbol{\theta}}^{(f(m))} = m\boldsymbol{\theta} + \boldsymbol{\varepsilon}^{(m)}$ where $\boldsymbol{\varepsilon}^{(m)}$ is a zeros-mean Gaussian process with a covariance given by the CRLB for a single LFM. Therefore, according to (3.24), we assume

that

$$\mathrm{cov}(\boldsymbol{\varepsilon}^{(m)}) = \frac{1}{|a_m|^2}\frac{\sigma_{v,m}^2}{\pi^2 N^3}\begin{bmatrix} 24 & -\frac{45}{N} \\ -\frac{45}{N} & \frac{90}{N^2} \end{bmatrix} \tag{3.33}$$

where $\sigma_{v,m}^2$ accounts for the additive noise and the interference of the other components. We further assume that the errors of any two components are uncorrelated, i.e. $E[(\boldsymbol{\varepsilon}^{(m)})^H \boldsymbol{\varepsilon}^{(k)}] = 0$ for $m \neq k$. The estimations of each component actually are correlated but we model that as an interference that contribute more noise. As noted in [23], analyzing $\sigma_{v,m}^2$ is very complicated. We can therefore conclude that

$$\mathrm{var}(\hat{\theta}_1) = \frac{24}{C_M \pi^2 N^3}\sum_{m=1}^{M}\frac{m\sigma_{v,m}^2}{|a_m|^2} \tag{3.34}$$

$$\mathrm{var}(\hat{\theta}_2) = \frac{90}{C_M \pi^2 N^5}\sum_{m=1}^{M}\frac{m\sigma_{v,m}^2}{|a_m|^2} \tag{3.35}$$

In order to compare the PHAF estimator to the optimal estimator, we examine the ratio between the variance of the MLE and that of the PHAF method

$$\begin{aligned}
\frac{\mathrm{var}(\hat{\theta}_k^{(\mathrm{PHAF})})}{\mathrm{var}(\hat{\theta}_k^{(\mathrm{MLE})})} &= \frac{\sum_{m=1}^{M} m\sigma_{v,m}^2/|a_m|^2}{C_M}\frac{\sum_{m=1}^{M} m^2|a_m|^2}{\sigma_v^2} \\
&> \frac{\sum_{m=1}^{M} m\sigma_v^2/|a_m|^2}{C_M}\frac{\sum_{m=1}^{M} m^2|a_m|^2}{\sigma_v^2} \\
&= \frac{\sum_{m=1}^{M} m/|a_m|^2}{C_M}\sum_{m=1}^{M} m^2|a_m|^2 \qquad (3.36) \\
&= \frac{1}{C_M}\Big(\sum_{m=1}^{M} m^3 + \sum_{m\neq p} mp^2|a_p/a_m|^2\Big) \\
&> \frac{\sum_{m=1}^{M} m^3}{\sum_{m=1}^{M} m^2} = \frac{3M}{2}\frac{M+1}{2M+1} \\
&> \frac{3M}{2}\frac{M+1}{2M+2} = \frac{3M}{4} \qquad (3.37)
\end{aligned}$$

for $k = 1, 2$. The MLE is asymptotically efficient. Therefore, from the last result, we get that for $M \geq 2$ the PHAF estimator cannot, even in high SNR, achieve the CRLB. As shown before, the MLE error improves by a factor of M^3. From the last result it seems that the PHAF estimator improves only by a factor of M^2. Generally, since $\sigma_{v,m}^2 > \sigma_v^2$, this is not a tight lower bound and the actual error should be even higher.

3.4.2 Computational Load

The construction of the PHAF in (3.27) involves calculation of a DTFT L times, each requires $\mathcal{O}(N)$ multiplications per frequency. The number of frequency rate candidates required to achieve the best possible approximation is in the order of $N^{5/2}/N$. The total number of multiplications required to construct (3.27) is therefore $\mathcal{O}(N^{5/2}L)$. Next, M DTFTs, one for each de-chirped signals are required. The number of frequencies in this step is in the order of $N^{3/2}$. The complexity of the initial frequencies estimation is therefore $\mathcal{O}(N^{5/2}M)$. The last step, the LS, requires $\mathcal{O}(M)$ multiplications which is negligible. To conclude, the PHAF method involves $\mathcal{O}(N^{5/2}(L+M))$ multiplications. Since L should be a small number, this is substantially less than the complexity of the Harmochirp-gram estimator.

3.5 The Harmonic Separate-Estimate Method

The use of the DTFT, as demonstrated in the numerical results, makes it possible to achieve the CRLB. However, it requires large number of computations. This complexity can be reduced using the discrete Fourier transform (DFT) which is more attractive due to its efficient implementation, the FFT. However, the frequency resolution of the DFT is limited proportionally to the inverse of the number of samples, i.e., $1/N$. To overcome this resolution limit but still exploits the low complexity of the DFT, we suggest a suboptimal estimator, the Harmonic-SEES.

We suggest a two-step method to estimate θ_1 and θ_2 of the harmonic chirps (see Fig. 3.3). First, separate the signal to its harmonic components and then jointly estimate the θ_1 and θ_2 from the phases of the signals using an LS approach. The computationally efficient DFT is used in a separate step to obtain a coarse normalized frequency rate estimate, and this estimate is further refined within the second step using the LS principle. We show that asymptotically, that is, given large number of data samples, the Harmonic-SEES estimator is unbiased, and obtain a closed-form expression for its theoretical covariance matrix.

The outputs of the separate step are M reconstructed harmonic components of the original signal. We design M processors where each processor is composed of three blocks (See Fig. 3.5): 1) de-chirping; 2) frequency filtering; 3) reconstruction. The first block eliminates the quadratic term of the phase of the mth harmonic component and retains

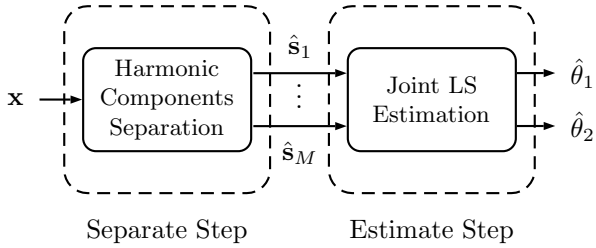

Figure 3.3: The Harmonic-SEES estimator.

the linear term of the phase only. The second block transforms the de-chirped signal to the frequency domain using DFT, and removes interferences from other harmonic components using a filter which is tuned to the frequency of the mth complex exponential. In the third block the de-chirped and filtered signal is back transformed to the time domain using inverse DFT (IDFT), and is multiplied by a chirp with a normalized frequency rate equals to the de-chirping frequency rate used in the first block of the mth processor. This processing chain assumes that the de-chirping value is given. Hence, we first perform a pre-processing step where we select the suitable de-chirping value. We next describe the separate step in details.

De-chirping selection

We define a set of L de-chirping normalized frequency rates ($L \gg M$) denoted by $\Omega = \{\theta_{2,1}, \ldots, \theta_{2,L}\}$. For each $\theta_{2,\ell} \in \Omega$, we define a corresponding harmonic de-chirping set, denoted by $\Omega_\ell = \{\theta_{2,\ell}, 2\theta_{2,\ell}, \ldots, M\theta_{2,\ell}\}$ and define the mth de-chirped signal, denoted by $\mathbf{x}_{\ell,m} = [x_{\ell,m}[0], \ldots, x_{\ell,m}[N-1]]^T$, where $m = 1, \ldots, M$ as

$$\mathbf{x}_{\ell,m} = \mathbf{D}(m\theta_{2,\ell})\mathbf{x} \tag{3.38}$$

$$\mathbf{D}(m\theta_{2,\ell}) = \mathrm{diag}(1, \ldots, e^{-j2\pi\frac{1}{2}m\theta_{2,\ell}(N-1)^2}) \tag{3.39}$$

If $\theta_{2,\ell}$ equals the true normalized frequency rate, we get an attenuated complex exponential in the presence of other interfering harmonic components and noise. We thus compute the DFT $x_{\ell,m}[n]$ at the kth frequency bin as $\bar{x}_{\ell,m}[k] = \sum_{n=0}^{N-1} x_{\ell,m}[n]e^{-j\frac{2\pi}{N}kn}$, $k = 0, \ldots, N-1$. By defining the DFT vector $\bar{\mathbf{x}}_{\ell,m} = [\bar{x}_{\ell,m}[0], \ldots, \bar{x}_{\ell,m}[N-1]]^T$ we obtain,

$$\bar{\mathbf{x}}_{\ell,m} = \mathbf{W}\mathbf{x}_{\ell,m} \overset{\text{by (3.38)}}{=} \mathbf{W}\mathbf{D}(m\theta_{2,\ell})\mathbf{x} \tag{3.40}$$

where $\mathbf{W}$ is the $N \times N$ DFT transformation matrix. If the de-chirping set $\Omega_\ell = \{\theta_{2,\ell}, 2\theta_{2,\ell}, \ldots, M\theta_{2,\ell}\}$ equals to the true set of normalized frequency rates of the M harmonic components, given by $\{\theta_{2,0}, 2\theta_{2,0}, \ldots, M\theta_{2,0}\}$, then $\bar{\mathbf{x}}_{\ell,m}$ is the sampled Dirichlet function where the value of the peak of $\bar{\mathbf{x}}_{\ell,m}$, is $N|a_m|$ (neglecting the noise). By summing the values of all peaks together, we obtain a value equals to $N^2 \sum_{m=1}^{M} |a_m|^2$, which is the energy of the harmonic signal. Any other hypothesized normalized frequency rate will result in a smaller value. Hence, we need to define a criterion for selecting the suitable de-chirping value. One possibility is to select the normalized frequency as,

$$\tilde{\theta}_2 = \underset{\theta_{2,\ell} \in \Omega}{\operatorname{argmax}} \sum_{m=1}^{M} |\bar{x}_{\ell,m}[k_m^{(\max)}(\theta_{2,\ell})]| \tag{3.41}$$

where $\bar{x}_{\ell,m}[k_m^{(\max)}(\theta_{2,\ell})]$ is the maximum value of $\bar{\mathbf{x}}_{\ell,m}[k]$, and the location of the maximum is,

$$k_m^{(\max)}(\tilde{\theta}_2) = \underset{k}{\operatorname{argmax}} |\bar{x}_{\ell,m}[k]|. \tag{3.42}$$

Another possibility is to use a Harmogram-like criterion that will exploit the relationship between the expected $\{k_m^{(\max)}(\tilde{\theta}_2)\}$. The normalized frequency is selected as

$$\tilde{\theta}_2 = \underset{\theta_{2,\ell} \in \Omega}{\operatorname{argmax}} \max_{k} \sum_{m=1}^{M} |\bar{x}_{\ell,m}[mk]|. \tag{3.43}$$

Other possible selection criteria can be based on computing the sparsity of $\bar{\mathbf{x}}_{\ell,m}$, e.g., its Kurtosis [81].

As an illustrative example, consider the case of a fundamental LFM where $\theta_1 = 0.1$, $\theta_2 = 10^{-5}$, $N = 1024$. The number of harmonic component is $M = 5$. By de-chirping with each candidate, and then calculating the magnitude of the DFT of each de-chirped signal, we obtain a de-chirping map. An example of the map is presented in Fig. 3.4. The map contains $M = 5$ peaks marked on the figure. The peaks are aligned on a straight line, also marked on the figure. The chirp rate selection in (3.43) can be thought of as summing M equispaced points along a straight line in the map.

Note that this process, as can be seen from the example, is very similar to the approximated MLE cost function maximization. However, there are two key differences. First, the number of candidate chirp rate required is very small relative to the MLE since this is only a coarse estimate. Second, the use of DFT, rather than the DTFT, reduces the complexity due to its efficient implementation, the FFT.

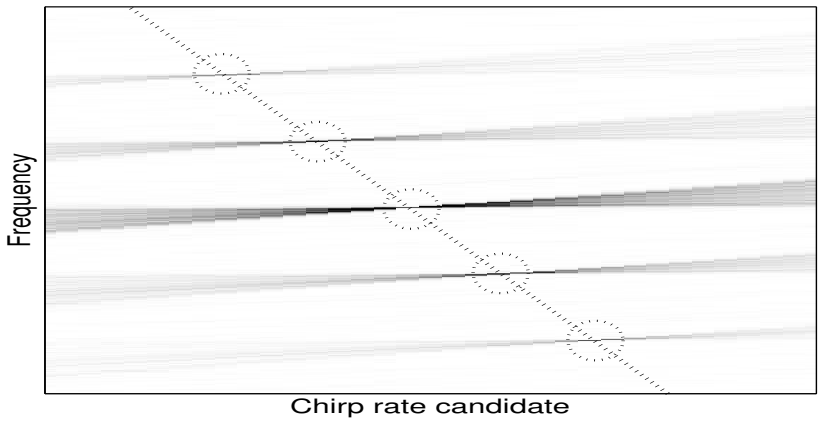

Figure 3.4: De-chriping map of $x[n]$ for $M = 5$. The 5 peaks are marked in circles aligned on the straight marked line.

Moreover, this process is also closely related to the FrFT (See Appendix B). Recall that the FrFT also involves a de-chirping process. Similarly, when the rotation angle of the FrFT is matched to the frequency rate, the result is a delta function. Therefore the optimal rotation order, and thus a coarse estimate of the frequency rate, can be obtained by sweeping through a set of rotation angles and using sparsity measures to select the optimal. This idea was used to create a high resolution time-frequency representation for chirps [82, 83] and for parameter estimation of multi-component LFM signals [34].

In order to compensate the poor resolution obtained by that process we preform LS estimation given the phase of each component. But first, the components must be separated.

Separating the harmonic components

Given $\tilde{\theta}_2$, We filter $\bar{\mathbf{x}}_{\ell,m}$ in the frequency domain with a bandpass filter of length δ (a pre-defined frequency interval that ensures the harmonic components are well separated) expressed by the matrix,

$$\mathbf{Y}_m = \text{diag}\left([\mathbf{0}^T_{k_m^{(\max)}(\tilde{\theta}_2)-\delta/2}, \mathbf{1}^T_\delta, \mathbf{0}^T_{N-k_m^{(\max)}(\tilde{\theta}_2)-\delta/2}]^T\right) \tag{3.44}$$

where $\mathbf{1}_n$ is the $n \times 1$ vector with all elements equal to one.

As mentioned above, when $\tilde{\theta}_2 = \theta_2$, then $\mathbf{x}_{\ell,m}$ is a complex exponential whose DFT, $\bar{\mathbf{x}}_{\ell,m}$, is a Dirichlet function. However, this is not the case in general. The mth component

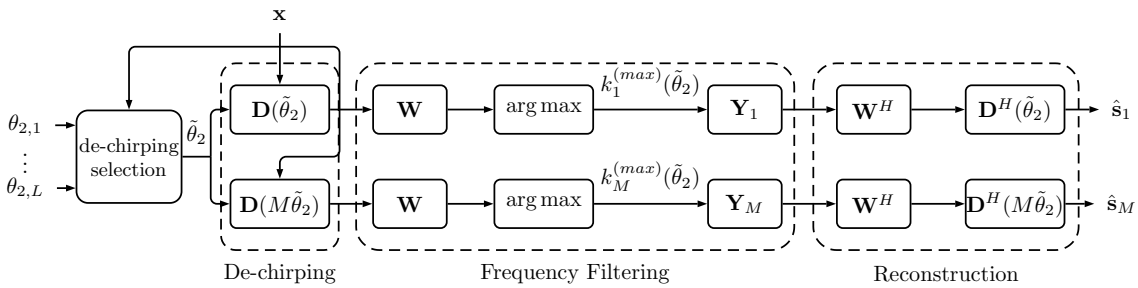

Figure 3.5: Scheme of the separate step.

in $\mathbf{x}_{\ell,m}$ should be an LFM with a very small bandwidth. Assume that the search grid $\{\theta_{2,\ell}\}_{\ell=1}^{L}$ is uniformly spaced such that $d = \theta_{2,\ell+1} - \theta_{2,\ell}$. Then the bandwidth of the LFM should be no more than Nd. Therefore, in order to avoid filtering the desired signal, the length of the filter should satisfy $\delta \geq Nd$. However, increasing the filter length introduces more noise into the filtered signal which can cause poor estimation.

The filtered signal in the frequency domain is,

$$\bar{\hat{\mathbf{s}}}_m = \mathbf{Y}_m \bar{\mathbf{x}}_{\ell,m} \overset{\text{by (3.40)}}{=} \mathbf{Y}_m \mathbf{W} \mathbf{D}_m(m\tilde{\theta}_2)\mathbf{x}. \tag{3.45}$$

Ideally, this process retains an attenuated complex exponential with a frequency equals to the normalized initial frequency of the mth harmonic component. To obtain the original harmonic component of the chirp, we perform an IDFT followed by a chirp multiplication, i.e.,

$$\hat{\mathbf{s}}_m(\boldsymbol{\theta}) = \mathbf{D}(m\tilde{\theta}_2)^H \mathbf{W}^H \bar{\hat{\mathbf{s}}}_m \overset{\text{by (3.45)}}{=} \mathbf{G}_m \mathbf{x} \tag{3.46}$$

where by substituting (3.45) into (3.46) we define

$$\mathbf{G}_m = \mathbf{D}(m\tilde{\theta}_2)^H \mathbf{W}^H \mathbf{Y}_m \mathbf{W} \mathbf{D}(m\tilde{\theta}_2). \tag{3.47}$$

We thus obtain a set of M reconstructed harmonic components, $\{\hat{\mathbf{s}}_1(\boldsymbol{\theta}), \ldots, \hat{\mathbf{s}}_M(\boldsymbol{\theta})\}$, of the observed signal.

Assume that $\{\hat{\mathbf{s}}_m(\boldsymbol{\theta})\}_{m=1}^{M}$ are filtered without interference from other harmonic components. We therefore get that,

$$\hat{s}_m[n;\boldsymbol{\theta}] = |a_m| e^{j\varphi_m} s_m[n;\boldsymbol{\theta}] + e_m[n] = |\hat{s}_m(n)| e^{j\hat{\phi}_m[n]} \tag{3.48}$$

where $|\hat{s}_m(n)|$ and $\hat{\phi}_m[n]$ are the absolute value and phase of $\hat{s}_m[n;\boldsymbol{\theta}]$, respectively, $e_m[n]$ is the nth element of $\mathbf{e}_m = \mathbf{G}_m\mathbf{v}$. Assuming that small errors are present, i.e., $|e_m[n]| \ll |a_m|$, $m = 1, \ldots, M$, it can be shown using a first order Taylor series that the magnitude and phase in (3.48) are approximately,

$$\begin{aligned}
|\hat{s}_m[n]| &= ||a_m|\cos(\phi_m[n] + \varphi_m) + \Re\{e_m[n]\} \\
&\quad + j(|a_m|\sin(\phi_m[n] + \varphi_m) + \Im\{e_m[n]\})| \\
&\cong |a_m| + \Re\{e_m[n]e^{-j\varphi_m}e^{-j\phi_m[n]}\} \qquad (3.49) \\
\hat{\phi}_m[n] &= \tan^{-1}\left(\frac{\sin(\phi_m[n] + \varphi_m) + \Im\{e_m[n]\}}{\cos(\phi_m[n] + \varphi_m) + \Re\{e_m[n]\}}\right) \\
&\cong \phi_m[n] + \varphi_m - \sin(\phi_m[n] + \varphi_m)\Re\{e_m[n]\} \\
&\quad + \cos(\phi_m[n] + \varphi_m)\Im\{e_m[n]\} \\
&\cong \phi_m[n] + \varphi_m + \Im\{e_m[n]e^{-j\varphi_m}e^{-j\phi_m[n]}\} \qquad (3.50)
\end{aligned}$$

We assume the magnitude of the filtered signal $\hat{s}_m[n;\boldsymbol{\theta}]$ is approximately $|a_m|$. The information on the normalized initial frequency and frequency rate is hidden in the wrapped phases $\{\hat{\phi}_m[n]\}_{n=0,m=1}^{N-1,M}$. However, to estimate the normalized initial frequency and frequency rate, we need to consider the unwrapped phase.

3.5.1 Phase Unwrapping

First, we present parameters estimation given the unwrapped phases of $\{\hat{\phi}_m[n]\}_{n=0}^{N-1}$, denoted by $\{\tilde{\phi}_m[n]\}_{n=0}^{N-1}$. In case of LFM signals, the unwrapped phase can be found by integrating the second derivative of the phase of the signal [29] given by

$$\begin{aligned}
\Delta^2\tilde{\phi}_m[n] &= \hat{\phi}_m[n] - 2\hat{\phi}_m[n-1] + \hat{\phi}_m[n-2] \\
&= \arg(\hat{s}_m[n](\hat{s}_m^*[n-1])^2\hat{s}_m[n-2]) \qquad (3.51)
\end{aligned}$$

for $n = 2, \ldots, N$. The motivation is that the second derivative of the phase of an LFM is constant and as such, can be extracted from the signal. By integrating $\Delta^2\tilde{\phi}_m[n]$ we obtain

$$\Delta\tilde{\phi}_m[n] = \Delta^2\tilde{\phi}_m[n] + \Delta\tilde{\phi}_m[n-1] \qquad (3.52)$$

where we define $\Delta\tilde{\phi}_m[1] = \arg(\hat{s}_m[0]\hat{s}_m^*[1])$. And the unwrapped phase is given by

$$\begin{aligned}\tilde{\phi}_m[0] &= \arg(\hat{s}_m[0]) \\ &= \hat{\phi}_m(0) \mod 2\pi \qquad (3.53)\\ \tilde{\phi}_m[n] &= \Delta\tilde{\phi}_m[n] + \tilde{\phi}_m[n-1],\ n = 1, \ldots, N. \qquad (3.54)\end{aligned}$$

We further assume that the noises are small enough such that they do not cause any π jumps in the unwrapping procedure. The unwrapped phase at the end of this step is

$$\tilde{\phi}_m[n] = \hat{\phi}_m[n] \cong \varphi_m + 2\pi m(\theta_1 n + \frac{1}{2}\theta_2 n^2) + \varepsilon_m[n] \qquad (3.55)$$

where we define the error term $\varepsilon_m[n] = \Im\{e_m[n]e^{-j\varphi_m}e^{-j\phi_m[n]}\}$. Define the vector of phase measurements obtained from the mth reconstructed harmonic component, $\hat{\mathbf{s}}_m(\boldsymbol{\theta})$, by $\tilde{\boldsymbol{\phi}}_m \triangleq [\tilde{\phi}_m[0], \ldots, \tilde{\phi}_m[N-1]]^T$. Collecting all the measurements in (3.55) we obtain an approximate linear model for θ_1 and θ_2 given $\tilde{\phi}_m[n]$, i.e.,

$$\tilde{\boldsymbol{\phi}}_m = \varphi_m \mathbf{1}_N + 2\pi m \mathbf{H}\boldsymbol{\theta} + \boldsymbol{\varepsilon}_m\,, m = 1, \ldots, M \qquad (3.56)$$

where $\mathbf{H} = [\mathbf{h}_1, \mathbf{h}_2]$ with $\mathbf{h}_1 = [0, 1, \ldots, N-1]^T$, and $\mathbf{h}_2 = [0^2/2, 1^2/2, \ldots, (N-1)^2/2]^T$.

Also, $\boldsymbol{\varepsilon}_m = [\varepsilon_m[0], \ldots, \varepsilon_m[N-1]]^T = \Im\{e^{-j\varphi_m}\mathbf{s}_m^*(\boldsymbol{\theta}) \odot \mathbf{e}_m\}$ where $\odot$ is the Hadamard (dot) product. The unknown parameters $\{\varphi_m\}_{m=1}^M$ and the unknown vector $\boldsymbol{\theta}$ are estimated using an LS method as follows,

$$[\{\hat{\varphi}_m\}_{m=1}^M, \hat{\boldsymbol{\theta}}^T]^T = \underset{\{\varphi_m\}_{m=1}^M, \boldsymbol{\theta}}{\operatorname{argmin}} \sum_{m=1}^{M} \|\tilde{\boldsymbol{\phi}}_m - \varphi_m \mathbf{1}_N - 2\pi m \mathbf{H}\boldsymbol{\theta}\|^2 \qquad (3.57)$$

Taking the derivative of (3.57) w.r.t. φ_m and equating the result to zero yields that $\hat{\varphi}_m = (\mathbf{1}_N^T\mathbf{1}_N)^{-1}\mathbf{1}_N^T(\tilde{\boldsymbol{\phi}}_m - 2\pi m\mathbf{H}\hat{\boldsymbol{\theta}})$. Substituting $\hat{\varphi}_m$ into (3.57), taking the derivative w.r.t. $\boldsymbol{\theta}$ and equating the result to zero yields that the estimate of $\boldsymbol{\theta}$ is,

$$\hat{\boldsymbol{\theta}} = (\mathbf{H}^T\mathbf{P}_1^\perp\mathbf{H})^{-1}\mathbf{H}^T\mathbf{P}_1^\perp\boldsymbol{\Psi} \qquad (3.58)$$

where $\mathbf{P}_1^\perp = \mathbf{I}_N - \mathbf{1}_N(\mathbf{1}_N^T\mathbf{1}_N)^{-1}\mathbf{1}_N^T$, $\boldsymbol{\Psi} = [\Psi[0], \ldots, \Psi[N-1]]^T = \frac{1}{2\pi C_M}\sum_{m=1}^M m\tilde{\boldsymbol{\phi}}_m$.

3.5.2 Joint Phase Unwrapping and Least Squares

The phase unwrapping process as described above assumes that the unwrapped phase does not change by more then π between two consecutive samples. That is, we assume that $|\Delta\tilde{\phi}_m[n]| < \pi$. If $|\Delta\tilde{\phi}_m[n]|$ is close to π, the processes becomes very sensitive to noise [41].

To overcome that problem, a joint phase unwrapping and parameters estimation method was proposed in [41] using a recursive processing. This eliminates the need to perform phase unwrapping prior to the estimation process. Rather, the unwrapping is performed sample at a time given the current estimation of the parameters yielding a more robust process.

Let $\hat{\boldsymbol{\eta}}[n] = [\hat{\boldsymbol{\varphi}}^T[n],\ \hat{\boldsymbol{\theta}}^T[n]]^T$, where $\hat{\boldsymbol{\varphi}}[n] = [\hat{\varphi}_1[n], \ldots, \hat{\varphi}_M[n]]^T$, be the estimated parameters at the nth step of the filter. Then, the unwrapped phase is given by

$$\hat{\boldsymbol{\phi}}[n] = \mathbf{H}[n]\hat{\boldsymbol{\eta}}[n] + \boldsymbol{\varepsilon}[n] \tag{3.59}$$

where

$$\mathbf{H}[n] = \begin{bmatrix} & 2\pi n & \pi n^2 \\ \mathbf{I}_M & \vdots & \vdots \\ & 2\pi M n & \pi M n^2 \end{bmatrix} \tag{3.60}$$

$\hat{\boldsymbol{\phi}}[n] = [\hat{\phi}_1[n], \ldots, \hat{\phi}_M[n]]^T$ and $\boldsymbol{\varepsilon}[n] = [\varepsilon_1[n], \ldots, \varepsilon_M[n]]^T$. The phase error of the mth harmonic component is defined as $\boldsymbol{\varepsilon}_m = \Im\{e^{-j\varphi_m}\mathrm{diag}(\mathbf{s}_m^*(\boldsymbol{\theta}))\mathbf{e}_m\}$.

The algorithm is initialized with an estimate given $L \geq M+2$ samples of the unwrapped phased using a conventional unwrapping algorithm, as suggested above,

$$\hat{\boldsymbol{\eta}}[L] = \left(\mathbf{H}_L^T\mathbf{H}_L\right)^{-1}\mathbf{H}_L^T\hat{\boldsymbol{\phi}}_L \tag{3.61}$$

where $\mathbf{H}_L = [\mathbf{H}^T[0], \ldots, \mathbf{H}^T[L-1]]^T$ and $\hat{\boldsymbol{\phi}}_L = [\hat{\boldsymbol{\phi}}^T[0], \ldots, \hat{\boldsymbol{\phi}}^T[L-1]]^T$. Following the initialization process, the algorithm iterates through three steps for $n = L+1, \ldots, N-1$.

1. **Predict:** $\hat{\boldsymbol{\phi}}[n+1|n] = \mathbf{H}[n+1]\hat{\boldsymbol{\eta}}[n]$
2. **Unwrap:** $\hat{\phi}_m[n+1] = \arg\left(\hat{s}_m[n+1]e^{-j\hat{\phi}_m[n+1|n]}\right) + \hat{\phi}_m[n+1|n]$
3. **Update:** $\hat{\boldsymbol{\eta}}[n+1] = \hat{\boldsymbol{\eta}}[n] + \mathrm{K}_{n+1}\left(\tilde{\boldsymbol{\phi}}[n+1] - \mathbf{H}[n+1]\hat{\boldsymbol{\eta}}[n]\right)$ where $\mathrm{K}_{n+1} = \left(\mathbf{H}_{n+1}^T\mathbf{H}_{n+1}\right)^{-1}\mathbf{H}^T[n+1]$. Note that K_{n+1} is not data dependent and can be computed off-line.

The estimated parameters are obtained from the final step, $\hat{\boldsymbol{\theta}}^{(\text{SEES})} = \boldsymbol{\theta}[N-1]$. The recursive processing used for the parameters estimation is equivalent to a batch LS estimation given the unwrapped phase [84]. That is,

$$\hat{\boldsymbol{\eta}} \triangleq \hat{\boldsymbol{\eta}}[N-1] = \left(\mathbf{H}^T\mathbf{H}\right)^{-1}\mathbf{H}^T\hat{\boldsymbol{\phi}} \tag{3.62}$$

where $\mathbf{H} \triangleq \mathbf{H}_{N-1}$ and $\hat{\boldsymbol{\phi}} \triangleq \hat{\boldsymbol{\phi}}_{N-1}$.

Again, once $\hat{\boldsymbol{\theta}}^{(\text{SEES})}$ is estimated, the number of harmonics can be selected by substituting the estimate into (3.6) instead of the $\hat{\boldsymbol{\theta}}^{(\text{MLE})}$ for each possible value of M.

3.5.3 Accuracy Analysis

We evaluate the bias and covariance of the estimate $\hat{\boldsymbol{\eta}}$ given in (3.62) when it is estimated in the presence of noise. Since both estimation method are equivalent, the analysis should hold to the estimate in (3.58). Substituting (3.56) into (3.62) yields that the estimate of $\boldsymbol{\eta}$ is given by

$$\hat{\boldsymbol{\eta}} = \boldsymbol{\eta} + \left(\mathbf{H}^T\mathbf{H}\right)^{-1}\mathbf{H}^T\boldsymbol{\varepsilon} \tag{3.63}$$

where $\boldsymbol{\varepsilon} = [\boldsymbol{\varepsilon}^T[0], \ldots, \boldsymbol{\varepsilon}^T[N-1]]^T$. Note that $E[\boldsymbol{\varepsilon}_m] = E[\Im\{e^{-j\varphi_m}\mathbf{s}_m^*(\boldsymbol{\theta}) \odot \mathbf{e}_m\}] = \Im\{e^{-j\varphi_m}\mathbf{s}_m^*(\boldsymbol{\theta}) \odot \mathbf{G}_m E[\mathbf{v}]\} = \mathbf{0}_N$, where we substitute $\mathbf{G}_m\mathbf{v}$ instead of $\mathbf{e}_m$. This means that $E[\boldsymbol{\varepsilon}] = \mathbf{0}_{NM}$ and therefore $\hat{\boldsymbol{\eta}}$ is approximately unbiased.

The covariance of $\hat{\boldsymbol{\eta}}$, is given by

$$\begin{aligned}\text{cov}(\hat{\boldsymbol{\eta}}) &= \left(\mathbf{H}^T\mathbf{H}\right)^{-1}\mathbf{H}^T\text{cov}(\tilde{\boldsymbol{\phi}})\mathbf{H}\left(\mathbf{H}^T\mathbf{H}\right)^{-1} \\ &= \left(\mathbf{H}^T\mathbf{H}\right)^{-1}\mathbf{H}^T\text{cov}(\boldsymbol{\varepsilon})\mathbf{H}\left(\mathbf{H}^T\mathbf{H}\right)^{-1}\end{aligned} \tag{3.64}$$

The covariance of the noise, $\text{cov}(\boldsymbol{\varepsilon})$, is a $NM \times NM$ block matrix composed of N^2 blocks of $M \times M$ matrices of the form $\text{cov}(\boldsymbol{\varepsilon}[n]\boldsymbol{\varepsilon}^H[k])$. Using the facts that $E[\Im\{\mathbf{v}\}\Re\{\mathbf{v}\}^T]$ is a zero matrix, while $E[\Re\{\mathbf{v}\}\Re\{\mathbf{v}\}^T] = E[\Im\{\mathbf{v}\}\Im\{\mathbf{v}\}^T] = \sigma_v^2/2\mathbf{I}_N$, it can be shown that

$$E[\boldsymbol{\varepsilon}_m\boldsymbol{\varepsilon}_{m'}] = \frac{\sigma_v^2}{2}\Re\{\text{diag}(\mathbf{s}_m^*(\boldsymbol{\theta}))\mathbf{G}_m\mathbf{G}_{m'}^H\text{diag}((\mathbf{s}_{m'}(\boldsymbol{\theta}))^T)\} \tag{3.65}$$

Substituting (3.65) in (3.64) yields the covariance matrix of $\hat{\boldsymbol{\theta}}$. In the simulation results we show that the asymptotic covariance in (3.64) coincides with the CRLB. However, this covariance result only holds for large N and small noise.

Table 3.1: Comparison of the Four Estimation Methods.
Threshold SNR and Efficiency From Fig. 3.7

Method	Complexity	Threshold SNR	Asymptotic Efficiency
MLE	$\mathcal{O}\left(N^5M\right)$	-10dB	Yes
Harmochirp-gram	$\mathcal{O}\left(N^4M\right)$	-10dB	Yes
PHAF	$\mathcal{O}(N^{5/2}(L+M))$	13dB	No
Harmonic-SEES	$\mathcal{O}\left(N^2\log NM\right)$	5dB	Yes

3.5.4 Computational Load

The first step in the Harmonic-SEES method is to create the vector $\bar{\mathbf{x}}_{\ell,m}$ in (3.40). This is done by multiplying the input with a diagonal matrix $\mathbf{D}$, which requires $2N$ multiplications, and performing DFT (using FFT), which involves $\mathcal{O}\left(N\log N\right)$ multiplications. This is done M times for each possible value. The total number of real multiplications required for the de-chirping selection is $\mathcal{O}\left(N\log N \cdot LM\right)$. Since the de-chirping process and the DFT block in the frequency filtering part is already performed in the de-chirping selection, no more multiplications are required. Next, the vectors $\bar{\hat{\mathbf{s}}}_m$ are created in (3.45) by multiplying each harmonic component with a diagonal matrix $\mathbf{Y}_m$, which requires $2N$ multiplications. The reconstruction of each harmonic component is $\mathcal{O}\left(N\log N\right)$ multiplications, similarly to the de-chirping selection. Therefore, the complexity of the separate step in total is $\mathcal{O}\left(N\log N \cdot (L+M)M\right)$. Finally, the estimation of both parameters is done by the recursive process. Since the gain is not data dependent, it can be computed off-line. Therefore each iteration requires $\mathcal{O}\left(M^2\right)$ multiplications. since there are N iterations, the total complexity of the estimation process is $\mathcal{O}\left(NM^2\right)$. Combining both steps and assuming $L \gg M$ results in a total of $\mathcal{O}\left(N\log N \cdot LM\right)$ multiplications. The de-chirping selection is only a rough estimate of θ_2, therefore there is no need to search with resolution that corresponds to the CRLB and L can be in the order of N. In that case, the total number of real multiplications for the Harmonic-SEES method is therefore $\mathcal{O}\left(N^2\log NM\right)$ which is substantially less than that of the Harmochirp-gram. A comparison between computational complexity of each method is presented in Table 3.1.

The low computational complexity of the proposed algorithm makes it more suitable for real-time applications. Furthermore, due to the recursive implementation of the estimation step, the estimated parameters can be updated on-line.

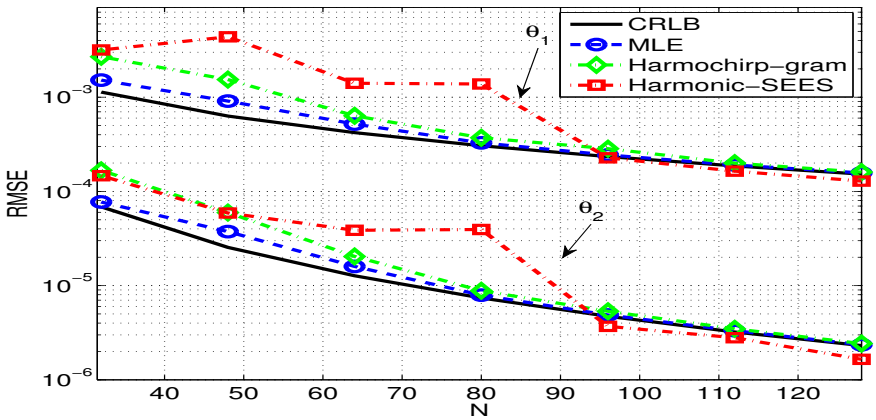

Figure 3.6: RMSE for the exact MLE, approximated MLE and Harmonic-SEES estimator including the CRLB vs. the number of samples.

3.6 Numerical Results

We present numerical examples that compare the performance of the MLE, Harmochirp-gram, PHAF and the proposed Harmonic-SEES methods. We start with synthetic simulations and then present real data results.

3.6.1 Simulations

In each simulation we consider $M = 3$ harmonics. The amplitudes of the harmonic components are given as $a_m = 2^{1-m}e^{j\varphi_m}, m = 1, \ldots, M$, where φ_m is a uniformly distributed phase. The noise power σ_v^2 is adjusted to give the desired SNR defined as $\text{SNR} = 10\log_{10}\left(\sum_{m=1}^{M}|a_m|^2/\sigma_v^2\right)$ [dB]. In each simulation we evaluated the root mean square error (RMSE) defined as $\text{RMSE}(\theta_k) = \sqrt{\frac{1}{Nexp}\sum_{i=1}^{N_{exp}}(\hat{\theta}_{k,i} - \theta_k)^2}$, $k = 1, 2$ where $\hat{\theta}_{1,i}$ and $\hat{\theta}_{2,i}$ are the estimate of θ_1 and θ_2 at the ith trial, respectively and $N_{exp} = 500$ is the number of Monte-Carlo independent trials. The phases of the amplitudes are generated once for all trials. For comparison, in each simulation we compared the results with the associated CRLB. First, we wish to examine the orthogonality assumption, presented in Section 3.3.2. The parameters of the fundamental chirp are given by $\theta_1 = 0.05$ and $\theta_2 = 10^{-4}$ and the SNR is set to 15dB. The requirement of the number of samples in (3.14) in this case is $N \geq 3/\delta = 3/\theta_1 = 60$. The filter's width for the harmonic components separation was 6 samples. We examine the performance of the exact and approximated MLE for number of samples ranging from $N = 16$ up to $N = 128$. The RMSE for both

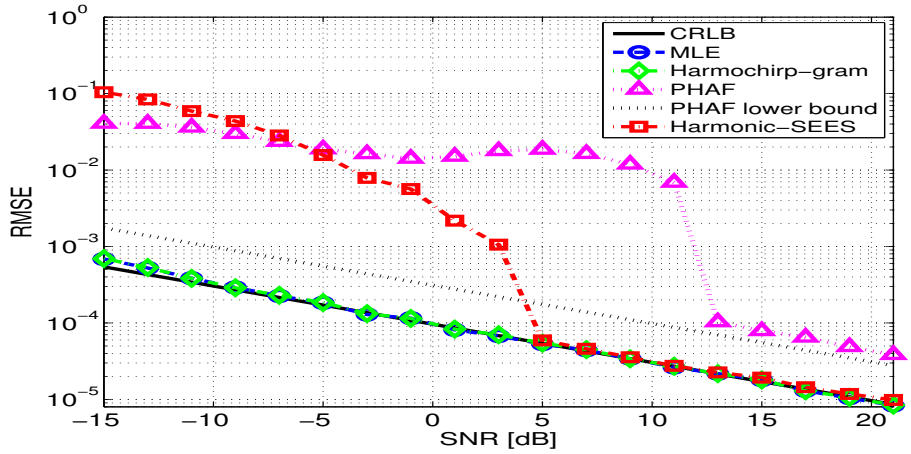

(a) θ_1, Normalized initial frequency

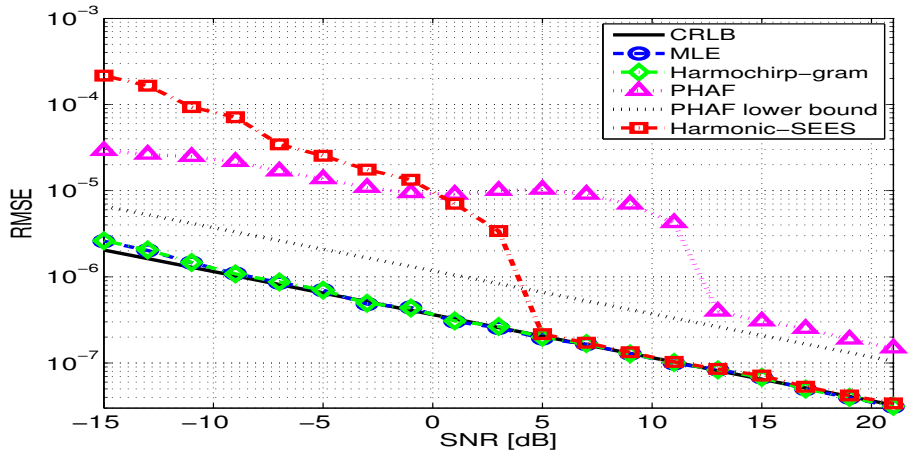

(b) θ_2, Normalized frequency rate

Figure 3.7: RMSE for each estimator including the CRLB vs. SNR.

parameters versus the number of samples is presented in Fig 3.6. It can be seen that when the number of samples satisfies (3.14), the Harmochirp-gram performs similarly to the MLE. The Harmonic-SEES method requires more samples and performs well in this case for $N \geq 96$. This is because for smaller number of samples the harmonic components are not well separated and cannot be properly filtered. The peaks of the PHAF becomes wider as the number of samples decreases. For the specified number of samples the peaks were not separable and the PHAF method was unable to detect the three components. Therefore the results are not presented for this case. Next, we compare the RMSE of the estimated normalized initial frequency and frequency rate versus the SNR for the MLE, Harmochirp-gram, PHAF and Harmonic-SEES methods. The parameters of the fundamental chirp are given by $\theta_1 = 0.1$ and $\theta_2 = 10^{-4}$. The number of samples is $N = 512$, far more than the requirement in (3.14). For the PHAF method, $L = 4$ lags are used with

$\boldsymbol{\tau} = [50, 100, 150, 200]$ samples. We consider SNR values from -15[dB] to 21[dB] in steps of 2[dB]. Those settings are used in the simulations hereafter unless otherwise stated. The RMSE results are presented in Fig 3.7. The CRLB and the theoretical lower bound of the PHAF method, according to (3.36), are also plotted for both parameters. The MLE and Harmochirp-gram perform similarly and achieve the CRLB for both parameters. For SNR above 5[dB] the Harmonic-SEES method also achieves the CRLB. The PHAF estimator does not reach its lower bound. This is expected as it is not a tight bound. The error seems to converge to around 1.5 times the lower bound for SNR of 13[dB] or more.

Fig 3.8 present the scattering of the estimate errors, i.e., $\varepsilon_1 = \hat{\theta}_1 - \theta_1$, $\varepsilon_2 = \hat{\theta}_2 - \theta_2$, of the MLE and Harmonic-SEES methods along with a theoretical and actual 50% confidence level ellipses for SNR values of -1[dB] and 7[dB]. For the lower SNR value, the Harmonic-SEES method does not achieve the CRLB and thus the actual confidence level ellipse is larger than the theoretical one. For the higher SNR the ellipse of the Harmonic-SEES coincides with that of the CRLB.

We now compare the performance of the model order selection using the MDL and AIC criteria for the MLE, PHAF and Harmonic-SEES methods. We evaluate the probability of detecting the correct model order, p_d defined as $p_d = \frac{1}{Nexp}\sum_{i=1}^{N_{exp}} \mathbb{1}_{\hat{M}=M}$ where $\mathbb{1}$ is the indicator function. The p_d versus SNR results are presented in Fig. 3.9. For both MDL and AIC criteria, the model order estimator that uses the Harmonic-SEES always estimates correctly for SNR values of 5[dB] or more. Not surprisingly, this is the threshold SNR for which the CRLB is achieved. The AIC performs slightly better then the MLE for both MLE and the Harmonic-SEES estimator. The PHAF method achieves perfect selection at around 11[dB] with both criteria perform equally.

Finally, we evaluate the sensitivity of the Harmonic-SEES method and the MLE to vibrations in the frequency. The mth harmonic component is simulated with an instantaneous frequency given by $f_m[n] = m(\theta_1(1 + \delta_f \cdot \sin(2\pi f_v n)) + \theta_2 n)$. The SNR is fixed to 10[dB] and we examine different values of both parameters, δ_f and f_v. The RMSE versus δ_f is presented in Fig. 3.10 for both estimated parameters, where each plot shows the error for different values of f_v. The PHAF performed poorly in this case and the results are not presented. Clearly, the estimator is very sensitive to changes in the assumed frequency model. The performance of the estimator is better for higher values of f_v. For the highest value of f_v, the proposed method performs similarly to the MLE for $\delta_f \leq 0.3$, which is 30% from the initial frequency.

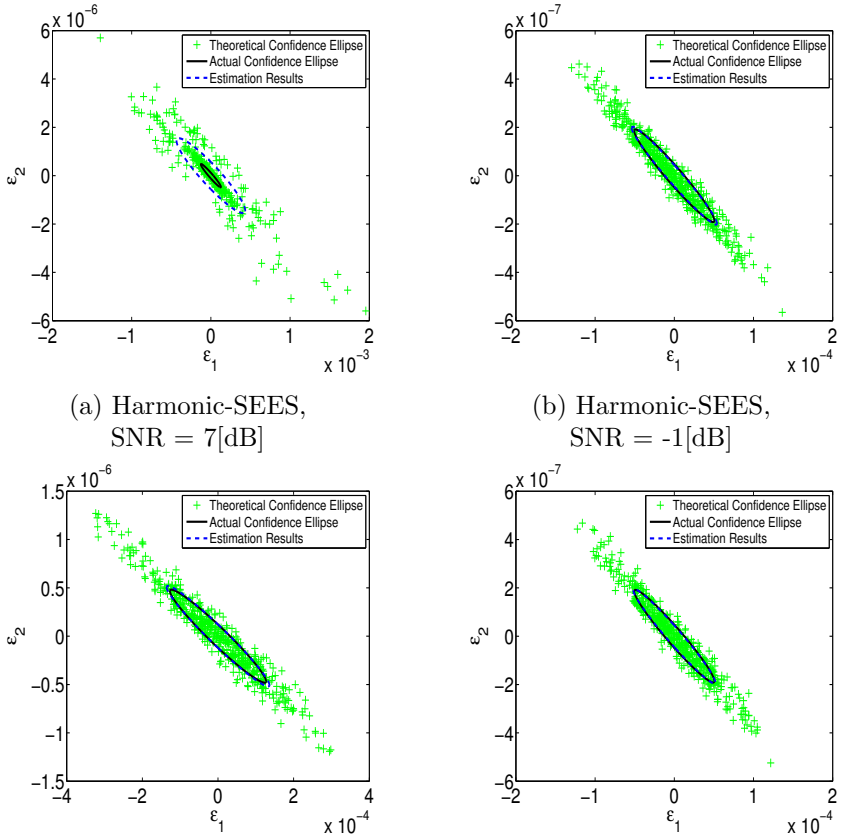

(a) Harmonic-SEES, SNR = 7[dB]

(b) Harmonic-SEES, SNR = -1[dB]

(c) MLE, SNR = 7[dB]

(d) MLE, SNR = -1[dB]

Figure 3.8: The estimates and confidence ellipses of the fundamental frequency and frequency rate for SNR=7[dB] (a,c) and for SNR=-1[dB] (b,d).

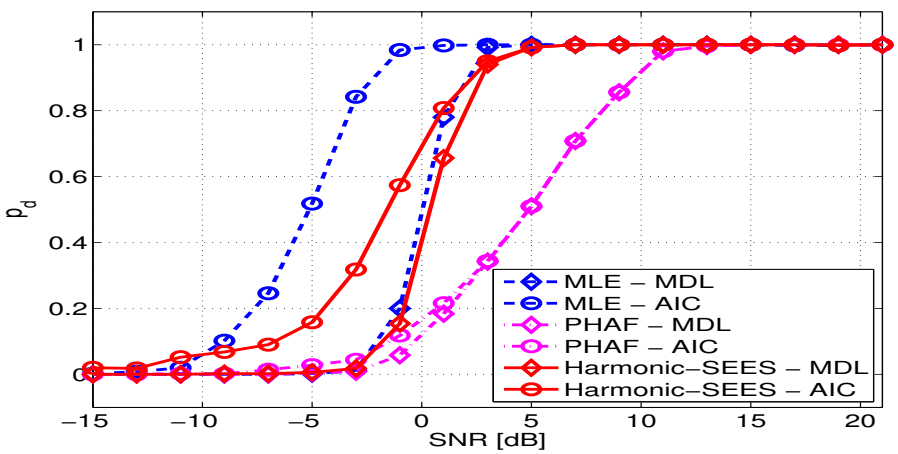

Figure 3.9: Probability of correct model order selection for each estimator.

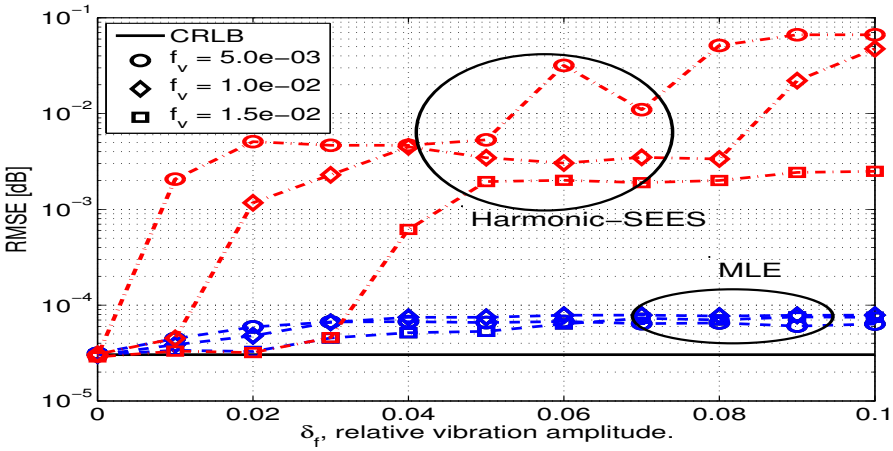

(a) θ_1, Normalized initial frequency

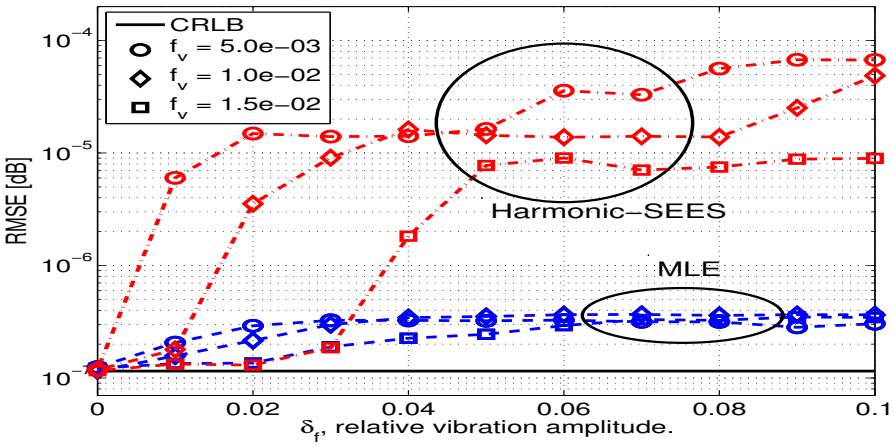

(b) θ_2, Normalized frequency rate

Figure 3.10: RMSE of the Harmonic-SEES estimator and the MLE versus vibrations in the instantaneous frequency.

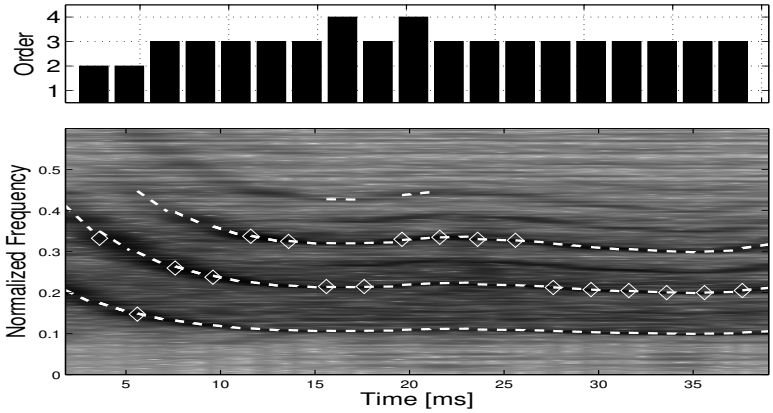

Figure 3.11: Model order selection and parameter estimation of an echolocation call produced by an *E. Nilssonii* bat. The diamonds mark peaks detection in the spectrogram.

3.6.2 Real Data

We demonstrate the model order selection and the parameter estimation of a recording of an echolocation call produced by an *E. nilssonii* bat [75]. The signal is about 40ms long and is sampled at $F_s = 250$kHz. It is divided into segments of $N = 300$ samples. In each segment, the parameter and model order were estimated using the AIC criterion. A spectrogram of the signal is presented in Fig. 3.11. The signal seems to have four harmonic components but the last one is very weak and is hardly detected. The estimated frequencies are plotted in dashes line on top of the spectrogram and the selected model order, using the AIC criterion, is plotted above. The results for the MDL were very similar and thus not presented. The markers on the spectrogram corresponds to a peak detection at each time frame. Clearly, the fundamental chirp is less dominant, yet it is detected the entire time.

Next, we demonstrate the model order selection and the parameter estimation of a recording of an echolocation call produced by a *G. melas* whale [76]. The signal is about 600ms long and is sampled to $F_s = 44.1$kHz. Again, the signal is divided into segments of $N = 300$ samples and the results are presented in Fig. 3.12 in the same format as the previous example. Once again, the AIC and MDL performed similarly and the latter is not presented. The fundamental frequency line is always detected. The higher harmonics, starting from the 5th, are very weak and not detected most of the time. The first part of the signal contains an interference which is not detected. The interference is relatively

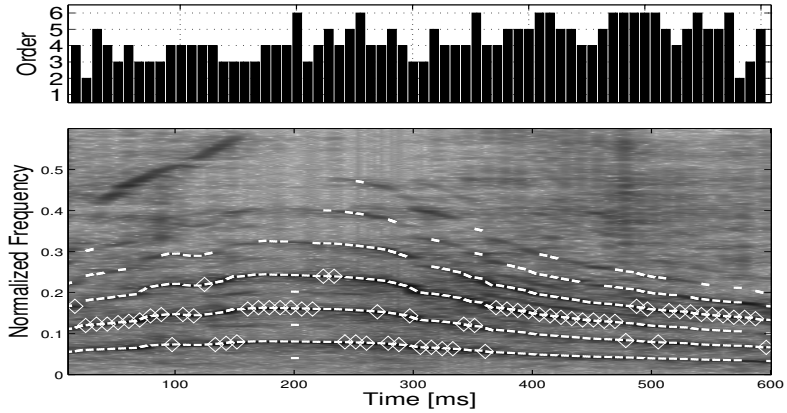

Figure 3.12: Model order selection and parameter estimation of an echolocation call produced by a *G. melas* whale. The diamonds mark peaks detection in the spectrogram.

strong, comparing to each harmonic component, but not strong enough when combining all the harmonic components together.

3.7 Conclusion

We considered the problem of estimating the parameters of harmonic linear chirps with constant amplitudes when the number of harmonic components is unknown. We started by presenting a model order selection criteria based on maximum likelihood, in order to estimate the number of harmonics. The exact and approximated MLE have large computation load due to a two-dimensional exhaustive search in the parameter space. We suggested a two-step estimation method, the Harmonic-SEES, that first separates the signal to its harmonic components, and then estimates the two parameters of interest using a joint least squares method given the phases of the harmonic components. The computational complexity of the proposed estimator is much smaller than that of the maximum likelihood estimators. We also presented the PHAF method and compared it to the proposed method. Simulations show that the proposed two-step estimator achieves the CRLB at moderate or high signal to noise ratio and that the suboptimal estimators can be used instead of the MLE in order to estimate the number of harmonics.

Chapter 4

Random Amplitude Model

4.1 Introduction

We now consider the case of harmonic LFM with time-varying amplitudes. We start by presenting the NLSEfor mono-component LFM with random amplitude in Section 4.2, and explain in Section 4.3 the difficulty in applying the same idea of nonlinear optimization to multi-component or harmonic LFM signals. In Section 4.4 we develop the IHNLSE, which is based on the NLSE and involves large number of computations as it requires high resolution search in the initial frequency and frequency rate parameter space. As an alternative, in Section 4.5 we suggest two sub-optimal low-complexity estimators. The first is based on the HAF, which reduces the problem to a one-dimensional search. The second method applies the Harmonic-SEES method, which was used for constant amplitude harmonic chirps. We present modifications of both methods for harmonic chirps with random amplitudes. We also provide a framework for estimating the number of harmonic components. Finally in Section 4.6 we present some numerical examples. Simulations show that the proposed IHNLSE achieves its asymptotic accuracy in medium to high SNR and while both low-complexity estimators perform well in high SNR. Real data examples demonstrate the performance of the Harmonic-SEES on random amplitude real-life signals.

4.2 Mono-Component NLSE

We present the NLSE of the parameters of harmonic linear chirp with random amplitudes. We start by presenting the estimator for a mono-component LFM with a random amplitude [58]. Next, we show that the maximization involved in the mono-component case cannot

be solved for a multi-component signal and provide a motivation for the iterative approach presented in the next section.

To start, consider a single LFM with a constant amplitude

$$x[n] = as[n;\boldsymbol{\theta}] + v[n] \tag{4.1}$$

where $s[n;\boldsymbol{\theta}] = e^{j2\pi(\theta_1 n + \frac{1}{2}\theta_2 n^2)}$ and a is a complex constant amplitude. The MLE of $\boldsymbol{\theta}$ is given by

$$\begin{aligned} \hat{\boldsymbol{\theta}} &= \arg\max_{\boldsymbol{\theta}} \frac{1}{N} \left| \sum_{n=0}^{N-1} x[n] e^{-j2\pi(\theta_1 n + \frac{1}{2}\theta_2 n^2)} \right|^2 \\ &\triangleq \arg\max_{\boldsymbol{\theta}} Q(x, \boldsymbol{\theta}). \end{aligned} \tag{4.2}$$

We see that the MLE is based on considering the maximum of the squared absolute of a matched filtering process where the signal $x[n]$ is matched to a complex conjugate chirp with the same model as the original chirp signal. An intuitive explanation of this estimator can be given be examining the values of $Q(x, \boldsymbol{\theta})$ at its maximum, the point where $\hat{\boldsymbol{\theta}}$ equals the true parameters of the signal, $\boldsymbol{\theta}$. In the absence of noise we get, by substituting (1.1) with $M = 1$ into (4.2), that

$$Q(x, \boldsymbol{\theta}) = \frac{1}{N} \left| \sum_{n=0}^{N-1} a \right|^2 = Na^2 \tag{4.3}$$

which is the entire energy of the signal.

We now generalize the previous case and consider a single chirp with random amplitude. The chirp parameters, $\boldsymbol{\theta}$, and amplitude, $a[n]$, can be estimated using NLS approach by minimizing the following criterion [58]

$$\hat{\boldsymbol{\theta}}, \hat{a}[n] = \arg\min_{\boldsymbol{\theta}, a[n]} \left| \sum_{n=0}^{N-1} x[n] - a[n] e^{-j2\pi(\theta_1 n + \frac{1}{2}\theta_2 n^2)} \right|^2 . \tag{4.4}$$

By taking the derivatives w.r.t. $a[n]$ and $\boldsymbol{\theta}$,and equating to zero, the NLSE for the chirp

parameters is [58, Appendix A]

$$\begin{aligned}\hat{\boldsymbol{\theta}} &= \arg\max_{\boldsymbol{\theta}} \frac{1}{N}\left|\sum_{n=0}^{N-1} x^2[n]e^{-j2\pi\cdot 2(\theta_1 n+\frac{1}{2}\theta_2 n^2)}\right| \\ &\triangleq \arg\max_{\boldsymbol{\theta}} \frac{1}{N}L(x,\boldsymbol{\theta}). \end{aligned} \tag{4.5}$$

From (4.5) it is clear that the NLSE for $\boldsymbol{\theta}$ has a similar structure as the MLE in (4.2) with two modifications: (1) the values of the chirp parameters are twice that of the original chirp, (2) the chirp is matched to $x^2[n]$ instead of $x[n]$ as with the MLE. The value of the NLSE at its maximum ignoring noise is given by

$$L(x,\boldsymbol{\theta}) = \left|\sum_{n=0}^{N-1} a^2[n]\right| = E_s \tag{4.6}$$

where E_s is the energy of the signal. When the amplitude is a random process, the squaring of the signal in the NLSE results in the energy of the signal just as in the MLE. That is, the NLSE extends the idea of the MLE to signals with random amplitude.

4.3 Harmonic Components NLSE

We now consider the case of harmonic chirp. We start by assuming that the number of harmonic components, M, is known. Similar to the estimator in (4.4), we define the NLS criterion, using (1.1), as

$$\begin{aligned}&\hat{\boldsymbol{\theta}}, \{\hat{a}_m[n]\}_{m=1}^M = \\ &\arg\min_{\boldsymbol{\theta},\{a_m[n]\}_{m=1}^M} \left|\sum_{n=0}^{N-1}\left(x[n] - \sum_{m=1}^{M} a_m[n]s_m[n;\boldsymbol{\theta}]\right)\right|^2. \end{aligned} \tag{4.7}$$

Attempting to take the derivatives w.r.t. $a_m[n]$ for each n and m and equate the results to zero yields a set of N equations with $M \cdot N$ unknowns, which is an under-determined problem. For a single component LFM, on the other hand, taking the derivatives of (4.4) w.r.t. $a[n]$ yields a set of N equations with N unknowns, which guaranties a solution to (4.4). Note that if we were to assume a specific model of the amplitudes, with a parameters vector λ, then (4.7) can be optimized w.r.t. λ [58].

We therefore wish to adapt the main idea of the NLSE solution for mono-component chirp, which is based on squaring the signal before the estimation process, in order to

sum its entire energy. For that purpose, we first explore the form of $x^2[n]$ in the multi-component case,

$$\begin{aligned} x^2[n] &= \sum_{k,p=1}^{M} a_k[n]a_p[n]s_k[n;\boldsymbol{\theta}]s_p[n;\boldsymbol{\theta}] \\ &\quad +2\sum_{m=1}^{M} a_m[n]s_m[n;\boldsymbol{\theta}]v[n] + v^2[n] \\ &= \sum_{m=2}^{2M} \tilde{a}_m[n]s_m[n;\boldsymbol{\theta}] \\ &\quad +2\sum_{m=1}^{M} a_m[n]s_m[n;\boldsymbol{\theta}]v[n] + v^2[n] \end{aligned} \tag{4.8}$$

where

$$\tilde{a}_m[n] = \sum_{k,p=1}^{M} a_k[n]a_p[n]\mathbb{1}_{k+p=m},\ m = 2,3,\ldots,2M \tag{4.9}$$

and $\mathbb{1}$ is the indicator function, that equals 1 if $k+p=m$ and 0 otherwise. Since the noise is a zero mean random process and it is uncorrelated with the amplitudes, the product between the harmonic components and the noise is regarded as additional noise rather than a harmonic signal that can be used in the estimation process. We can therefore define

$$x^2[n] = \sum_{m=2}^{2M} \tilde{a}_m[n]s_m[n;\boldsymbol{\theta}] + \tilde{v}[n] \tag{4.10}$$

where $\tilde{v}[n]$ is composed of the squared noise, $v^2[n]$, and all the products in (4.8) between the noise and the harmonic components. Note that in low SNR, by squaring the signal the noise is actually amplified and we can expect degraded performance. It can be seen that $x^2[n]$ is composed of $2M-1$ LFM components where the first component has parameters that are twice that of the original fundamental LFM. That is, $2M-1$ harmonic LFM components with the fundamental chirp absent. Clearly, squaring the signal imposes a constraint on the possible range for the parameters. In order to avoid aliasing, we assume that the initial frequency and frequency rate satisfy that $f_{max} < 1$, where $f_{max} = 2M\theta_1$ or $f_{max} = 2M(\theta_2 + N\theta_2)$ for decreasing or increasing chirp, respectively.

Example 1: As an illustrative example, consider the case of a fundamental LFM where $\theta_1 = 0.1$, $\theta_2 = 10^{-5}$, $N = 1024$. The number of harmonic components is $M = 3$ and the amplitudes are generated as an independent Gaussian processes with mean 1 and variance 0.25 each. The NLSE cost function defined in (4.5), $L(x,\boldsymbol{\theta})$, is presented in Fig. 4.1(a).

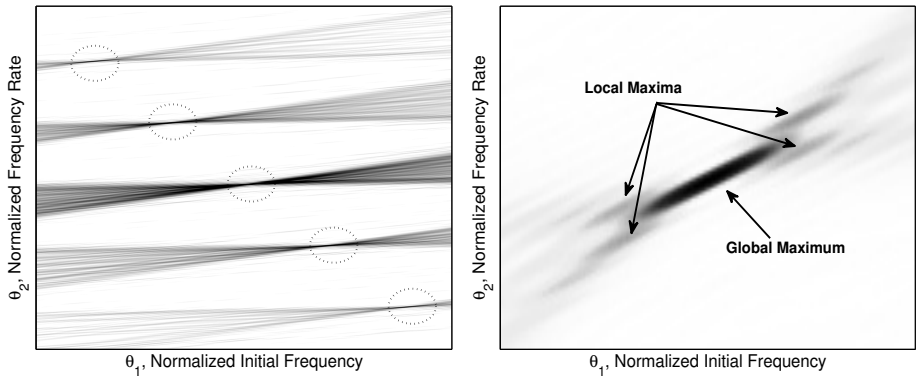

(a) (b)

Figure 4.1: The NLSE cost function, $L(x, \boldsymbol{\theta})$. (a) The entire range of possible parameters, (b) Enlarged area around the strongest peak.

There are five peaks, marked in circles, corresponding to the five harmonic components in $x^2[n]$. The peaks are well separated. In a close region around each peak, $L(x, \boldsymbol{\theta})$ is similar to that of a single component signal. Surrounding each peak there are a few minor peaks. Figure 4.1(b) shows a small area around the strongest peak, surrounding the local maxima. These peaks can be higher than those belong to the other components, as is the case with the strong peak in the middle. Due to the presence of these minor peaks, it is impossible to estimate the parameters by simply locating the $2M - 1$ highest peaks in $L(x, \boldsymbol{\theta})$. A possible estimation approach is suggested in the next section.

4.4 Iterative NLSE for Harmonic Chirps

We suggest an iterative approach based on the NLSE for a single component chirp, which we term for simplicity as the IHNLSE. We start by presenting an estimator and derive its asymptotic bias and variance under the assuming that the number of components is known. Next, we show how peakedness measures of the spectrum of the signal can be used to estimate the number of components when it is unknown.

4.4.1 Known Model Order

Recall that $L(x, \boldsymbol{\theta})$ has $2M - 1$ peaks corresponding to the harmonic components in $x^2[n]$. At each iteration, the global maximum of $L(x, \boldsymbol{\theta})$ is located. Then, the component corresponding to the peak found is filtered from the signal using a de-modulation and filtering scheme proposed in [85]. Note that standard band-pass linear filtering cannot be applied

since the harmonic components may overlap in frequency.

More specifically, we use $x_1[n] = x^2[n]$ and estimate its strongest component using (4.5). The estimated parameters are denoted by $\hat{\boldsymbol{\theta}}^{(1)} = [\theta_1^{(1)}, \theta_2^{(1)}]$. Next, we wish to filter the components whose parameters were found from the signal, so that in the next iteration, $L(x, \boldsymbol{\theta})$ will not have a global maximum at $\hat{\boldsymbol{\theta}}^{(1)}$. The random amplitude is not estimated, therefore we cannot reconstruct the component and subtract it from the signal. The estimated parameters, $\hat{\boldsymbol{\theta}}^{(1)}$, are used to construct the normalized chirp

$$s[n; 2\hat{\boldsymbol{\theta}}^{(1)}] = e^{j2\pi \cdot 2(\theta_1^{(1)} n + \frac{1}{2}\theta_2^{(1)} n^2)}. \tag{4.11}$$

In order to filter the estimated component, the signal is modulated by $s^*[n; 2\hat{\boldsymbol{\theta}}^{(1)}]$, filtered with a high-pass filter designed to remove frequencies around zero and then modulated back by $s[n; 2\hat{\boldsymbol{\theta}}^{(1)}]$. The resulted signal is given by

$$x_2[n] = ((x_1[n] s^*[n; 2\hat{\boldsymbol{\theta}}^{(1)}]) * h[n]) s[n; 2\hat{\boldsymbol{\theta}}^{(1)}] \tag{4.12}$$

where $h[n]$ is the high-pass filter and $*$ denotes convolution. Note that the random amplitudes are not subtracted from the signal, only their chirp modulation. The resulted signal can be approximated as

$$x_2[n] \approx \sum_{m \neq p} \tilde{a}_m[n] s_m[n; \boldsymbol{\theta}] + \bar{a}_p[n] + \tilde{v}[n] \tag{4.13}$$

where

$$\bar{a}_p[n] = ((\tilde{a}_p[n] s^*[n; 2\hat{\boldsymbol{\theta}}^{(1)}]) * h[n]) s[n; 2\hat{\boldsymbol{\theta}}^{(1)}] \tag{4.14}$$

for some $p \in \{2, \ldots, 2M\}$. We assume that filtering any signal, $y[n]$, with $h[n]$ yields $y[n] * h[n] \approx y[n] - 1/N \sum_{n=0}^{N-1} y[n]$. Therefore

$$\bar{a}_p[n] \approx \tilde{a}_p[n] - \mu_{\tilde{a}_p} \tag{4.15}$$

where $\mu_{\tilde{a}_p} = E\{\tilde{a}_p[n]\}$. The process is repeated with $x_2[n]$ to obtain $\hat{\boldsymbol{\theta}}^{(2)}$ and so on, with a total of $2M-1$ times to obtain the set $\hat{\boldsymbol{\theta}}^{(1)}, \ldots, \hat{\boldsymbol{\theta}}^{(2M-1)}$. Since the number of components, M, is assumed to be known, the stopping condition for the iterative process is also known (i.e. after $2M-1$ iterations). If this assumption does not hold then a stopping condition, or model order selection rule, is required. This matter is discussed in detail later.

Each of the $2M-1$ vectors estimated above is a multiple of the parameter vector of the fundamental chirp, $\boldsymbol{\theta}$. Thus, the parameters of interest can be estimated by properly averaging the estimated components. But first we have to associate each vector, $\hat{\boldsymbol{\theta}}^{(m)}$, with the right component, as there is no guaranty that it belongs to the m'th component. In order to do so we sort the set of estimated parameters. We define a mapping, $f(m) : [2, 2M] \rightarrow [1, 2M-1]$, such that $\hat{\theta}_1^{(f(2))} < \hat{\theta}_1^{(f(3))} < \ldots < \hat{\theta}_1^{(f(2M))}$. Then, the parameters can be estimated by solving the following LS problem

$$\hat{\boldsymbol{\theta}} = \arg\min_{\boldsymbol{\theta}} \|\mathbf{A}_M \boldsymbol{\theta} - \boldsymbol{\theta}_M\|^2 \tag{4.16}$$

where

$$\mathbf{A}_M = \begin{bmatrix} \mathbf{g}_M & \mathbf{0}_M \\ \mathbf{0}_M & \mathbf{g}_M \end{bmatrix} \tag{4.17}$$

where $\mathbf{0}_n$ is the $n \times 1$ vector with all elements equal to zero, $\mathbf{g}_M = [2, \ldots, 2M]^T$ and $\boldsymbol{\theta}_M = [\boldsymbol{\theta}_M^{(1)}, \boldsymbol{\theta}_M^{(2)}]^T$. Where $\boldsymbol{\theta}_M^{(k)} = [\hat{\theta}_k^{(f(2))}, \ldots, \hat{\theta}_k^{(f(2M))}]$, for $k = 1, 2$. Solving the above optimization problem yields

$$\hat{\boldsymbol{\theta}} = (\mathbf{A}_M^T \mathbf{A}_M)^{-1} \mathbf{A}_M^T \boldsymbol{\theta}_M = \frac{1}{C_M} \sum_{m=2}^{2M} m \hat{\boldsymbol{\theta}}^{(f(m))} \tag{4.18}$$

where $C_M = \sum_{m=2}^{2M} m^2 = \frac{1}{6}(M+1)M(2M+1)$. The complete process is summarized in Algorithm 1.

Algorithm 1 Iterative Harmonic-NLSE (IHNLSE)

Input:
$x[n]$ - Input signal
M - Model order

Output:
$\hat{\boldsymbol{\theta}}$ - Estimated parameters

$x_1[n] \leftarrow x^2[n]$
for $m \leftarrow 1, \ldots, 2M-1$ **do**
  $\hat{\boldsymbol{\theta}}^{(m)} \leftarrow \arg\max_{\boldsymbol{\theta}} L(x_m, \boldsymbol{\theta})$
  $x_{m+1}[n] \leftarrow ((x_m[n] s^*[n; 2\hat{\boldsymbol{\theta}}^{(m)}]) * h[n]) s[n; 2\hat{\boldsymbol{\theta}}^{(m)}]$
end for
$\hat{\boldsymbol{\theta}} \leftarrow (\mathbf{A}_M^T \mathbf{A}_M)^{-1} \mathbf{A}_M^T \boldsymbol{\theta}_M = \frac{1}{C_M} \sum_{m=2}^{2M} m \hat{\boldsymbol{\theta}}^{(f(m))}$

4.4.2 Accuracy Analysis

We evaluate the accuracy of the proposed IHNLSE by examining its bias and variance. At each step the signal of interest can be expressed as

$$x_p^2[n] = \tilde{a}_p[n]s_p[n;\boldsymbol{\theta}] + \tilde{v}_p[n]. \tag{4.19}$$

The noise, $\tilde{v}_p[n]$, is composed of the other harmonics as well as the squared noise. Without loss of generality, we assume that the components are estimated in order, i.e. $f(p) = p$. From (4.8) and (4.13) it can be seen that, when estimating $\hat{\boldsymbol{\theta}}^{(p)}$, $p = 2, \ldots, 2M$, the noise is given by

$$\begin{aligned} \tilde{v}_p[n] &= \sum_{m=2}^{p-1} \bar{a}_m[n] + \sum_{m=p+1}^{2M} \tilde{a}_m[n]s_m[n;\boldsymbol{\theta}] \\ &\quad +2\sum_{m=1}^{M} a_m[n]s_m[n;\boldsymbol{\theta}]v[n] + v^2[n]. \end{aligned} \tag{4.20}$$

We start by deriving the asymptotic bias and variance of $\hat{\boldsymbol{\theta}}^{(p)}$. Assuming the amplitudes, $a_m[n]$, and noise, $v[n]$, are uncorrelated, it can be shown that

$$E\{x_p^2[n]\} = \sum_{m=p}^{2M} \mu_{\tilde{a}_m} s_m[n;\boldsymbol{\theta}]. \tag{4.21}$$

In order to show that the estimator is asymptotically unbiased, we show that, asymptotically, $L(x_p, \hat{\boldsymbol{\theta}}^{(p)})/N$ achieves a global maximum at $\hat{\boldsymbol{\theta}}^{(p)} = p\boldsymbol{\theta}$ [58]

$$\begin{aligned} L_\infty(x_p, \hat{\boldsymbol{\theta}}^{(p)}) &= \lim_{N\to\infty} \frac{1}{N} \left| L(x_p, \hat{\boldsymbol{\theta}}^{(p)}) \right| \\ &= \lim_{N\to\infty} \frac{1}{N} \left| \sum_{n=0}^{N-1} x_p^2[n]s_1[n;\hat{\boldsymbol{\theta}}^{(p)}] \right|. \end{aligned} \tag{4.22}$$

Following [58], it can be shown that

$$\begin{aligned} &\lim_{N\to\infty} \frac{1}{N} \sum_{n=0}^{N-1} x_p^2[n]s_1[n;\hat{\boldsymbol{\theta}}^{(p)}] = \\ &\lim_{N\to\infty} \frac{1}{N} \sum_{n=0}^{N-1} E\{x_p^2[n]\}s_1[n;\hat{\boldsymbol{\theta}}^{(p)}] \end{aligned} \tag{4.23}$$

and therefore we obtain

$$\begin{aligned} L_\infty(x_p, \hat{\boldsymbol{\theta}}^{(p)}) &= \lim_{N\to\infty} \frac{1}{N} \left| \sum_{n=0}^{N-1} E\{x_p^2[n]\} s_1[n; \hat{\boldsymbol{\theta}}^{(p)}] \right| \\ &= \lim_{N\to\infty} \frac{1}{N} \left| \sum_{n=0}^{N-1} \sum_{m=p}^{2M} \mu_{\tilde{a}_m} \right. \\ &\qquad \left. \cdot s_m[n; \boldsymbol{\theta}] s_1[n; \hat{\boldsymbol{\theta}}^{(p)}] \right| . \end{aligned} \tag{4.24}$$

The cross-product of two chirps with different parameters is negligible w.r.t. N for sufficiently large value of N. Therefore

$$L_\infty(x_p, \hat{\boldsymbol{\theta}}^{(p)}) = \left| \sum_{m=p}^{2M} \mu_{\tilde{a}_m} \delta(\hat{\boldsymbol{\theta}}^{(p)} - m\boldsymbol{\theta}) \right| . \tag{4.25}$$

That is, $L(x_{p+1}, \hat{\boldsymbol{\theta}}^{(p)})/N$ has $2M-p+1$ peaks at each $m\boldsymbol{\theta}$ for $m = p, \ldots, 2M$ with a magnitude of $\mu_{\tilde{a}_m}$. Since we assume that the components are estimated in order, the last result implies that $\mu_{\tilde{a}_2} > \mu_{\tilde{a}_3} > \ldots > \mu_{\tilde{a}_{2M}}$ and consequently $L(x_p, p\boldsymbol{\theta}) > L(x_p, m\boldsymbol{\theta})$, $\forall m > p$. Therefore we conclude that

$$\arg\max_{\hat{\boldsymbol{\theta}}^{(p)}} \left\{ L_\infty(x_p, \hat{\boldsymbol{\theta}}^{(p)}) \right\} = p\boldsymbol{\theta} \tag{4.26}$$

and thus the estimator is asymptotically unbiased.

Proposition 1: *The asymptotic variance of* $\hat{\boldsymbol{\theta}}^{(p)}$ *is given by*

$$var(\hat{\theta}_1^{(p)}) = \frac{24}{\pi^2 N^3} \frac{tr\{R_a\}\sigma_v^2 + 0.5\sigma_v^4}{\mu_{\tilde{a}_p}^2} \tag{4.27}$$

$$var(\hat{\theta}_2^{(p)}) = \frac{90}{\pi^2 N^5} \frac{tr\{R_a\}\sigma_v^2 + 0.5\sigma_v^4}{\mu_{\tilde{a}_p}^2} \tag{4.28}$$

where R_a *is the* $M \times M$ *cross-correlation matrix of the amplitudes whose elements are given by*

$$R_a[k, \ell] = E\{a_k[n] a_\ell[n]\}. \tag{4.29}$$

PROOF: See Appendix D. ■

Proposition 2: *For a single harmonic, i.e.* $M = 1$, *the results* (4.27) *and* (4.28) *converge to the asymptotic variance presented in [58] for the NLSE of a mono-component LFM.*

PROOF: For $M = 1$, we get that $tr\{R_a\} = R_a = E\{a_1^2\}$. In addition, $\tilde{a}_1 = a_1^2[n]$ and therefore $\mu_{\tilde{a}_1}^2 = E\{a_1^2\}^2$. Substituting $tr\{R_a\}$ and $\mu_{\tilde{a}_1}^2$ into (4.27) and (4.28) yields the same result as in [58], except for a small difference in the frequency normalization, i.e. a factor of 2π and π for the initial frequency and frequency rate, respectively. ■

So far we obtained the asymptotic bias and variance of the estimator in each step of the IHNLSE. In order to evaluate the overall asymptotic bias and variance of the IHNLSE, we assume that the estimators are approximately uncorrelated. This is not accurate, but can be assumed since the components are well separated in $L(x, \boldsymbol{\theta})$. Since the mono-component estimator is asymptotically unbiased, it is clear that the IHNLSE is also asymptotically unbiased. The asymptotic variance is given by

$$\begin{aligned} \mathrm{var}(\hat{\theta}_1) &= \frac{1}{C_M^2} \sum_{m=2}^{2M} m^2 \cdot \mathrm{var}(\hat{\theta}_1^{(f(m))}) \\ &= \frac{24}{\pi^2 N^3 C_M^2} r_M \end{aligned} \tag{4.30}$$

$$\begin{aligned} \mathrm{var}(\hat{\theta}_2) &= \frac{1}{C_M^2} \sum_{m=2}^{2M} m^2 \cdot \mathrm{var}(\hat{\theta}_2^{(f(m))}) \\ &= \frac{90}{\pi^2 N^5 C_M^2} r_M \end{aligned} \tag{4.31}$$

where $r_M = (tr\{R_a\}\sigma_v^2 + 0.5\sigma_v^4) \sum_{m=2}^{2M} m^2/\mu_{\tilde{a}_m}^2$.

Note that the last result implies that in order to achieve the optimal accuracy, a search resolution of $N^{3/2}$ and $N^{5/2}$ is required for the initial frequency and frequency rate, respectively.

4.4.3 Computational Load

We evaluate the computational complexity of the IHNLSE by calculating the number of on-line multiplications. Each iteration of the process involves a two-dimensional search. In order to achieve the possible accuracy, a search resolution of $1/N^{3/2}$ and $1/N^{5/2}$ is required for the initial frequency and frequency rate, respectively. That means that there are an order of $N^{3/2} \cdot N^{5/2}/N = N^3$ search point. Each point requires the calculation of the cost function, $L(x, \boldsymbol{\theta})$, which can be done using $\mathcal{O}(N)$ multiplications. The modulation and filtering of the signal is also perform using $\mathcal{O}(N)$ multiplications. Therefore, the complexity of each iteration is $\mathcal{O}(N^4)$. Since there are $2M - 1$ iterations, the total computational complexity of the IHNLSE is $\mathcal{O}(N^4 M)$.

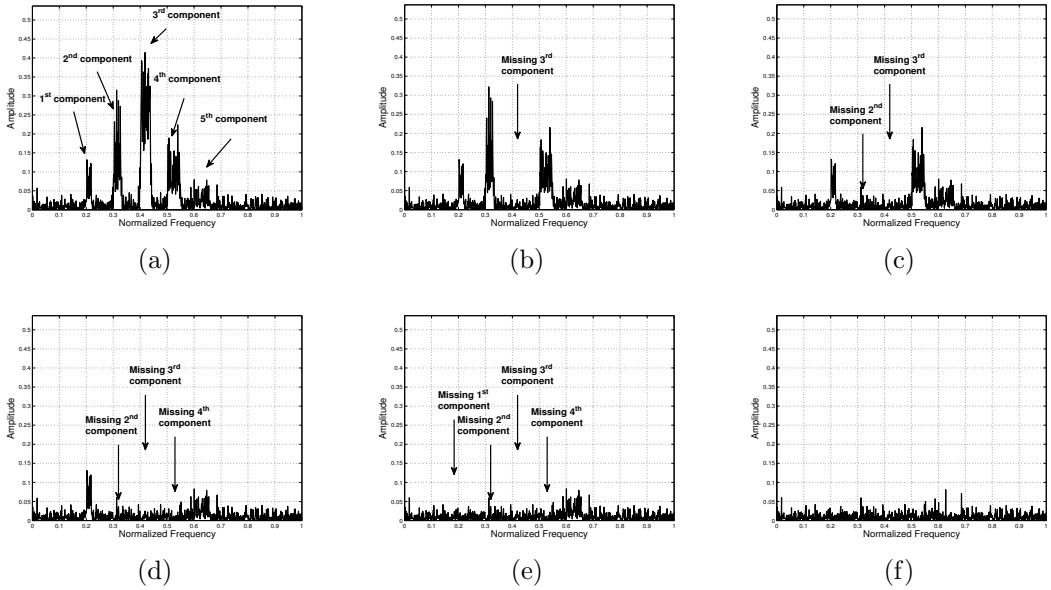

Figure 4.2: Spectrum of x_m for (a) $m = 1$ (i.e. x^2), (b) $m = 2$, (c) $m = 3$,(d) $m = 4$, (e) $m = 5$, (f) $m = 6$ (i.e. $2M$).

4.4.4 Unknown Model Order

As mentioned above, when the number of harmonic components is unknown, a model order selection criterion is required. Methods such as MDL or AIC are commonly used and successfully applied to multicomponent and harmonic chirps in the previous chapter. Both involve the maximum likelihood cost function [78], which requires estimates of the parameters and amplitudes of each component. Since that the IHNLSE cannot be used to estimate the amplitudes, these criteria are not useful. We therefore suggest to incorporate a detection process in the IHNLSE to determine the number of components.

Example 1 (cont.): As an example, to illustrate the idea of this process, Fig. 4.2 presents the spectrum of $x_m[n]$ for each iteration of the IHNLSE, i.e. $m = 1, \ldots, 2M$, where $x[n]$ is the same signal as in Example 1. Figure 4.2(a) shows the spectrum of $x_1[n] = x^2[n]$, with the five harmonic components apparent. After the first iteration, the strongest component is filtered using the process described in the previous subsection, as can be seen in Fig. 4.2(b). The process is repeated $2M - 1$ times. Finally, when all harmonic components are filtered, the spectrum, showed in Fig. 4.2(f), has no major peaks and its power is overall lower than the previous iterations.

We can therefore detect the number of harmonic components by examining a peakedness measure of the spectrum of $x_m[n]$. Such measures were presented in [81]. Particularly,

Table 4.1: Definition of Peakedness Measures for $X^{(m)}[k]$

Measure	Definition
Energy Level	$\sum_k \lvert X^{(m)}[k]\rvert^2$
Kurtosis	$\frac{\sum_k \lvert X^{(m)}[k]\rvert^4}{(\sum_k \lvert X^{(m)}[k]\rvert^2)^2}$
Hoyer	$\sqrt{N} - \frac{\sum_k \lvert X^{(m)}[k]\rvert}{\sqrt{\sum_k \lvert X^{(m)}[k]\rvert^2}}$
H_S	$\sum_k \lvert X^{(m)}[k]\rvert \log\lvert X^{(m)}[k]\rvert^2$
H_G	$\sum_k \log\lvert X^{(m)}[k]\rvert^2$

we examine the Kurtosis, Hoyer, Shannon entropy (H_S) and Gaussian entropy (H_G) measures. In addition, we examine the energy level of the signal as a measure. Definitions for all measures are presented in Table 4.1 for the spectrum of $x_m[n]$, denoted by $X^{(m)}[n]$. The measures for the signal from Example 1 are presented in Fig 4.3. The measures are normalized so that they equal 1 at $m = 1$. All measures reach a certain level at $m = 2M$ and change very little afterwards, with the exception of the Gaussian entropy measure which is almost not effected and thus not suitable for our purpose. The number of harmonic components can estimated as

$$\hat{M} = \arg\min_m \{Sp(2m) + p_r(2m)\} \tag{4.32}$$

where $Sp(m)$ is a spectrum peakedness measure at the m'th iteration and p_r is a monotonically increasing (w.r.t. m) regularization to prevent over estimation. The iterative harmonic-NLSE with model order selection (IHNLSE-MO) is summarized in Algorithm 2.

4.5 Low Complexity Estimators

In order to avoid the high resolution, two-dimensional search required for the IHNLSE, We present two low complexity estimators. The first is a modification of the HAF estimator [58] for a single component LFM with a random amplitude. The second is a modification of the Harmonic-SEES, for constant-amplitude harmonic chirps.

4.5.1 A Modified HAF Estimator

In order to avoid the high-resolution two-dimensional search involved in the NLSE, a suboptimal estimation method was proposed in [58] based on the HAF. We first explain

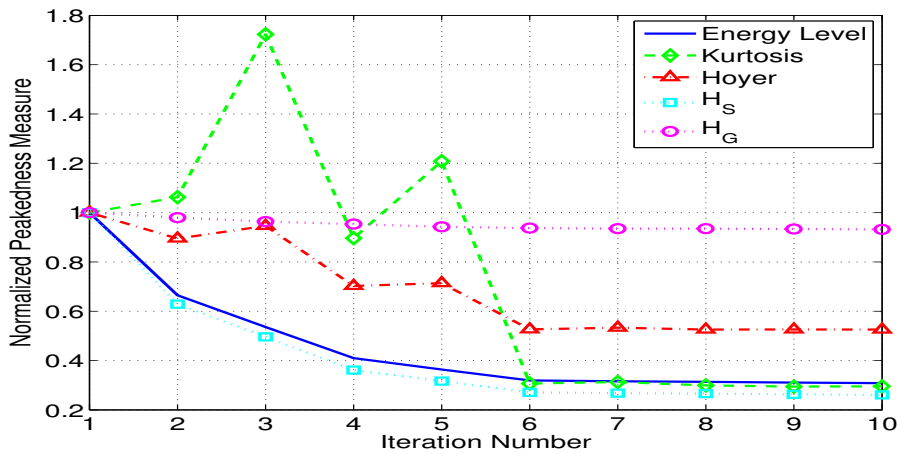

Figure 4.3: Peakedness measures and energy level of the spectrum of x_m for Example 1. Measures are normalized so that they equal 1 at $m = 1$.

Algorithm 2 Iterative Harmonic-NLSE for Unknown Model Order (IHNLSE-MO)

Input:

$x[n]$ - Input signal

D - Maximum possible model order

Output:

$\hat{\boldsymbol{\theta}}$ - Estimated parameters

$\hat{M}$ - Estimated model order

$x_1[n] \leftarrow x^2[n]$

for $m \leftarrow 1, \ldots, D$ **do**

$Sp(m) \leftarrow$ Peakedness measure of $x_m[n]$

$\hat{\boldsymbol{\theta}}^{(m)} \leftarrow \arg\max_{\boldsymbol{\theta}} L(x_m, \boldsymbol{\theta})$

$x_{m+1}[n] \leftarrow ((x_m[n]s^*[n; 2\hat{\boldsymbol{\theta}}^{(m)}]) * h[n])s[n; 2\hat{\boldsymbol{\theta}}^{(m)}]$

end for

$\hat{M} = \arg\min_m \{Sp(2m) + p_r(2m)\}$

$\hat{\boldsymbol{\theta}} \leftarrow= \frac{1}{C_{\hat{M}}} \sum_{m=2}^{2\hat{M}} m\hat{\boldsymbol{\theta}}^{(f(m))}$

in short the HAF method for a mono-component case. For a single LFM, the discrete ambiguity function is given by

$$\begin{aligned}\rho_k[n] &= x^*[n]x[n+k] \\ &= a[n]a[n+k]e^{j2\pi(\theta_1 k+\frac{1}{2}\theta_2 k^2)}e^{j2\pi(\theta_2 kn)} \\ &\quad +v_\rho[n] \end{aligned} \tag{4.33}$$

for some constant k, where $v_\rho[n]$ is the transformed noise given by $v_\rho[n] = a[n]^* s^*[n,\boldsymbol{\theta}]v[n+k]+v^*[n]a[n+k]s[n+k,\boldsymbol{\theta}]+v^*[n]v[n+k]$. The signal $\rho_k[n]$ is a sinusoid with a time-varying random amplitude in presence of non-Gaussian noise. The chirp rate, θ_2, can be obtained from ρ_k using the LS approach again. This time, however, the result is a one dimensional search problem. It can be shown that [58]

$$\hat{\theta}_2 = \frac{1}{2k}\arg\max_{\tilde{\theta}_2}\left|\sum_{n=0}^{N-1}\rho_k^2[n]e^{-j2\pi\tilde{\theta}_2 n^2}\right|. \tag{4.34}$$

Once θ_2 is estimated according to (4.34), we determine θ_1 as

$$\hat{\theta}_1 = \frac{1}{2k}\arg\max_{\tilde{\theta}_1}\left|\sum_{n=0}^{N-1}x^2[n]e^{-j2\pi\hat{\theta}_2 n^2}e^{-j2\pi\cdot 2\tilde{\theta}_1 n}\right|. \tag{4.35}$$

Note that (4.34) and (4.35) essentially find the maximum of the absolute value of the DTFT of $\rho_k^2[n]$ and $x^2[n]$, respectively. Additionally, it is worth noting that $\rho_k^2[n]$ is equivalent to the second order ambiguity function of $x^2[n]$. As can be seen, the solution for random-amplitude signal is similar to the constant amplitude except the squaring of the signal, just as in the NLSE.

Now, we return to the problem of harmonic signals. We wish to obtain an expression for $\rho_k[n]$:

$$\begin{aligned}\rho_k[n] &= \sum_{m,m'=1}^{M} a_m[n]a_{m'}[n+k]s_m^*[n;\boldsymbol{\theta}]s_{m'}[n+k;\boldsymbol{\theta}] \\ &\quad +v_\rho[n] \\ &= \sum_{m=1}^{M} a_m[n]a_m[n+k]s_m^*[n;\boldsymbol{\theta}]s_m[n+k;\boldsymbol{\theta}] \\ &\quad + \sum_{m\neq m'} a_m[n]a_{m'}[n+k]s_m^*[n;\boldsymbol{\theta}]s_{m'}[n+k;\boldsymbol{\theta}] \\ &\quad +v_\rho[n]. \end{aligned} \tag{4.36}$$

From (4.33) we know that the first sum results in harmonic sinusoids of order M at frequencies $k\theta_2, 2k\theta_2, \ldots, Mk\theta_2$ with random amplitudes. The second sum in (4.36) is the cross terms between the harmonic components. Substituting (1.2) into (4.36), it can be shown that

$$\begin{aligned} s_m^*[n;\boldsymbol{\theta}]s_{m'}[n+k;\boldsymbol{\theta}] &= e^{j2\pi(m'-m)(\tilde{\theta}_1 n+\frac{1}{2}\theta_2 n^2)} \\ &\quad \cdot e^{-j2\pi m'(\theta_1 k+\frac{1}{2}\theta_2 k^2)} \end{aligned} \tag{4.37}$$

where $\tilde{\theta}_1 = \theta_1 + m'k\theta_2/(m'-m)$. That is, the cross terms in (4.36) are also LFM signals. So the problem becomes estimating from $\rho_k[n]$ the fundamental frequency of harmonic sinusoid with random amplitude in presence of the transformed noise and LFM signals. From (4.36) and (4.8), it can be shown that $\rho_k^2[n]$ contains random amplitude harmonic sinusoids of order $2M$ with the fundamental frequency missing. That is, $2M-1$ sinusoids at frequencies $2k\theta_2, 3k\theta_2, \ldots, 2Mk\theta_2$. The LS approach used to obtain (4.34) and (4.35), results in maximizing a DTFT. In case of harmonic signals, instead of using the DTFT, we apply the idea of the Harmogram [7], a method for estimating the fundamental frequency of an harmonic series of sinusoids. The chirp rate, θ_2, can be estimated using a modified Harmogram criterion

$$\hat{\theta}_2 = \frac{1}{k}\arg\max_{\tilde{\theta}_2} \sum_{m=2}^{2M} \left| \sum_{n=0}^{N-1} \rho_k^2[n] e^{-j2\pi m\tilde{\theta}_2 n^2} \right|. \tag{4.38}$$

Once $\hat{\theta}_2$ is estimated, we define the set of the following M signals

$$x_m[n] = x[n]e^{j2\pi\frac{m}{2}\hat{\theta}_2 n^2} \tag{4.39}$$

This is termed de-chirping since that for $\hat{\theta}_2 = \theta_2$, each $x_m[n]$ is a single sinusoid with random amplitude in the presence of other harmonic components and noise. Finally, θ_1 is estimated using a modified Harmogram approach as well

$$\hat{\theta}_1 = \frac{1}{2}\arg\max_{\tilde{\theta}_1} \sum_{m=1}^{M} \left| \sum_{n=0}^{N-1} x_m^2[n] e^{-j2\pi m\tilde{\theta}_1 n} \right|. \tag{4.40}$$

Note that for $M = 1$, (4.38) is clearly the same as (4.34). Then, by substituting (4.39) for $m = 1$ into (4.40), we obtain the exact expression as in (4.35). That is, for $M = 1$, the solution is exactly the same as the mono-component case.

The HAF based method reduces the problem to two one-dimensional problems, but does not change the search resolution required to achieve optimal performance. The construction of the cost function in (4.38) requires $\mathcal{O}(NM)$ multiplications per frequency. The number of frequency rates required is in the order of $N^{5/2}/N$. The total number of multiplications required for the frequency rate estimation is therefore $\mathcal{O}(N^{5/2}M)$. Next, M DTFTs, one for each de-chirped signal, are required. The number of frequencies in this step is in the order of $N^{3/2}$. The complexity of the initial frequencies estimation is therefore $\mathcal{O}(N^{5/2}M)$. To conclude, HAF method involves $\mathcal{O}(N^{5/2}M)$ multiplications.

4.5.2 The Harmonic Separate-Estimate Method

We now extend the Harmonic-SEES to the random amplitude model. Similarly to the two previous methods, in order to do so, we define a pre-processing step of squaring the signal, before applying the Harmonic-SEES. As noted before, the squared signal contains $2M$ harmonics but the fundamental component is missing. That is, $2M-1$ components overall. Therefore, the second modification to the Harmonic-SEES is to take into account that the fundamental component, whose parameters are those we wish to estimate, is missing. When the number of harmonic components is known, the HRA-SEES method is very similar to the Harmonic-SEES method. The model order selection for constant amplitude model involves the MDL or AIC criteria. Both are not applicable for this case as explained above. Therefore the model order selection presented in the next subsection differs from the Harmonic-SEES method.

The first step is separating the signal into $2M-1$ harmonic components. This is achieved exactly as in the Harmonic-SEES method. However, note that the maximization in (3.41), used to select the optimal de-chirping value, becomes

$$\tilde{\theta}_2 = \underset{\theta_{2,\ell}\in\Omega}{\operatorname{argmax}} \sum_{m=2}^{2M} |\bar{x}_{\ell,m}[k_m^{(\max)}(\theta_{2,\ell})]| \tag{4.41}$$

where $\bar{\mathbf{x}}_{\ell,m}[k]$ is the DFT of the de-chirped squared signal.

The output of the separate step in this case is a set of $2M-1$ reconstructed harmonic components, $\{\hat{s}_2[n],\ldots,\hat{s}_{2M}[n]\}$, of the observed signal. And the LS problem in (3.57), used to estimate the parameters from the unwrapped phases, now becomes

$$[\{\hat{\tilde{\varphi}}_m\}_{m=2}^{2M}, \hat{\boldsymbol{\theta}}^T]^T = \underset{\{\tilde{\varphi}_m\}_{m=2}^{2M},\boldsymbol{\theta}}{\arg\min} \sum_{m=2}^{2M} \|\tilde{\boldsymbol{\phi}}_m - \tilde{\varphi}_m \mathbf{1}_N - 2\pi m \mathbf{H}\boldsymbol{\theta}\|^2 \tag{4.42}$$

where $\tilde{\boldsymbol{\phi}}_m$ is the unwrapped phase of the m'th component, $\mathbf{1}_N$ is the $N \times 1$ vector with all elements equal to one and $\mathbf{H} = [\mathbf{h}_1, \mathbf{h}_2]$ with $\mathbf{h}_1 = [0, 1, \ldots, N-1]^T$, and $\mathbf{h}_2 = [0^2/2, 1^2/2, \ldots, (N-1)^2/2]^T$. The estimate of $\boldsymbol{\theta}$ is given by

$$\hat{\boldsymbol{\theta}} = (\mathbf{H}^T \mathbf{P}_1^{\perp} \mathbf{H})^{-1} \mathbf{H}^T \mathbf{P}_1^{\perp} \boldsymbol{\Psi} \tag{4.43}$$

where $\mathbf{P}_1^{\perp} = \mathbf{I}_N - \mathbf{1}_N(\mathbf{1}_N^T \mathbf{1}_N)^{-1}\mathbf{1}_N^T$, $\boldsymbol{\Psi} = \frac{1}{2\pi C_M} \sum_{m=2}^{2M} m\tilde{\boldsymbol{\phi}}_m$.

The linear model for the recursive process is now given by

$$\hat{\boldsymbol{\phi}}[n] = \mathbf{H}[n]\hat{\boldsymbol{\eta}}[n] + \boldsymbol{\varepsilon}[n] \tag{4.44}$$

where

$$\mathbf{H}[n] = \begin{bmatrix} & 4\pi n & 2\pi n^2 \\ \mathbf{I}_M & \vdots & \vdots \\ & 4\pi M n & 2\pi M n^2 \end{bmatrix} \tag{4.45}$$

and $\hat{\boldsymbol{\eta}}[n] = [\hat{\boldsymbol{\varphi}}^T[n],\ \hat{\boldsymbol{\theta}}^T[n]]^T$, where $\hat{\boldsymbol{\varphi}}[n] = [\hat{\varphi}_2[n], \ldots, \hat{\varphi}_{2M}[n]]^T$.

Note that the computational complexity of the HRA-SEES method is exactly the same as the Harmonic-SEES method, presented in the previous chapter, i.e. $\mathcal{O}\left(N^2 \log NM\right)$ online multiplications.

4.5.3 Unknown Model Order

So far, in both low complexity estimation methods, the number of harmonic components was assumed to be known. Therefore, similarly to the IHNLSE, a model order selection rule is required. The IHNLSE works iteratively. That is, in each step one component is estimated and removed. However, both low complexity methods suggested use all the components at once. Thus, the methods must be applied for every possible M. Using the same approach as in the IHNLSE, for a given M, once the parameters are estimated, M harmonic components are filtered from the original signal, $x[n]$, using the same demodulation scheme. Note that in this case the filtering is performed on $x[n]$ rather than $x^2[n]$ as in the IHNLSE. Again, peakedness measures of the spectrum of the filtered signal can be calculated to obtain a model order selection criterion. The model order selection framework is summarized in Algorithm 3. The estimation step can be achieved either with the HAF based estimation or with the suggested HRA-SEES method.

Algorithm 3 Model Order Selection Framework

Input:
$x[n]$ - Input signal
D - Maximum possible model order
Output:
$\hat{\boldsymbol{\theta}}$ - Estimated parameters
$\hat{M}$ - Estimated model order

for $m = 1$ to D **do**
  Estimate parameters of $x[n]$, $\hat{\boldsymbol{\theta}}^{(m)}$, assuming m harmonics.
  $x^{(m)}[n] \leftarrow x[n]$
  for $k = 1$ to m **do**
    $x^{(m)}[n] \leftarrow ((x^{(m)}[n]s^*[n; k\hat{\boldsymbol{\theta}}^{(m)}]) * h[n])s[n; k\hat{\boldsymbol{\theta}}^{(m)}]$
  end for
  $Sp(m) \leftarrow$ Peakedness measure of $x_m[n]$
end for
$\hat{M} \leftarrow \underset{m=1,\ldots,D}{\arg\min} \{Sp(m) + p_r(m)\}$
$\hat{\boldsymbol{\theta}} \leftarrow \hat{\boldsymbol{\theta}}^{(\hat{M})}$

4.6 Numerical Results

We now present examples to compare the performances of the IHNLSE, HAF and HRA-SEES methods. First, we compare the RMSE and p_d, the probability of selecting the correct model order for all three methods. We consider a signal with $M = 3$ harmonic components. The parameters of the fundamental chirp are given by $\theta_1 = 0.15$ and $\theta_2 = 10^{-5}$. The number of samples is $N = 1024$. The phases of all component, φ_m, are generated from a uniform distribution, i.e. $\varphi_m \sim U(0, 2\pi)$. We consider two different models for the random amplitude. The first is a normally distributed amplitudes, in which $\alpha_m[n] \sim \mathcal{N}(1, 0.25)$. In the second model each amplitude is an AR(2) process with parameters $\{1, 0.97, -0.35\}$. The noise power σ_v^2 is adjusted to give the desired SNR defined as SNR $= 10\log_{10}\left(E\{x^2\}/\sigma_v^2\right) = 10\log_{10}\left(tr\left\{R_a\right\}/\sigma_v^2\right)$ [dB], where $E\{\cdot\}$ denotes the expectation operator. In all simulations we use a lag of $\tau = N/2$ samples in the HAF based estimation method [58].

We start by evaluating the RMSE of the estimators when the number of harmonic components is known. The RMSE is defined as $\text{RMSE}(\theta_k) = \sqrt{\frac{1}{Nexp}\sum_{i=1}^{N_{exp}}(\hat{\theta}_{k,i} - \theta_k)^2}$, $k = 1, 2$ where $\hat{\theta}_{1,i}$ and $\hat{\theta}_{2,i}$ are the estimate of θ_1 and θ_2 at the ith trial, respectively and $N_{exp} = 500$ is the number of Monte-Carlo independent trials. Simulation results for the normally distributed amplitudes and AR(2) amplitudes are presented in Fig. 4.4 and 4.5, respectively. The results include the RMSE for each estimator and the theoretical RMSE

of the IHNLSE is plotted. In addition, we include the RMSE of the Harmonic-SEES estimator, that assumes constant amplitudes. As can be expected, the IHNLSE yields the best results and almost achieves the theoretical RMSE for SNR above 3dB. The difference between the theoretical and actual errors can be accounted for by the approximations and assumptions used in deriving the theoretical error. The HAF based estimator and the HRA-SEES method perform similarly. The HAF has a slightly better threshold SNR while the HRA-SEES has a slightly better RMSE. Both low-complexity methods fail to achieve the performance of the IHNLSE for the normally distributed amplitudes, but still achieve very low errors w.r.t. to the values of the parameters and can be used to initiate a two dimensional search of the IHNLSE. The Harmonic-SEES method performed worse in high SNR, due to the inaccurate assumption of constant amplitudes. However, its threshold SNR is lower. This is probably because that in low SNR the squared noise in the random amplitude methods becomes very strong.

Next we evaluate the model order selection criteria, by calculating the p_d for various values of SNR. The probability, p_d, is defined as $p_d = \frac{1}{Nexp}\sum_{i=1}^{N_{exp}} \mathbb{1}_{\hat{M}=M}$. The regularization, $p_r(m)$, used is defined by $p_r(m) = m/c_p$ where c_p is a normalization constant to ensure $\sum p_r(m) = 1$. Simulation results for the normally distributed amplitudes and AR(2) amplitudes are presented in Fig. 4.6 and 4.7, respectively. For both the HAF based estimation and the HRA-SEES method, there is very little difference between the performance for the different peakedness measures. For the IHNLSE, the Shannon entropy and the energy level criteria perform better than the others.

We now demonstrate the HRA-SEES method with the model order selection for estimating the parameters of two real-data examples of echolocation calls of a bat and a whale [75, 76]. The same examples were used in the previous chapter, where the amplitudes assumed to be constant at each observation window. The signals are divided into segments of $N = 1000$ samples. At each segment the parameters and the number of harmonic components are estimated using the HRA-SEES method with the Shannon entropy measure.

The first example is an echolocation call produced by an *E. nilssonii* bat [75]. The signal is about 40ms long and is sampled at $F_s = 250$kHz. A spectrogram of the signal is presented in Fig. 3.11. The call has four harmonic components with the last one being very weak. The estimated frequencies are plotted in dashes line on top of the spectrogram and the selected model order is plotted above. The markers on the spectrogram corresponds

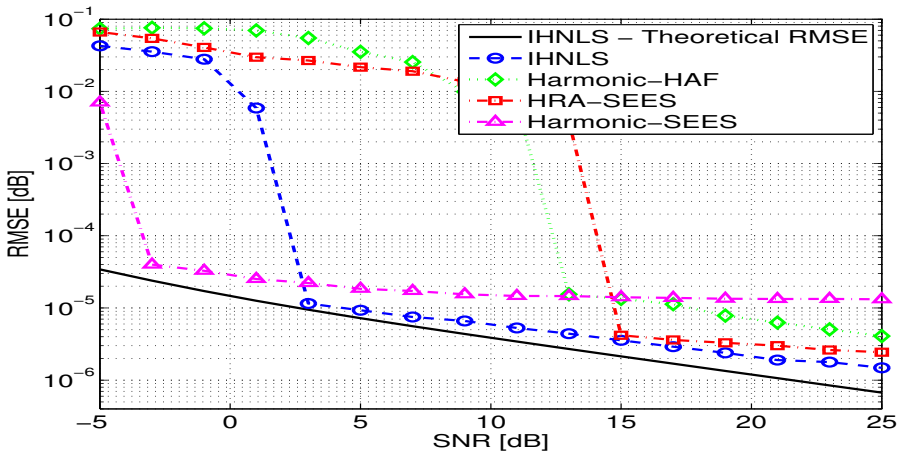

(a) θ_1, Normalized initial frequency

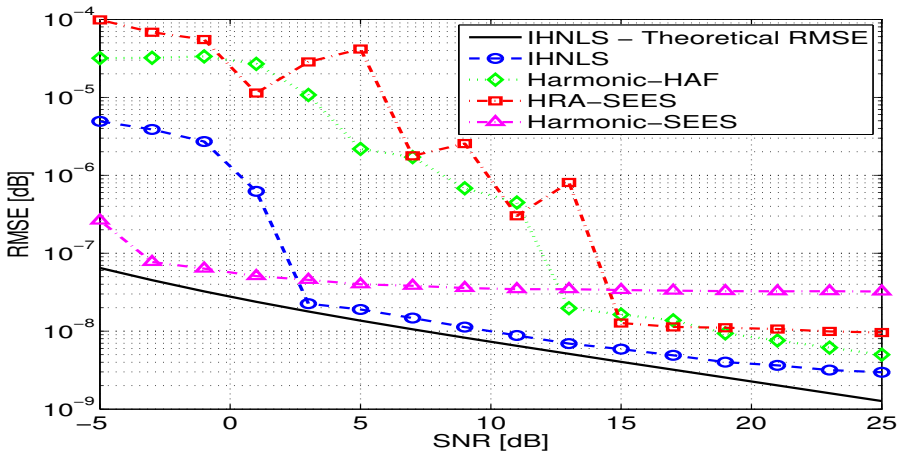

(b) θ_2, Normalized frequency rate

Figure 4.4: RMSE of each estimator vs. SNR for normally distributed amplitudes.

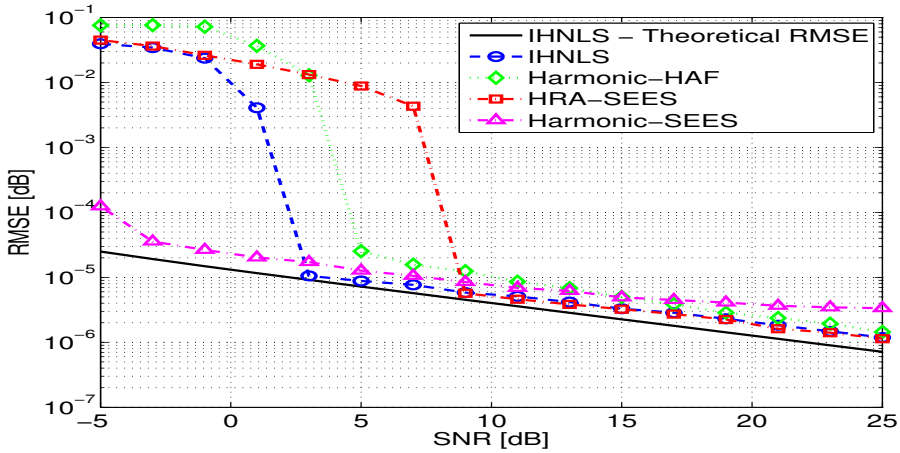

(a) θ_1, Normalized initial frequency

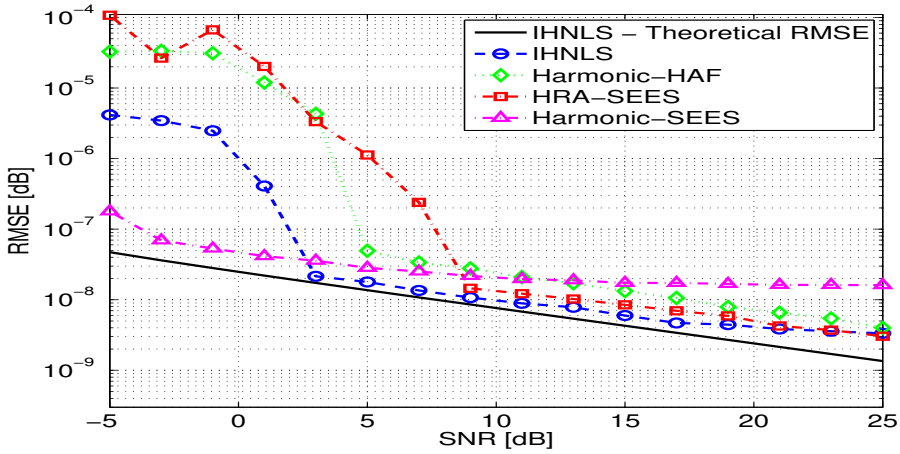

(b) θ_2, Normalized frequency rate

Figure 4.5: RMSE of each estimator vs. SNR for AR(2) amplitudes.

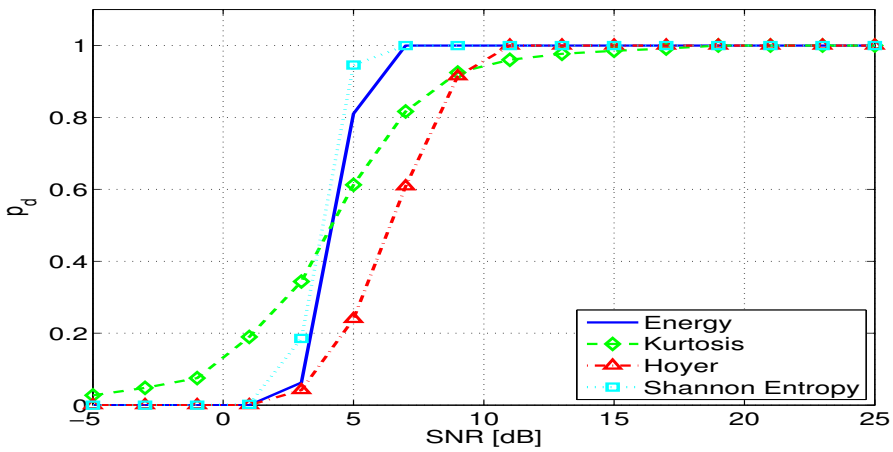

(a) IHNLSE

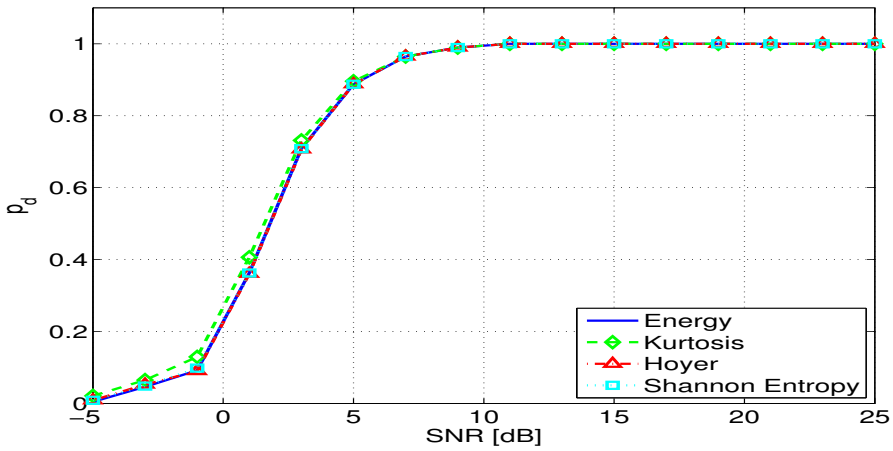

(b) HAF

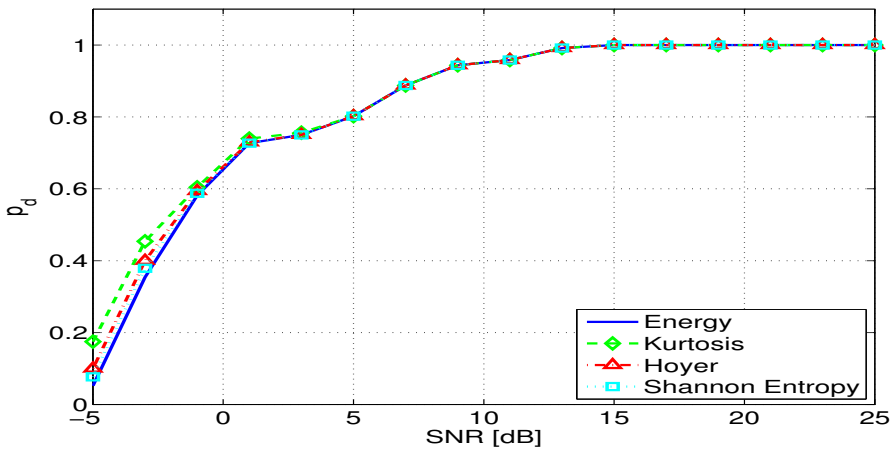

(c) HRA-SEES

Figure 4.6: p_d of each estimator vs. SNR for normally distributed amplitudes.

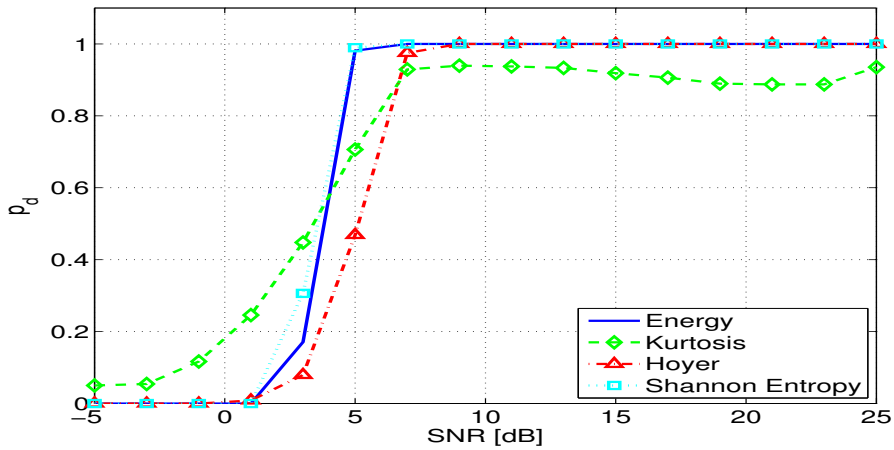

(a) IHNLSE

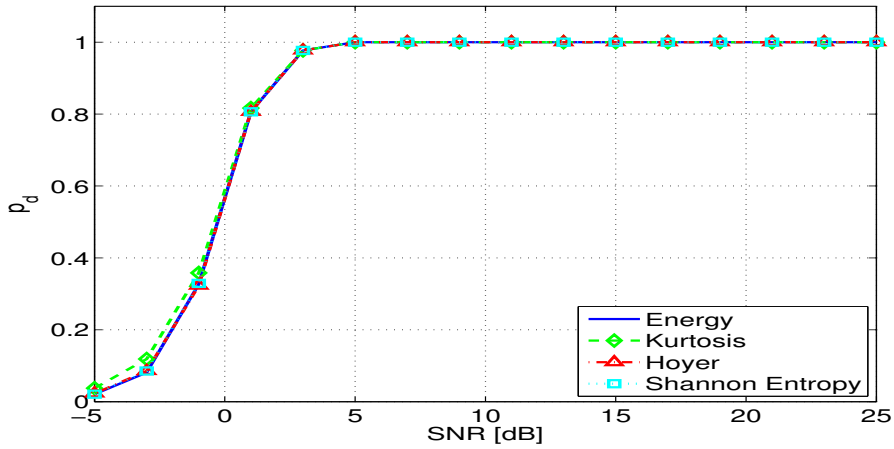

(b) HAF

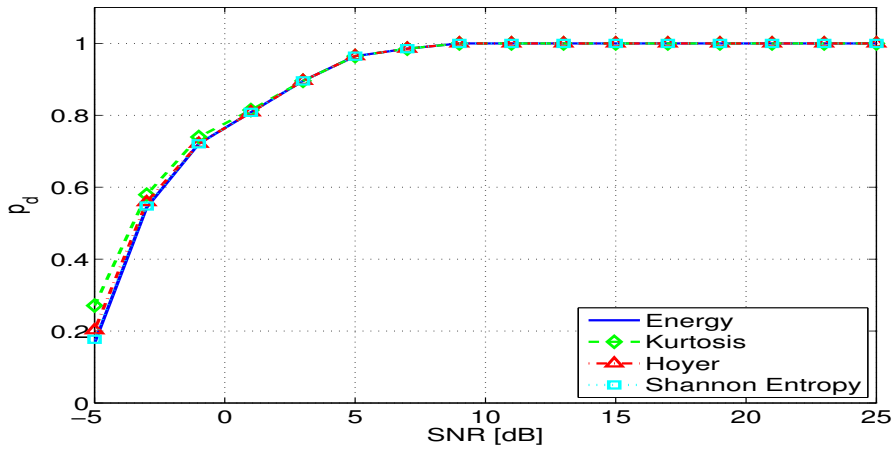

(c) HRA-SEES

Figure 4.7: p_d of each estimator vs. SNR for AR(2) amplitudes.

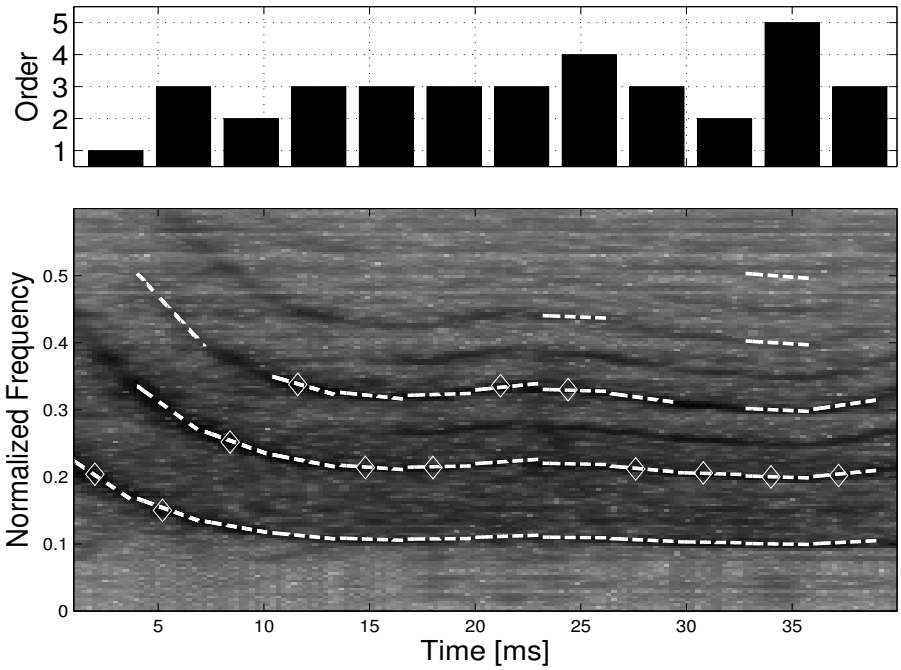

Figure 4.8: Model order selection and parameter estimation of an echolocation call produced by an *E. Nilssonii* bat. The diamonds mark peaks detection in the spectrogram.

to a peak detection at each time frame. The peak detection shows that the fundamental chirp is not the most dominant. However, the HRA-SEES method successfully estimated the correct fundamental frequency at each observation window.

The second example is an echolocation call produced by a *G. melas* whale [76]. The signal is about 600ms long and is sampled to $F_s = 44.1$kHz. The results are presented in Fig. 3.12 in the same format as the previous example. The fundamental frequency line is detected in all segments except for one.

4.7 Conclusion

We considered the problem of estimating the parameters of harmonic linear chirps with random amplitudes when the number of harmonic components is unknown. We showed that the statistical model order selection criteria that were used for constant amplitude model, are not applicable. Consequently, we proposed an iterative framework for model order selection based on peakedness measures of the spectrum of the signal. We suggested three estimation methods for time-varying amplitudes. The first is based on the NLSE, which requires two-dimensional high resolution search. The second is a modification of the

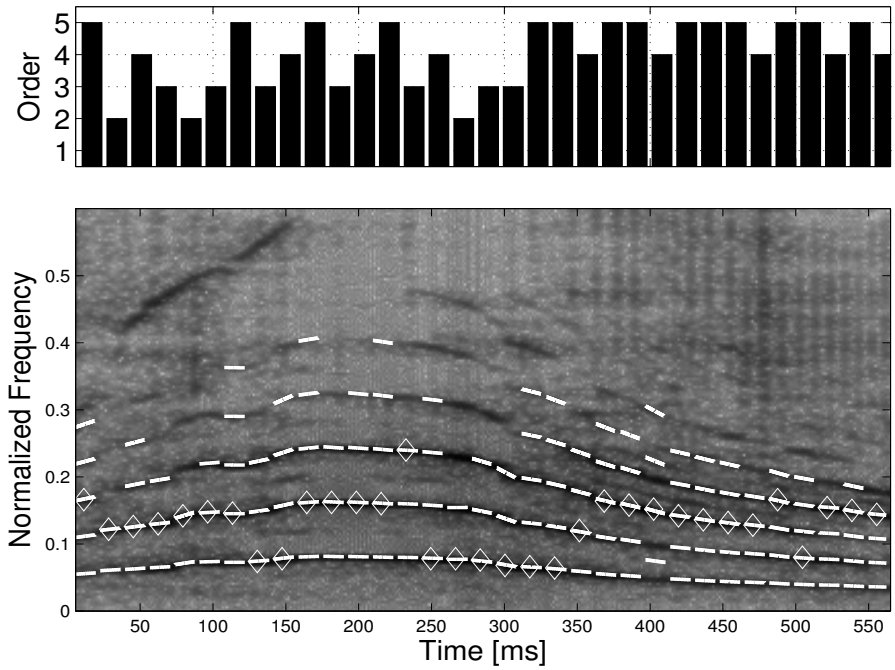

Figure 4.9: Model order selection and parameter estimation of an echolocation call produced by a *G. melas* whale. The diamonds mark peaks detection in the spectrogram.

HAF based estimation for mono-component LFM and the third is a modification of the Harmonic-SEES for harmonic LFM with random amplitudes, the HRA-SEES. Once again, the computational complexity of th proposed method, the HRA-SEES, is substantially smaller than the other two estimators. We showed through simulations that the IHNLSE achieves its asymptotic variance at medium to high SNR and that the two low-complexity methods perform well in high SNR. We also showed that the peakedness measures of the spectrum of the signal can be successfully used in order to estimate the number of components in all three methods.

Chapter 5

Conclusion

5.1 Summary

We have considered the problem of estimating the fundamental initial frequency and frequency rate of harmonic linear chirps when the number of harmonic components is unknown. We started with the simpler model of constant amplitudes and then extended the work to a more general and realistic case of time-varying amplitude.

Previous research can be divided into two categories. Either the fundamental frequency of the signal is assumed to be constant, or a multi-component signal with time-varying frequency is assumed where the different components are not related. In the first case, the possible observation length is very short in order for the assumption to hold. In the second, the parameters of each component are estimated separately and the harmonic relation is not exploited. In this work, we assumed a model of harmonic linear chirps. This allowed us to increase the observation length, and consequently improved the estimation accuracy, comparing to the constant frequency approach. We further improved the accuracy, comparing to multi-component parameter estimation problems, by exploiting the harmonic relation.

For each model (i.e. constant and random amplitudes), we started by developing an optimal estimator. In the constant amplitude model we presented the exact and approximated MLE. We later showed that the MLE is not applicable for random amplitudes and we developed the IHNLSE, an iterative process based on the NLS approach. In both cases, the estimator requires two-dimensional high-resolution search in the parameter space and therefore has high computational complexity.

We then introduced two low-complexity estimation methods for each model. The first

is based on HAF, which transforms the problem to two one-dimensional problems. We presented a modification to the HAF based estimation for harmonic linear chirps with constant amplitude and also a modification for random amplitudes. The second is a two-step estimation method which we termed Harmonic-SEES for the constant amplitude model. The Harmonic-SEES method first separates the signal to its harmonic components, and then estimates the two parameters of interest using a joint least squares method given the phases of the harmonic components. We also provided an extension of the method, which we termed HRA-SEES, for random amplitudes model. We also considered the case where the number of harmonic components is unknown and presented criteria for model order selection.

Simulation results showed that the proposed estimation method, for constant and random amplitudes, achieves the performance of the optimal estimators for high SNR and outperforms the HAF based estimation.

5.2 Future Research

The work presented in this thesis can be further extended in a number of interesting directions:

1. In this work we assumed that the signal can be modeled as a sum of harmonic LFM components in each observation window. Thus, we allow longer segments, compared to existing methods that assume constant frequency model. We can further increase the segment length by assuming a model of harmonic PPS. The difficulty in doing so is with the first step of the coarse estimation. Currently, this is done by searching for the optimal de-chirping, which for Pth order PPS would require $P-1$ dimensional search. A possible approach to obtain the coarse estimation is to extend the quasi-maximum-likelihood [86], originally proposed for mono-component PPS, to multi-component signals.

2. In this work we assumed the signal is a sum of linear chirps that satisfy an harmonic relation. An interesting research direction is to consider a more general model of multi-component LFM signals, which received much attention in literature. The Harmonic-SEES and HRA-SEES methods can be easily modified for such signals and can offer very low complexity estimators.

3. In the second part of the work we considered signals with random amplitudes. However, no specific model of the random amplitudes was assumed. In some applications the random amplitudes can be modeled as a parametric process (e.g. autoregressive process). In such cases the NLS optimization in (4.7) can be solved w.r.t. the amplitudes parameters. It would be interesting to compare the performance of the parametric NLS estimator for random amplitude harmonic LFM with the IHNLSE and the other estimators suggested in this work.

4. In some scenarios, there is more than one source present. For example, two people speaking at the same time, or in a group of dolphins or bats. Generally, it can be considered a multi-component signal. However, as in the single speaker scenario, if the signal of each speaker contains harmonic components than it is a different problem from multi-component signal. The harmonic relation of each speaker can be exploited to separate the speakers and estimate the parameters of the fundamental component of each one.

5. In this work we assumed that the chirp is always present. This is not the necessarily the case. Usually the start and end times of the chirp are not known. In addition, long signals often contain times where no chirp is present. The Harmonic-SEES method can be extended to perform chirp detection by using the same property that is used for the coarse estimation. The presence of a chirp can be detected by the existence of a significant peak in the de-chirping map.

6. The proposed Harmonic-SEES and HRA-SEES methods were tested on real-life example of complex echolocation chirps. The signals were divided into segments and the parameters were estimated for each segment separately. Obviously, the segments are related to each other and we expect the time-varying frequency of the signal to be smooth. This information can be used to improve the estimation by tracking the frequency. For example, we can assume the signal is a high order PPS and predict (e.g. using Kalman filtering) the parameters for the next step. The prediction can replace the first step of de-chirping selection. Furthermore, the last step can be replaced with a constraint LS optimization. The model order can also be tracked, for example, using hidden Markov models, which can perhaps replace the model order selection criteria.

Appendix A

Harmogram

The Harmogram was presented by Hinich [7] as a simple method to detect the fundamental frequency of a constant frequency harmonic signal. The method operates on the frequency domain of the signal. As such, the performance deteriorates when the fundamental frequency is not aligned with a DFT frequency bin, i.e. not a multiple of $1/N$. The number of harmonic components was assumed to be known as well as the spectrum of the noise. The Harmogram was later generalized for the case of unknown noise spectrum and unknown number of harmonics by Planquette et al. [87]. In addition they proposed a modification to improve the performance, in terms of probability of detection, when the fundamental frequency is not aligned with a DFT frequency bin.

Consider a signal with M harmonic components given by

$$x[n] = \sum_{m=1}^{M} a_m e^{2\pi jmn\theta} + v[n] \tag{A.1}$$

where a_m is the constant and complex amplitude of the m'th component and $v[n]$ is an additive noise whose spectrum is given by $S_v(\theta_k)$. Denote by $X(\theta_k)$, the DFT of $x[n]$ where $\theta_k = k/N$ for $k = 0, \ldots, N-1$. The Harmogram of $x[n]$ is given by

$$H_x(\theta_k) = \sum_{m=1}^{M} S_v^{-1}(m\theta_k) \left|X(m\theta_k)\right|^2 . \tag{A.2}$$

When $\theta_k = \theta$, in high SNR conditions the Harmogram is approximately

$$H_x(\theta) \cong N \sum_{m=1}^{M} S_v^{-1}(m\theta) \left|a_m\right|^2 . \tag{A.3}$$

That is, the Harmogram sums the entire energy of the signal. Any other candidate frequency will result in a smaller value. Therefore the fundamental frequency can be obtained as

$$\hat{\theta} = \arg\max_{\theta_k} \{H_x(\theta_k)\}. \tag{A.4}$$

Note that if $v[n]$ is a zero mean Gaussian noise with variance σ_v^2, then $S_v(\theta_k) = \sigma_v^2$. In that case we get

$$\begin{aligned} \hat{\theta} &= \arg\max_{\theta_k} \{H_x(\theta_k)\} \\ &= \arg\max_{\theta_k} \left\{ \sum_{m=1}^{M} \left| X(m\theta_k)/\sigma_v^2 \right|^2 \right\} \\ &= \arg\max_{\theta_k} \left\{ \sum_{m=1}^{M} \left| X(m\theta_k) \right|^2 \right\} \end{aligned} \tag{A.5}$$

which means hat the noise level is not actually required. For simplicity, in what follows we assume a Gaussian noise and discard the noise normalization in the Harmogram.

The number of harmonic components is not necessarily known. Incorrect estimation of the number of harmonics can severely impact the estimation [87]. Denote by N_k the maximal number of harmonic components possible for the fundamental frequency θ_k, i.e. $N_k = \lfloor N/(2k) \rfloor$. The modified Harmogram estimator, when the number of harmonics is unknown, is given by [87]

$$H_x(\theta_k) = \frac{\sum_{m=1}^{N_k} \left| X(m\theta_k) \right|^2 - N_k}{\sqrt{N_k}}. \tag{A.6}$$

As mentioned before, the performance of the Harmogram is greatly effected by the DFT resolution. To overcome this problem, the fundamental frequency can be scanned at a higher resolution than the DFT [87]. More specifically, the fundamental frequency is scanned at a resolution of $1/(QN)$, for some integer Q, rather than $1/N$. For simplicity we assume that the number of harmonic components is known. Extension to unknown number of harmonics is straightforward. The modified Q-Harmogram is given by [87]

$$H_x(\theta_k^{(Q)}) = \sum_{m=1}^{M} \left| X(\theta_{mk}) \right|^2 + \left| X(\theta_{mk} + 1/N) \right|^2 \tag{A.7}$$

where $\theta_k^{(Q)} = k/(QN)$ and $\theta_{mk} = \lfloor Nm\theta_k^{(Q)} \rfloor / N = \lfloor mk/Q \rfloor / N$. Note that for each har-

monic, the two nearest frequency bins are summed as opposed to the original Harmogram.

Appendix B

Fractional Fourier Transform

The FrFT received its first attention in optics [88, 89], and in recent years also in signal processing applications [15, 34, 82, 83, 90, 91]. Formally, the continuous FrFT of $x(t)$ is defines as [92]

$$\mathcal{F}^{\alpha}\{x(t)\} = X_{\alpha}(\xi) = \int_{-\infty}^{\infty} K_{\alpha}(\xi, t)x(t)\, dt \tag{B.1}$$

where

$$K_{\alpha}(\xi, t) = \frac{e^{-j(\frac{\pi}{4}\mathrm{sign}(\alpha)-\frac{1}{2}\alpha)}}{\sqrt{2\pi|\sin(\alpha)|}} e^{j\frac{1}{2}\xi^2 \cot\alpha} e^{j(-\frac{t\xi}{\sin\alpha}+\frac{1}{2}t^2\cot\alpha)} \tag{B.2}$$

is the FrFT kernel, $0 \leq \alpha < 2\pi$ is transform order and ξ is the fractional frequency. The FrFT can be described as a four steps transformation [82, 92]. First, the signal is multiplied by a linear chirp with an initial frequency equals to zero, $e^{\frac{1}{2}jt^2\cot\alpha}$. Next, a scaled Fourier transform is performed by multiplying the resulted signal with $e^{-j\frac{t\xi}{\sin\alpha}}$ and integrating. The third step involves chirp multiplication in the frequency domain, i.e. $e^{j\frac{1}{2}\xi^2\cot\alpha}$ and finally, scaling by $\frac{e^{-j(\frac{\pi}{4}\mathrm{sign}(\alpha)-\frac{1}{2}\alpha)}}{\sqrt{2\pi|\sin(\alpha)|}}$. The two chirp multiplications can be described as a rotation of the time-frequency plane by an angle of α [92]. There are four special cases of the FrFT worth mentioning. First, when $\alpha = 0$ the result is the identity transformation. That is, $\mathcal{F}^0\{x(t)\} = x(t)$. Second, when $\alpha = \pi/2$, the FrFT is equivalent to the classical Fourier transform, $\mathcal{F}^{\pi/2}\{x(t)\} = \mathcal{F}\{x(t)\}$. Next, when $\alpha = \pi$, the FrFT becomes the parity transform, equivalent to applying twice the Fourier transform, i.e. $\mathcal{F}^{\pi}\{x(t)\} = \mathcal{F} \circ \mathcal{F}\{x(t)\} = x(-t)$. Finally, the FrFT of order $\alpha = \pi$ is the inverse Fourier transform, $\mathcal{F}^{3\pi/2}\{x(t)\} = \mathcal{F} \circ \mathcal{F} \circ \mathcal{F}\{x(t)\} = \mathcal{F}^{-1}\{x(t)\}$. Note that the zero-order transform, the identity transform, is also equivalent to the composition of four Fourier transforms. The classical Fourier transform can operate in four different rotation angles of the time-frequency plane. The FrFT thus fills the gap and provides arbitrary rotation

angle.

Just as the classical Fourier transform is suited for a constant frequency signals, the FrFT is suited for LFM signals. Consider a continuous-time LFM given by

$$x(t) = a \cdot e^{j(\theta_1 t + \frac{1}{2}\theta_2 t^2)}. \tag{B.3}$$

The rotation angle of the FrFT can be selected to match the frequency rate of $x(t)$. That is

$$\frac{1}{2}t^2 \cot\alpha = -\frac{1}{2}\theta_2 t^2 \Rightarrow \alpha = -\cot^{-1}\theta_2. \tag{B.4}$$

By substituting (B.3) and (B.4) into (B.1) we obtain

$$X_\alpha(\xi) = \frac{e^{-j(\frac{\pi}{4}\mathrm{sign}(\alpha) - \frac{1}{2}\alpha)}}{\sqrt{2\pi|\sin(\alpha)|}} e^{j\frac{1}{2}\xi^2 \cot\alpha} \int_{-\infty}^{\infty} a \cdot e^{j\theta_1 t} e^{-j\frac{t\xi}{\sin\alpha}}\, dt. \tag{B.5}$$

The integral term above is a scaled Fourier transform. Therefore we obtain

$$X_\alpha(\xi) = \frac{e^{-j(\frac{\pi}{4}\mathrm{sign}(\alpha) - \frac{1}{2}\alpha)}}{\sqrt{2\pi|\sin(\alpha)|}} e^{j\frac{1}{2}\xi^2 \cot\alpha} \cdot a \cdot \delta(\xi - \theta_1 \sin\alpha) \tag{B.6}$$

where $\delta(\xi)$ is the delta function. That is, the FrFT of an LFM signal is a delta function at a fractional frequency that depends on the initial frequency of the LFM, if the rotation angle is matched to the frequency rate of the signal. This property of the FrFT can be used for the parameter estimation of LFM signals [34]. The optimal rotation angle can be obtained, for example, by searching for the angle that produces the most delta-like result.

A discrete implementation of the FrFT can be achieved by numerical integration of (B.1), by spectral decomposition of the kernel, $K_\alpha(\xi, t)$, or by kernel approximation and the FFT [89, 92].

Appendix C

Derivation of the FIM

In this appendix we present a detailed derivation of the sub-matrices of the FIM in (3.15) following [78].

The $(1,1)$th element of $J_{\boldsymbol{\theta},\boldsymbol{\theta}}$ is given by

$$J_{\theta_1,\theta_1} = \frac{2}{\sigma_v^2}\Re\{\frac{\partial(\mathbf{Sa})^H}{\partial\theta_1}\frac{\partial\mathbf{S}}{\partial\theta_1}\} = \frac{2}{\sigma_v^2}\Re\{\mathbf{a}^H\frac{\partial\mathbf{S}^H}{\partial\theta_1}\frac{\partial\mathbf{S}}{\partial\theta_1}\mathbf{a}\} \tag{C.1}$$

where $\partial\mathbf{S}/\partial\theta_1 = [\partial\mathbf{s}_1/\partial\theta_1, \cdots, \partial\mathbf{s}_M/\partial\theta_1]$. By substituting $\mathbf{s}_m$ we get that $\frac{\partial\mathbf{s}_m}{\partial\theta_1} = j2\pi m\mathbf{q}\odot\mathbf{s}_m$, where $\mathbf{q} = [0,1,\ldots,N-1]^T$. Substituting $\partial\mathbf{s}_m/\partial\theta_1$ in $\partial\mathbf{S}/\partial\theta_1$ results in $\frac{\partial\mathbf{S}}{\partial\theta_1} = j2\pi\mathbf{q}\mathbf{p}^T\odot\mathbf{S}$, where $\mathbf{p} = [1,2,\ldots,M]^T$ and $\odot$ is the Hadamard (dot) product. Using $\partial\mathbf{S}/\partial\theta_1$ yields,

$$J_{\theta_1,\theta_1} = \frac{2}{\sigma_v^2}(2\pi)^2\|(\mathbf{q}\mathbf{p}^T\odot\mathbf{S})\mathbf{a}\|^2 = \frac{8\pi^2}{\sigma_v^2}\|\mathbf{QSDa}\|^2 \tag{C.2}$$

where in the second transition we used the result $(\mathbf{q}\mathbf{p}^T\odot\mathbf{S})\mathbf{a} = \mathbf{q}\odot(\mathbf{SDa}) = \mathbf{QSDa}$, and in the second transition we used the identity $\mathbf{a}\odot\mathbf{b} = \mathrm{diag}(\mathbf{a})\odot\mathbf{b}$ for two vectors with identical dimensions, $\mathbf{a}$ and $\mathbf{b}$.

The $(2,2)$th element of $\mathbf{J}_{\boldsymbol{\theta},\boldsymbol{\theta}}$ is given by

$$J_{\theta_2,\theta_2} = \frac{2}{\sigma_v^2}\Re\{\frac{\partial(\mathbf{Sa})^H}{\partial\theta_2}\frac{\partial\mathbf{Sa}}{\partial\theta_2}\} = \frac{2}{\sigma_v^2}\Re\{\mathbf{a}^H\frac{\partial\mathbf{S}^H}{\partial\theta_2}\frac{\partial\mathbf{S}}{\partial\theta_2}\mathbf{a}\} \tag{C.3}$$

where $\partial\mathbf{S}/\partial\theta_2 = [\partial\mathbf{s}_1/\partial\theta_2, \cdots, \partial\mathbf{s}_M/\partial\theta_2]$. By substituting $\mathbf{s}_m$ we get that $\partial\mathbf{s}_m/\partial\theta_2 = j\pi m\mathbf{u}\odot\mathbf{s}_m$, where $\mathbf{u} = [0,1^2,\ldots,(N-1)^2]^T$. Substituting $\partial\mathbf{s}_m/\partial\theta_2$ in $\partial\mathbf{S}/\partial\theta_2$ yields $\partial\mathbf{S}/\partial\theta_2 = j\pi\mathbf{u}\mathbf{p}^T\odot\mathbf{S}$. Using $\partial\mathbf{S}/\partial\theta_2$ yields,

$$J_{\theta_2,\theta_2} = \frac{2}{\sigma_v^2}(\pi)^2\|(\mathbf{u}\mathbf{p}^T\odot\mathbf{S})\mathbf{a}\|^2 = \frac{2\pi^2}{\sigma_v^2}\|\mathbf{Q}^2\mathbf{SDa}\|^2 \tag{C.4}$$

where in the second transition we used a similar result to the identity expressed in (C.2) where the vector $\mathbf{q}$ is replaced by the vector $\mathbf{u}$.

The $(1,2)$th element of $\mathbf{J}_{\boldsymbol{\theta},\boldsymbol{\theta}}$ is given by

$$J_{\theta_1,\theta_2} = \frac{2}{\sigma_v^2}\Re\{\frac{\partial(\mathbf{Sa})^H}{\partial\theta_1}\frac{\partial\mathbf{Sa}}{\partial\theta_2}\} = \frac{2}{\sigma_v^2}\|\mathbf{a}^H\frac{\partial\mathbf{S}^H}{\partial\theta_1}\frac{\partial\mathbf{S}}{\partial\theta_2}\mathbf{a}\|^2. \tag{C.5}$$

Using $\partial\mathbf{S}/\partial\theta_1$ and $\partial\mathbf{S}/\partial\theta_2$ yields,

$$\begin{aligned} J_{\theta_1,\theta_2} &= \frac{2}{\sigma_v^2}(2\pi)(\pi)\Re\{\mathbf{a}^H(\mathbf{qp}^T\odot\mathbf{S})^H(\mathbf{up}^T\odot\mathbf{S})\mathbf{a}\} \\ &= \frac{4\pi^2}{\sigma_v^2}\Re\{(\mathbf{a}^H\mathbf{D}^T\mathbf{S}^H\mathbf{Q}^T)\mathbf{Q}^2\mathbf{SDa}\} \\ &= \frac{4\pi^2}{\sigma_v^2}\|\mathbf{Q}^{3/2}\mathbf{SDa}\|^2. \end{aligned} \tag{C.6}$$

We next derive the sub-matrices of the FIM $\mathbf{J}_{\mathbf{a},\mathbf{a}}$. We use the identity $\Re\{jx\} = -\Im\{x\}$ for a complex scalar x.

The upper-left sub-matrix of $\mathbf{J}_{\mathbf{a},\mathbf{a}}$ is given by

$$J_{\mathbf{a}_r,\mathbf{a}_r} = \frac{2}{\sigma_v^2}\Re\{\frac{\partial(\mathbf{Sa})^H}{\partial\mathbf{a}_r}\frac{\partial\mathbf{Sa}}{\partial\mathbf{a}_r}\} = \frac{2}{\sigma_v^2}\Re\{\mathbf{S}^H\mathbf{S}\}. \tag{C.7}$$

Similarly, we define the other sub-matrices of $\mathbf{J}_{\mathbf{a},\mathbf{a}}$.

The upper-left sub-matrix of $\mathbf{J}_{\boldsymbol{\theta},\mathbf{a}}$ is given by

$$\mathbf{J}_{\theta_1,\mathbf{a}_r} = \frac{2}{\sigma_v^2}\Re\{\frac{\partial(\mathbf{Sa})^H}{\partial\theta_1}\frac{\partial\mathbf{Sa}}{\partial\mathbf{a}_r}\} = \frac{4\pi}{\sigma_v^2}\Im\{\mathbf{a}^H\mathbf{D}^T\mathbf{S}^H\mathbf{QS}\} \tag{C.8}$$

where we used the expression of $\partial\mathbf{S}/\partial\theta_1$. In a similar way we derive $\mathbf{J}_{\theta_1,\mathbf{a}_i}$. The lower-left sub-matrix of the $\mathbf{J}_{\boldsymbol{\theta},\mathbf{a}}$ is given by

$$\mathbf{J}_{\theta_2,\mathbf{a}_r} = \frac{2}{\sigma_v^2}\Re\{\frac{\partial(\mathbf{Sa})^H}{\partial\theta_2}\frac{\partial\mathbf{Sa}}{\partial\mathbf{a}_r}\} = \frac{2\pi}{\sigma_v^2}\Im\{\mathbf{a}^H\mathbf{D}^T\mathbf{S}^H\mathbf{Q}^2\mathbf{S}\} \tag{C.9}$$

where we used again the expression for $\partial\mathbf{S}/\partial\theta_2$. In a similar way we derive $\mathbf{J}_{\theta_2,\mathbf{a}_i}$. This concludes the derivation of the FIM.

Appendix D

Derivation of the NLS Asymptotic Variance

In this section we derive the asymptotic variance of NLSE for harmonic linear chirps. Recall the signal of interest at a single iteration of the NLSE estimator

$$x_{p+1}^2[n] = \tilde{a}_p[n]s_p[n;\boldsymbol{\theta}] + \tilde{v}_p[n] \tag{D.1}$$

for some $p \in \{2, \ldots, 2M\}$ and

$$\begin{aligned}\tilde{v}_p[n] &= \sum_{m=2}^{p-1} \bar{a}_m[n] + \sum_{m=p+1}^{2M} \tilde{a}_m[n]s_m[n;\boldsymbol{\theta}] \\ &\quad +2\sum_{m=1}^{M} a_m[n]s_m[n;\boldsymbol{\theta}]v[n] + v^2[n]\end{aligned} \tag{D.2}$$

is an additive non Gaussian noise. We now derive the second order statistics of the noise. The second moment of that noise is given by

$$\begin{aligned}&E\left\{\tilde{v}_p[n]\tilde{v}_p^*[n']\right\} = \\ &\quad E\left\{\sum_{m=2}^{p-1} \bar{a}_m[n]\tilde{v}_p^*[n']\right\} \\ &+E\left\{\sum_{m=p+1}^{2M} \tilde{a}_m[n]s_m[n;\boldsymbol{\theta}] \sum_{k=p+1}^{2M} \tilde{a}_k^*[n']s_k^*[n';\boldsymbol{\theta}]\right\} \\ &+E\left\{4\sum_{m=1}^{M} a_m[n]s_m[n;\boldsymbol{\theta}]v[n] \sum_{k=1}^{M} a_k^*[n']s_k^*[n';\boldsymbol{\theta}]v^*[n']\right\}\end{aligned}$$

$$
\begin{aligned}
&+E\left\{v^2[n]\left(v^2[n']\right)^*\right\}\\
&+E\left\{2\sum_{m=p+1}^{2M}\tilde{a}_m[n]s_m[n;\boldsymbol{\theta}]\sum_{k=1}^{M}a_k^*[n']s_k^*[n';\boldsymbol{\theta}]v^*[n']\right\}\\
&+E\left\{2\sum_{m=p+1}^{2M}\tilde{a}_m^*[n]s_m^*[n;\boldsymbol{\theta}]\sum_{k=1}^{M}a_k[n']s_k[n';\boldsymbol{\theta}]v[n']\right\}\\
&+E\left\{\sum_{m=p+1}^{2M}\tilde{a}_m[n]s_m[n;\boldsymbol{\theta}]\left(v^2[n']\right)^*\right\}\\
&+E\left\{\sum_{m=p+1}^{2M}\tilde{a}_m^*[n']s_m^*[n';\boldsymbol{\theta}]v^2[n]\right\}\\
&+E\left\{2\sum_{m=1}^{M}a_m[n]s_m[n;\boldsymbol{\theta}]v[n]\left(v^2[n']\right)^*\right\}\\
&+E\left\{2\sum_{m=1}^{M}a_m^*[n']s_m^*[n';\boldsymbol{\theta}]v^*[n']v^2[n]\right\}. \qquad \text{(D.3)}
\end{aligned}
$$

Since $v[n]$ is a zero-mean circularly-symmetric complex normal variable, $E\left\{v^*[n']v^2[n]\right\} = 0$ and $E\left\{v^2[n]\right\} = 0$. In addition, the noise is assumed to be uncorrelated with the amplitudes. Hence,

$$E\left\{\tilde{a}_m[n]s_m[n;\boldsymbol{\theta}]a_k^*[n']s_k^*[n';\boldsymbol{\theta}]v^*[n']\right\} = 0 \qquad \text{(D.4)}$$

$$E\left\{\tilde{a}_m^*[n']s_m^*[n';\boldsymbol{\theta}]a_k[n]s_k[n;\boldsymbol{\theta}]v[n]\right\} = 0 \qquad \text{(D.5)}$$

$$E\left\{\tilde{a}_m[n]s_m[n;\boldsymbol{\theta}]\left(v^2[n']\right)^*\right\} = 0 \qquad \text{(D.6)}$$

$$E\left\{\tilde{a}_m^*[n']s_m^*[n';\boldsymbol{\theta}]v^2[n]\right\} = 0 \qquad \text{(D.7)}$$

$$E\left\{a_m[n]s_m[n;\boldsymbol{\theta}]v[n]\left(v^2[n']\right)^*\right\} = 0 \qquad \text{(D.8)}$$

$$E\left\{a_m^*[n']s_m^*[n';\boldsymbol{\theta}]v^*[n']v^2[n]\right\} = 0 \qquad \text{(D.9)}$$

for any $m, k \in \{1, \ldots, M\}$. Recall that $E\{\bar{a}_m[n]\} = 0$. Therefore

$$E\left\{\sum_{m=2}^{p-1}\bar{a}_m[n]\tilde{v}_p^*[n']\right\} = \sum_{m=2}^{p-1}E\left\{\bar{a}_m[n]\bar{a}_m[n']\right\}\delta(n-n'). \qquad \text{(D.10)}$$

Assuming that the amplitudes are uncorrelated, we get

$$E\left\{4\sum_{m=1}^{M}a_m[n]s_m[n;\boldsymbol{\theta}]v[n]\sum_{k=1}^{M}a_k^*[n']s_k^*[n';\boldsymbol{\theta}]v^*[n']\right\}$$

$$
\begin{aligned}
&= 4E\left\{\sum_{m=1}^{M} a_m[n]a_m^*[n']\right\}\sigma_v^2\delta(n-n') \\
&= (4tr\left\{R_a\right\}\sigma_v^2)\delta(n-n') \qquad \text{(D.11)}
\end{aligned}
$$

where R_a is the cross-correlation matrix of the amplitudes whose elements are given by

$$
R_a[k,\ell] = E\{a_k[n]a_\ell^*[n]\}. \qquad \text{(D.12)}
$$

Therefore we obtain

$$
\begin{aligned}
E\left\{\tilde{v}_p[n]\tilde{v}_p^*[n']\right\} &= (4tr\left\{R_a\right\}\sigma_v^2 + 2\sigma_v^4)\delta(n-n') \\
&\quad + \left(\sum_{m=2}^{p-1} E\left\{\bar{a}_m[n]\bar{a}_m^*[n']\right\}\right)\delta(n-n') \\
&\quad + E\left\{\sum_{m=p+1}^{2M} \tilde{a}_m[n]s_m[n;\boldsymbol{\theta}]\right. \\
&\quad \left.\cdot \sum_{k=p+1}^{2M} \tilde{a}_k^*[n']s_k^*[n';\boldsymbol{\theta}]\right\} \\
&= (4tr\left\{R_a\right\}\sigma_v^2 + 2\sigma_v^4)\delta(n-n') \\
&\quad + \left(\sum_{m=2}^{p-1} E\left\{\bar{a}_m[n]\bar{a}_m^*[n']\right\}\right)\delta(n-n') \\
&\quad + \sum_{m=p+1}^{2M}\sum_{k=p+1}^{2M} E\left\{\tilde{a}_m[n]\tilde{a}_k^*[n']\right\} \\
&\quad \cdot s_m[n;\boldsymbol{\theta}]s_k^*[n';\boldsymbol{\theta}]. \qquad \text{(D.13)}
\end{aligned}
$$

Similarly it can be shown that

$$
\begin{aligned}
E\left\{\tilde{v}_p[n]\tilde{v}_p[n']\right\} &= \sum_{m=p+1}^{2M}\sum_{k=p+1}^{2M} E\left\{\tilde{a}_m[n]\tilde{a}_k[n']\right\} \\
&\quad \cdot s_m[n;\boldsymbol{\theta}]s_k[n';\boldsymbol{\theta}] \\
&\quad + \sum_{m=2}^{p-1} E\left\{\bar{a}_m[n]\bar{a}_m[n']\right\}\delta(n-n'). \qquad \text{(D.14)}
\end{aligned}
$$

As noted in [58], the optimization problem in (4.4), used to estimate the parameters of $x_p^2[n]$ is equivalent to

$$\hat{\boldsymbol{\theta}}^{(p)}, \hat{A}_p = \underset{\boldsymbol{\theta}, A_p}{\arg\min} \left| \sum_{n=0}^{N-1} x_p^2[n] - A_p e^{-j2m\pi(\theta_1 n + \frac{1}{2}\theta_2 n^2)} \right|^2 . \tag{D.15}$$

where A_p is constant such that $\hat{A}_p \to \mu_{\tilde{a}_p}$, and $\mu_{\tilde{a}_p} = E\{\tilde{a}_p\}$. Following the same steps as in [58, Appendix B], it can be shown that

$$\text{var}\left(\psi^{(p)}\right) = \frac{1}{\mu_{\tilde{a}_p}^2} \Lambda_N^{-1} R_\epsilon \Lambda_N^{-1} \tag{D.16}$$

where $\psi^{(p)} = [\tilde{\varphi}_p, (\hat{\boldsymbol{\theta}}^{(p)})^T]^T$,

$$\Lambda_N = \pi^2 \begin{bmatrix} N^{1/2} \cdot 1 & N^{1/2} \cdot 2/2 & N^{1/2} \cdot 1/3 \\ N^{3/2} \cdot 2/2 & N^{3/2} \cdot 4/3 & N^{3/2} \cdot 2/4 \\ N^{5/2} \cdot 1/3 & N^{5/2} \cdot 2/4 & N^{5/2} \cdot 1/5 \end{bmatrix} \tag{D.17}$$

and

$$\begin{aligned} R_\epsilon(k,\ell) &= \lim_{N\to\infty} \frac{g(k)g(\ell)}{8N} \sum_{n,n'=0}^{N-1} \left(\frac{n}{N}\right)^k \left(\frac{n'}{N}\right)^\ell \\ &\quad \cdot \Re\{E\left\{\tilde{v}_p[n]\tilde{v}_p^*[n']\right\} - E\left\{\tilde{v}_p[n]\tilde{v}_p[n']\right\}\} \end{aligned} \tag{D.18}$$

for $k, \ell = 0, 1, 2$, where $g(k)$ is the frequency normalization for each parameter, i.e. $g(0) = 1$ for the constant phase, $g(1) = 2\pi$ for the initial frequency and $g(2) = \pi$ for the frequency rate. Note that (D.17) and (D.18) are different from [58] due to different frequency normalization, but otherwise similar. Substituting (D.13) and (D.14) into (D.18) yields

$$\begin{aligned} R_\epsilon(k,\ell) &= \lim_{N\to\infty} \frac{g(k)g(\ell)}{8N} \sum_{n,n'=0}^{N-1} \left(\frac{n}{N}\right)^k \left(\frac{n'}{N}\right)^\ell \\ &\quad \cdot \Re\Bigg\{ (4tr\left\{R_a\right\}\sigma_v^2 + 2\sigma_v^4)\delta(n-n') \\ &\quad -2j \sum_{m=p+1}^{2M} \sum_{k=p+1}^{2M} E\left\{\tilde{a}_m[n]\tilde{a}_k[n']\right\} \\ &\quad \cdot s_m[n;\boldsymbol{\theta}]\Im\{s_k[n';\boldsymbol{\theta}]\}\Bigg\} \end{aligned}$$

$$
\begin{aligned}
&= \lim_{N\to\infty} \frac{g(k)g(\ell)}{8N} \sum_{n,n'=0}^{N-1} \left(\frac{n}{N}\right)^k \left(\frac{n'}{N}\right)^\ell \\
&\quad \cdot \Bigg[(4tr\left\{R_a\right\}\sigma_v^2 + 2\sigma_v^4)\delta(n-n') \\
&\quad +2 \sum_{m=p+1}^{2M} \sum_{k=p+1}^{2M} E\left\{\tilde{a}_m[n]\tilde{a}_k[n']\right\} \\
&\quad \cdot \Im\{s_m[n;\boldsymbol{\theta}]\}\Im\{s_k[n';\boldsymbol{\theta}]\} \Bigg]. \qquad \text{(D.19)}
\end{aligned}
$$

In order get a large sample approximation of the result, we assume that $E\left\{\tilde{a}_m[n]\tilde{a}_k[n']\right\}$ is time independent. That is, we assume the $E\left\{\tilde{a}_m[n]\tilde{a}_k[n']\right\} = R_{m,k}$ for any m, k. This assumption holds, for example, when the amplitudes are independent and normally distributed. We now wish to examine the elements in the sum in (D.19)

$$
\begin{aligned}
& \lim_{N\to\infty} \frac{1}{N} \sum_{n,n'=0}^{N-1} \left(\frac{n}{N}\right)^k \left(\frac{n'}{N}\right)^\ell E\left\{\tilde{a}_m[n]\tilde{a}_k[n']\right\} \\
& \cdot\Im\{s_m[n;\boldsymbol{\theta}]\}\Im\{s_k[n';\boldsymbol{\theta}]\} \\
= \quad & R_{m,k} \lim_{N\to\infty} \frac{1}{N} \sum_{n,n'=0}^{N-1} \left(\frac{n}{N}\right)^k \left(\frac{n'}{N}\right)^\ell \\
& \cdot\Im\{s_m[n;\boldsymbol{\theta}]\}\Im\{s_k[n';\boldsymbol{\theta}]\} \\
< \quad & R_{m,k} \lim_{N\to\infty} \frac{1}{N} \sum_{n,n'=0}^{N-1} \Im\{s_m[n;\boldsymbol{\theta}]\}\Im\{s_k[n';\boldsymbol{\theta}]\} \\
= \quad & R_{m,k} \underbrace{\lim_{N\to\infty} \frac{1}{N} \sum_{n=0}^{N-1} \Im\{s_m[n;\boldsymbol{\theta}]\}}_{\to 0} \\
& \cdot \sum_{n=0}^{N-1} \Im\{s_k[n';\boldsymbol{\theta}]\} \\
\underset{N\to\infty}{\to} \quad & 0. \qquad \text{(D.20)}
\end{aligned}
$$

Therefore, for large number of samples we get

$$
\begin{aligned}
R_\epsilon(k,\ell) \quad &\approx \quad \lim_{N\to\infty} \frac{g(k)g(\ell)}{8N} \sum_{n,n'=0}^{N-1} \left(\frac{n}{N}\right)^k \left(\frac{n'}{N}\right)^\ell \\
& \quad \cdot(4tr\left\{R_a\right\}\sigma_v^2 + 2\sigma_v^4)\delta(n-n') \\
&= \quad (4tr\left\{R_a\right\}\sigma_v^2 + 2\sigma_v^4) \lim_{N\to\infty} \frac{1}{8N} \sum_{n=0}^{N-1} \left(\frac{n}{N}\right)^{k+\ell}
\end{aligned}
$$

$$= \quad (tr\,\{R_a\}\,\sigma_v^2 + 0.5\sigma_v^4)\frac{g(k)g(\ell)}{2(k+\ell+1)}. \tag{D.21}$$

Finally, substituting (D.21) into (D.16) yields (4.27) and (4.28). This concludes the derivation of the asymptotic variance of the NLSE.

Bibliography

[1] M. G. Christensen, P. Stoica, A. Jakobsson, and H. S. Jensen, "Multi-pitch estimation," *Signal Processing*, vol. 88, no. 4, pp. 972–983, Apr. 2008.

[2] M. G. Christensen, S. H. Jensen, A. Jakobsson, and S. H. Jensen, "Optimal filter designs for fundamental frequency estimation," *IEEE Signal Process. Lett.*, vol. 15, no. 7, pp. 745–748, Dec. 2008.

[3] C. Dubois and M. Davy, "Joint detection and tracking of time varying harmonic components: A flexible bayesian approach," *IEEE Trans. Audio, Speech, Language Process.*, vol. 15, no. 4, pp. 1283–1295, May 2007.

[4] H. Li, P. Stoica, and J. Li, "Computationally efficient parameter estimation for harmonic sinusoidal signals," *Signal Processing*, vol. 80, no. 9, pp. 1937–1944, Sept. 2000.

[5] K. W. Chan and H. C. So, "Accurate frequency estimation for real harmonic sinusoids," *IEEE Signal Process. Lett.*, vol. 11, no. 7, pp. 609–612, July 2004.

[6] A. Nehorai and B. Porat, "Adaptive comb filtering for harmonic signal enhancement," *IEEE Trans. Acoust., Speech, Signal Process.*, vol. 34, no. 5, pp. 1124–1138, Oct. 1986.

[7] M. Hinich, "Detecting a hidden periodic signal when its period is unknown," *IEEE Trans. Acoust., Speech, Signal Process.*, vol. 30, no. 5, pp. 747–750, Oct. 1982.

[8] T. W. Eddy, "Maximum likelihood detection and estimation for harmonic sets," *J. Acoust. Soc. Am.*, vol. 68, no. 1, pp. 149–155, July 1980.

[9] A. Swami and M. Ghogho, "Cramer-Rao bounds for coupled harmonics in noise," in *Proc. 31st Asilomar Conf. Signals, Syst. Comput.*, vol. 1. Pacific Grove, CA, Nov. 1997, pp. 483–487.

[10] G. W. Chang and C. Chen, "An accurate time domain procedure for harmonics and inter-harmonics detection," *IEEE Trans. Power Del.*, vol. 25, no. 3, pp. 1787–1795, July 2010.

[11] S. K. Jain and S. N. Singh, "Exact model order ESPRIT technique for harmonics and inter-harmonics estimation," *IEEE Trans. Instrum. Meas.*, vol. 61, no. 7, pp. 1915–1923, July 2012.

[12] E. Chassande-Moffin and P. Flandrin, "On the time frequency detection of chirps," *Applied Computational Harmonics Analysis*, vol. 6, no. 2, pp. 252–181, Mar. 1999.

[13] M. Vespe, G. Jones, and C. Baker, "Lessons for radar: waveform diversity in echolocating mammals," *IEEE Signal Process. Mag.*, vol. 26, no. 1, pp. 65–75, Jan. 2009.

[14] Y. Kopsinis, E. Aboutanios, D. A. Waters, and S. McLaughlin, "Time-frequency and advanced frequency estimation techniques for the investigation of bat echolocation calls," *J. Acoust. Soc. Am.*, vol. 127, no. 2, pp. 1124–1134, Feb. 2010.

[15] M. Bennett, S. McLauglin, T. Anderson, and N. McDicken, "Filtering of chirped ultrasound echo signals with the fractional Fourier transform," in *IEEE Ultrasonics Symposium*, vol. 3, Aug. 2004, pp. 2036–2040.

[16] T. H. Chung and J. Cheung, "Maximum likelihood estimation of direction of arrival and frequency sweeping rate with linear chirp signals," *IEEE Signal Process. Lett.*, vol. 2, no. 8, pp. 163–165, Aug. 1995.

[17] R. Aouada, A. Belouchrani, and K. Abed-Meraim, "Multipath parameter estimation of linear chirp signals using sensor arrays," in *Proc. IEEE-SAM*, July 2004, pp. 313–317.

[18] S. Peleg and B. Porat, "Estimation and classification of polynomial-phase signals," *IEEE Trans. Inf. Theory*, vol. 37, no. 2, pp. 422–430, Mar. 1991.

[19] S. Peleg and B. Friedlander, "The discrete polynomial-phase transform," *IEEE Trans. Signal Process.*, vol. 43, no. 8, pp. 1901–1914, Aug. 1995.

[20] A. Amar, A. Leshem, and A. J. van-der Veen, "A computationally efficient blind estimator of polynomial phase signals observed by a sensor array," *IEEE Trans. Signal Process.*, vol. 58, no. 9, pp. 4674–4683, Sept. 2010.

[21] R. P. Perry, R. C. DiPietro, and R. Fante, "SAR imaging of moving targets," *IEEE Trans. Aerosp. and Electron. Syst.*, vol. 35, no. 1, pp. 188–200, Jan. 1999.

[22] N. Rankine, M. Stevenson, M. Mesbah, and B. Boashash, "A nonstationary model of newborn EEG," *IEEE Trans. Biomed. Eng.*, vol. 54, no. 1, pp. 19–28, Jan. 2007.

[23] S. Barbarossa, A. Scaglione, and G. Giannakis, "Product high-order ambiguity function for multicomponent polynomial-phase signal modeling," *IEEE Trans. Signal Process.*, vol. 46, no. 3, pp. 691–708, Mar. 1998.

[24] G. T. Whipps and R. L. Moses, "A combined order selection and parameter estimation algorithm for coupled harmonics," in *Military Sensing Symposium (MSS) Specialty Group on Battlefield Acoustic and Seismic Sensing, Magnetic and Electric Field Sensors.* Laurel, MD, 2003.

[25] T. J. Abatzoglou, "Fast maximum likelihood joint estimation of frequency and frequency rate," *IEEE Trans. Aerosp. and Electron. Syst.*, vol. 22, no. 6, pp. 708–715, Nov. 1986.

[26] R. Kumaresan and S. Verma, "On estimating the parameters of chirp signals using rank reduction techniques," in *Proc. 21st Asilomar Conf. Signals, Syst. Comput.* Pacific Grove, CA, Nov. 1988, pp. 555–558.

[27] B. Volcker and B. Ottersten, "Chirp parameter estimation using rank reduction," in *Proc. 32nd Asilomar Conf. Signals, Syst. Comput.*, vol. 2. Pacific Grove, CA, Nov. 1998, pp. 1443–1446.

[28] S. Peleg and B. Porat, "Linear FM signal parameter estimation from discrete-time observations," *IEEE Trans. Aerosp. and Electron. Syst.*, vol. 27, no. 4, pp. 607–616, July 1991.

[29] P. M. Djuric and S. M. Kay, "Parameter estimation of chirp signals," *IEEE Trans. Acoust., Speech, Signal Process.*, vol. 38, no. 12, pp. 2118–2126, Dec. 1990.

[30] P. O'Shea, "Fast parameter estimation algorithms for linear FM signals," in *Proc. IEEE Int. Conf. Acoust., Speech, Signal Process. (ICASSP)*, vol. 4. Adelaide, Australia, Apr. 1994, pp. 17–20.

[31] S. Barbarossa, "Analysis of multicomponent LFM signals by a combined Wigner-Hough transform," *IEEE Trans. Signal Process.*, vol. 43, no. 6, pp. 1511–1515, June 1995.

[32] S. Saha and S. M. Kay, "Maximum likelihood parameter estimation of superimposed chirps using Monte Carlo importance sampling," *IEEE Trans. Signal Process.*, vol. 50, no. 2, pp. 224–230, Feb. 2002.

[33] C. Lin and P. M. Djuric, "Estimation of chirp signals by MCMC," in *Proc. IEEE Int. Conf. Acoust., Speech, Signal Process. (ICASSP)*, vol. 1. Istanbul, Turkey, June 2000, pp. 265–268.

[34] L. Qi, R. Tao, S. Zhou, and Y. Wang, "Detection and parameter estimation of multicomponent LFM signal based on the fractional Fourier transform," *Science in China Series F: Information Sciences*, vol. 47, no. 2, pp. 184–198, Mar. 2004.

[35] P. Wang, H. Li, and B. Himed, "Parameter estimation of linear frequency-modulated signals using integrated cubic phase function," in *Proc. 42nd Asilomar Conf. Signals, Syst. Comput.* Pacific Grove, CA, Oct. 2008, pp. 487–491.

[36] B. Porat, *Digital processing of random signals: theory and methods.* Prentice-Hall, Inc., 1994.

[37] S. Peleg and B. Friedlander, "A technique for estimating the parameters of multiple polynomial phase signals," in *1992 Symp. Time-Frequency Time-Scale Anal.* Victoria, BC, Oct. 1992, pp. 119–122.

[38] ——, "Multicomponent signal analysis using the polynomial-phase transform," *IEEE Trans. Aerosp. and Electron. Syst.*, vol. 32, no. 1, pp. 378–387, Jan. 1996.

[39] Y. Wang and G. Zhou, "On the use of high-order ambiguity function for multi-component polynomial phase signals," *Signal Processing*, vol. 65, no. 2, pp. 283–296, Mar. 1998.

[40] J. Kitchen, "A method for estimating the coefficients of a polynomial phase signal," *Signal Processing*, vol. 37, no. 3, pp. 463–470, June 1994.

[41] B. J. Slocumb and J. Kitchen, "A polynomial phase parameter estimation-phase unwrapping algorithm," in *Proc. IEEE Int. Conf. Acoust., Speech, Signal Process. (ICASSP)*, vol. 4. Adelaide, Australia, Apr. 1994, pp. 129–132.

[42] S. Barbarossa, "Detection and estimation of the instantaneous frequency of polynomial-phase signals by multilinear time-frequency representations," in *Proc. IEEE Signal Process. Workshop Higher Order Stat.* Lake Tahoe, CA, June 1993, pp. 168–172.

[43] M. Z. Ikram, K. Abed-Meraim, and Y. Hua, "Estimating the parameters of chirp signals: an iterative approach," *IEEE Trans. Signal Process.*, vol. 46, no. 12, pp. 3436–3441, Dec. 1998.

[44] B. Barkat and B. Boashash, "Instantaneous frequency estimation of polynomial FM signals using the peak of the PWVD: statistical performance in the presence of additive Gaussian noise," *IEEE Trans. Signal Process.*, vol. 47, no. 9, pp. 2480–2490, Sept. 1999.

[45] J. Angeby, "Estimating signal parameters using the nonlinear instantaneous least squares approach," *IEEE Trans. Signal Process.*, vol. 48, no. 10, pp. 2721–2732, Oct. 2000.

[46] M. Farquharson, P. O'Shea, and G. Ledwich, "A computationally efficient technique for estimating the parameters of polynomial-phase signals from noisy observations," *IEEE Trans. Signal Process.*, vol. 53, no. 8, pp. 3337–3342, Aug. 2005.

[47] P. Wang, I. Djurovic, and J. Yang, "Generalized high-order phase function for parameter estimation of polynomial phase signal," *IEEE Trans. Signal Process.*, vol. 56, no. 7, pp. 3023–3028, July 2008.

[48] P. Wang, H. Li, I. Djurovic, and B. Himed, "Instantaneous frequency rate estimation for high-order polynomial-phase signals," *IEEE Signal Process. Lett.*, vol. 16, no. 9, pp. 782–785, Sept. 2009.

[49] Y. Wu, H. C. So, and H. Liu, "Subspace-based algorithm for parameter estimation of polynomial phase signals," *IEEE Trans. Signal Process.*, vol. 56, no. 10, pp. 4977–4983, Oct. 2008.

[50] D. S. Pham and A. M. Zoubir, "Analysis of multicomponent polynomial phase signals," *IEEE Trans. Signal Process.*, vol. 55, no. 1, pp. 56–65, Jan. 2007.

[51] P. O'Shea, "Improving polynomial phase parameter estimation by using nonuniformly spaced signal sample methods," *IEEE Trans. Signal Process.*, vol. 60, no. 7, pp. 3405–3414, July 2012.

[52] G. Zhou and G. Giannakis, "Harmonics in multiplicative and additive noise: performance analysis of cyclic estimators," *IEEE Trans. Signal Process.*, vol. 43, no. 6, pp. 1445–1460, June 1995.

[53] O. Besson and P. Stoica, "Sinusoidal signals with random amplitude: least-squares estimators and their statistical analysis," *IEEE Trans. Signal Process.*, vol. 43, no. 11, pp. 2733–2744, Nov. 1995.

[54] S. Shamsunder, G. Giannakis, and B. Friedlander, "Estimating random amplitude polynomial phase signals: a cyclostationary approach," *IEEE Trans. Signal Process.*, vol. 43, no. 2, pp. 492–505, Feb. 1995.

[55] A. Swami, "Cramer-rao bounds for deterministic signals in additive and multiplicative noise," *Signal Processing*, vol. 53, no. 2-3, pp. 231–244, Sept. 1996.

[56] B. Senadji and B. Boashash, "A mobile communications application of time-varying higher order spectra to FM signals affected by multiplicative noise," in *Proc. IEEE Int. Conf. Info., Commun. and Signal Process. (ICICS)*, vol. 3, Sept. 1997, pp. 1489–1492.

[57] B. Boashash and B. Ristic, "Polynomial time-frequency distribution and time-varying higher order spectra: Application to the analysis of multicomponent FM signals and to the treatment of multiplicative noise," *Signal Processing*, vol. 67, no. 1, pp. 1–23, May 1998.

[58] O. Besson, M. Ghogho, and A. Swami, "Parameter estimation for random amplitude chirp signals," *IEEE Trans. Signal Process.*, vol. 47, no. 12, pp. 3208–3219, Dec. 1999.

[59] M. Morelande and A. Zoubir, "On the performance of cyclic moments-based parameter estimators of amplitude modulated polynomial phase signals," *IEEE Trans. Signal Process.*, vol. 50, no. 3, pp. 590–606, Mar. 2002.

[60] P. Tsiakoulis and A. Potamianos, "Statistical analysis of amplitude modulation in speech signals using an AM-FM model," in *Proc. IEEE Int. Conf. Acoust., Speech, Signal Process. (ICASSP)*, Apr. 2009, pp. 3981–3984.

[61] M. Pineda-Sanchez, M. Riera-Guasp, J. Roger-Folch, J. Antonino-Daviu, J. Perez-Cruz, and R. Puche-Panadero, "Diagnosis of induction motor faults in time-varying conditions using the polynomial-phase transform of the current," *IEEE Trans. Ind. Electron.*, vol. 58, no. 4, pp. 1428–1439, Apr. 2011.

[62] O. Besson and P. Stoica, "Nonlinear least-squares approach to frequency estimation and detection for sinusoidal signals with arbitrary envelope," *Digital Signal Processing*, vol. 9, no. 1, pp. 45–56, Jan. 1999.

[63] M. Ghogho, A. Swami, and A. Nandi, "Non-linear least squares estimation for harmonics in multiplicative and additive noise," in *Proc. 9th IEEE SSAP Workshop*, Sept. 1998, pp. 407–410.

[64] O. Besson and P. Stoica, "Two subspace-based methods for frequency estimation of sinusoidal signals with random amplitude," *Proc. Inst. Elect. Eng., Radar, Sonar and Navigation*, vol. 144, no. 4, pp. 169–176, Aug. 1997.

[65] G. Zhou and G. Giannakis, "On estimating random amplitude-modulated harmonics using higher order spectra," *IEEE J. Oceanic Eng.*, vol. 19, no. 4, pp. 529–539, Oct. 1994.

[66] A. Swami, "Multiplicative noise models: Parameter estimation using cumulants," *Signal Processing*, vol. 36, no. 3, pp. 355–373, Apr. 1994.

[67] M. Ghogho, A. Swami, and T. Durrani, "Frequency estimation in the presence of doppler spread: performance analysis," *IEEE Trans. Signal Process.*, vol. 49, no. 4, pp. 777–789, Apr. 2001.

[68] G. Zhou, G. Giannakis, and A. Swami, "On polynomial phase signals with time-varying amplitudes," *IEEE Trans. Signal Process.*, vol. 44, no. 4, pp. 848–861, Apr. 1996.

[69] B. Barkat and B. Boashash, "IF estimation of linear FM signals corrupted by multiplicative and additive noise: a time-frequency approach," in *Proc. IEEE Int. Conf. Acoust., Speech, Signal Process. (ICASSP)*, vol. 2. Istanbul, Turkey, June 2000, pp. 661–664.

[70] B. Barkat, "Instantaneous frequency estimation of nonlinear frequency-modulated signals in the presence of multiplicative and additive noise," *IEEE Trans. Signal Process.*, vol. 49, no. 10, pp. 2214–2222, Oct. 2001.

[71] P. Stoica and Y. Selen, "Model order selection: a review of information criterion rules," *IEEE Signal Process. Mag.*, vol. 21, no. 4, pp. 36–47, July 2004.

[72] P. M. Djuric, "A model selection rule for sinusoids in white Gaussian noise," *IEEE Trans. Signal Process.*, vol. 44, no. 7, pp. 1744–1751, July 1996.

[73] M. G. Christensen, A. Jakobsson, and S. H. Jensen, "Sinusoidal order estimation using angles between subspaces," *EURASIP J. Adv. Signal Process.*, vol. 2009, pp. 1–11, Jan. 2009.

[74] M. G. Christensen, L. J. Højvang, A. Jakobsson, and S. H. Jensen, "Joint fundamental frequency and order estimation using optimal filtering," *EURASIP J. Adv. Signal Process.*, vol. 2011, no. 1, pp. 1–18, June 2011.

[75] G. Pfalzer. Avisoft bioacoustics, European bat calls. [Online]. Available: http://www.batcalls.com

[76] Interdisciplinary center for bioacoustics and environmental research. [Online]. Available: http://www.unipv.it/cibra/

[77] S. Raimund. Avisoft bioacoustics. [Online]. Available: http://www.avisoft.com

[78] H. Van Trees, *Detection, Estimation, and Modulation Theory - Part IV, Optimum Array Processing.* Wiley, 2004.

[79] X. G. Xia, "Discrete chirp-Fourier transform and its application to chirp rate estimation," *IEEE Trans. Signal Process.*, vol. 48, no. 11, pp. 3122–3133, Nov. 2000.

[80] F. J. Harris, "On the use of windows for harmonic analysis with the discrete Fourier transform," *Proc. IEEE*, vol. 66, no. 1, pp. 51–83, Jan. 1978.

[81] N. Hurley and R. Scott, "Comparing measures of sparsity," *IEEE Trans. Inf. Theory*, vol. 55, no. 10, pp. 4723–4741, Oct. 2009.

[82] C. Capus and K. Brown, "Short-time fractional Fourier methods for the time-frequency representation of chirp signals," *J. Acoust. Soc. Am.*, vol. 113, no. 6, pp. 3253–3263, June 2003.

[83] A. T. Catherall and D. P. Williams, "High resolution spectrograms using a component optimized short-term fractional Fourier transform," *Signal Processing*, vol. 90, no. 5, pp. 1591–1596, May 2010.

[84] J. M. Mendel, *Lessons in digital estimation theory.* Prentice-Hall, Inc., 1986.

[85] M. Polad and B. Friedlander, "Separation of co-channel FM/PM signals using the discrete polynomial-phase transform," in *Sixth IEEE Digital Signal Processing Workshop*, Oct. 1994, pp. 3–6.

[86] I. Djurović and L. Stanković, "Quasi-maximum-likelihood estimator of polynomial phase signals," *IET Signal Processing*, vol. 8, no. 4, pp. 347–359, June 2014.

[87] G. Planquette, C. Le Martret, and G. Vezzosi, "Detecting and estimating the fundamental of harmonics series when the number of harmonics is unknown," in *Military Communications Conference (MILCOM'95)*, vol. 3, Nov. 1995, pp. 998–1002.

[88] V. Namias, "The fractional order Fourier transform and its application to quantum mechanics," *IMA Journal of Applied Mathematics*, vol. 25, no. 3, pp. 241–265, Mar. 1980.

[89] H. M. Ozaktas, M. A. Kutay, and D. Mendlovic, "Introduction to the fractional Fourier transform and its applications," *Advances in imaging and electron physics*, vol. 106, pp. 239–291, 1999.

[90] L. Stanković, T. Alieva, and M. J. Bastiaans, "Time-frequency signal analysis based on the windowed fractional Fourier transform," *Signal Processing*, vol. 83, no. 11, pp. 2459–2468, Nov. 2003.

[91] R. Tao, Y. Li, and Y. Wang, "Short-time fractional Fourier transform and its applications," *IEEE Trans. Signal Process.*, vol. 58, no. 5, pp. 2568–2580, May 2010.

[92] H. M. Ozaktas, Z. Zalevsky, and M. A. Kutay, *The fractional Fourier transform with Applications in Optics and Signal Processing.* Wiley, 2001.

הסטטיסטיים לבחירת סדר המודל בהם השתמשנו בחלק הקודם. אנו מפתחים שיטת שערוך איטרטיבית המבוססת על שיטת הריבועים הפחותים הלא לינארית (Nonlinear Least Squares), שפותחה במקור עבור אות בודד בעל תדר המשתנה לינארית עם אמפליטודה אקראית. המשערך המתקבל בשיטה זו מאוד דומה למשערך הסבירות המירבית של אות עם אמפליטודה קבועה למעט שלב עיבוד מקדים, שנוסף לפני ביצוע השערוך. גם שיטה זו דורשת חיפוש דו מימדי ברזולוצייה גבוהה ונדרשת סיבוכיות חישובית גבוהה על מנת להגיע לביצועים אופטימליים, בדומה למשערך הסבירות המירבית. בנוסף אנו מראים כיצד ניתן לשערך את מספר הרכיבים ההרמוניים על ידי שימוש במדדי ריכוזיות של הספקטרום של האות. גם עבור מודל זה של האות אנו מציגים הרחבה של שיטה המבוססת על HAF. גם במקרה זה, השיטה המתקבלת דומה למשערך מבוסס HAF שהוצג עבור מודל של אמפליטודה קבועה, וכוללת את אותו שלב עיבוד מקדים של משערך הריבועים הפחותים. לבסוף אנו מראים כיצד ניתן להרחיב את שיטת השערוך Harmonic Separate-Estimate, שהצענו בחלק הקודם, עבור המודל הנוכחי של אותות עם אמפליטודה אקראית. גם עבור מקרה זה ההרחבה מתבצעת, בין היתר, על ידי הוספת אותו שלב מקדים כמו במשערך הריבועים הפחותים. גם בשיטה המוצעת, מספר הרכיבים ההרמוניים משעורך בעזרת מדדי הריכוזיות של הספקטרום. השיטה המתקבלת משיגה ביצועים טובים בתנאי יחס אות לרעש גבוה. גם במקרה זה אנו מדגימים את ביצועי השיטה על אותות אמיתיים.

כלומר מספר הרכיבים ההרמוניים. הקריטריונים המוצגים דומים והם מבוססים על משערך הסבירות המירבית של הפרמטרים של תדר הבסיס. משערך זה הינו אופטימלי במובן שגיאה ריבועית ממוצעת, אולם אנו מראים כי לא קיים פתרון סגור עבורו והוא דורש לבצע חיפוש דו־מימדי ברזולוציה מאוד גבוהה במרחב הפרמטרים. עקב חיפוש זה משערך הסבירות המירבית הינו בעל סיבוכיות חישובית גבוהה מאוד. כדי להתגבר על הבעיה, אנו מציעים שיטת שערוך תת־אופטימלית, בסיבוכיות נמוכה, המכונה Harmonic Separate־Estimate. השיטה מורכבת משני חלקים. בחלק הראשון, מבצעים שערוך גס של הפרמרים באמצעות Fast Fourier Transform. אנו מראים כי שימוש בהתמרה זו מהווה קירוב של פונקציית המחיר של משערך הסבירות המירבית, אולם הדיוק המתקבל מקירוב זה אינו מספק, ונדרש לבצע שלב נוסף לצורך שיפור הדיוק. השערוך הגס משמש לצורך הפרדת הרכיבים ההרמוניים אחד מהשני. בשלב השני, משערכים את הפרמטרים בצורה מדויקת מתוך הפאזות של האותות המופרדים. השערוך מתבצע על ידי פתרון בעיית הריבועים הפחותים במשותף לכל הרכיבים ההרמוניים, מה שמאפשר לנצל את הקשר בינהם. בניגוד למשערך הסבירות המירבית, במקרה זה מתקבל פתרון סגור שאינו דורש חיפוש במרחב המימדים. בנוסף, לצורך השוואה לשיטה המוצעת, אנו מציגים הרחבה של שיטת שערוך פופולרית המבוססת על High־Order Ambiguity Function (HAF). שערוך מבוסס HAF פותח במקור עבור אותות מרובי רכיבים ואנו מבצעים התאמה של שיטה זו לאותות הרמוניים. השימוש ב HAF על אותות בעלי תדר המשתנה לינארית, מאפשר להמיר את בעיית החיפוש הדו־מימדי לשתי בעיות חיפוש חד מימדיות. תכונה זו מורידה את הסיבוכיות החישובית באופן ניכר. אולם רזולוציית החיפוש בכל אחד מהפרמטרים, הנדרשת לקבלת ביצועים מיטביים, זהה למשערך הסבירות המירבית. ניתוח הסיבוכיות החישובית של שלושת השיטות מראה כי מושג חיסכון משמעותי ביותר על ידי השיטה המוצעת, ביחס למשערך הסבירות המירבית. כמו כן לשיטה המוצעת סיבוכיות חישובית נמוכה מזו של שערוך מבוסס HAF. אנו מראים כי השיטה המוצעת, Harmonic Separate־Estimate, מגיעה לביצועים דומים, מבחינת השגיאה הריבועית הממוצעת, כמו משערך הסבירות המירבית בתנאים של יחס אות לרעש בינוני־גבוה וביצועים טובים יותר ביחס לשערוך המבוסס על HAF. כמו כן אנו מראים שניתן להשתמש בשיטת השערוך המוצעת במקום משערך הסבירות המירבית בקריטריונים לבחירת סדר המודל. בנוסף אנו מדגימים את ביצועי המשערך והקריטריון לבחירת סדר המודל על אותות גילוי של עטלף ולוויתן.

בחלק השני, אנו מרחיבים את הבעיה ומניחים מודל בו האמפליטודה של כל רכיב משתנה בזמן. תחת ההנחה הזאת, האמפליטודות עשויות להיות למשל תהליכים אקראים בלתי תלויים סטטיסטית או כאלו המשתנות בהתאם לדינמיקה לא ידועה כלשהי, למשל תהליך אוטו־רגרסיבי עם פרמטרים לא ידועים. אמפליטודה אקראית יכולה להופיע למשל במערכות מכ"ם, סונאר ותקשורת כתוצאה מפיזור של האות או מתופעת רב־נתיב ובמערכות לזיהוי כשלים מכניים. בנוסף, אמפליטודה אקראית יכולה לשמש כמודל עבור אותות דיבור. עבור המודל הזה, של אמפליטודה אקראית, אנו מראים כי בניגוד לאות עם אמפליטודות קבועות, לא ניתן להשתמש במשערך הסבירות המירבית ובקריטריונים

תקציר

בעבודה זו אנו מתמקדים בניתוח תדר של אות הניתן לקירוב על ידי סדרה הרמונית של אותות קצרים לא סטציונריים (CHIRPS). כלומר אות מרובה רכיבים, כאשר התדר של כל אחד מן הרכיבים הינו כפולה שלמה של תדר, המשתנה בזמן, של אות בסיס כלשהו. אותות הרמוניים כאלו נוצרים למשל על ידי מעבר בתווך לא לינארי במערכות מכ"ם, סונאר ותקשורת. בנוסף, אותו אלו משמשים לקירוב של אותות מורכבים יותר כגון אותות דיבור ומוזיקה או אותות במערכות לזיהוי כשלים מכניים. במקרים מסוימים ההרמוניות נוצרות במכוון כדי לשפר את הגילוי, למשל אותות גילוי וניווט של עטלפים ולויתנים או במערכות אולטראסאונד רפואי.

קיימים פתרונות רבים בספרות לבעיית שערוך התדר הבסיסי של אותות הרמוניים. בכולם ההנחה היא שהתדר אינו משתנה במשך זמן ההתבוננות באות הנקלט. הנחה זו מגבילה את זמן ההתבוננות לזמנים קצרים מאוד, שכן אותות בהם התדר אכן קבוע אינם נפוצים. אם לעומת זאת נניח מודל שבו התדר אכן משתנה בזמן, ניתן להאריך את זמן ההתבוננות וכתוצאה מכך לשפר את הדיוק של שיערוך התדר. בעבודה זאת אנו מניחים מודל בו בכל מסגרת זמן, האות אינו סטציונרי וניתן לקירוב כסכום של אותות הרמוניים כאשר התדר של הרכיב הבסיסי משתנה בצורה לינארית ומספר הרכיבים ההרמוניים אינו ידוע. תחת הנחה זו, אנו מפתחים שיטות לשערוך הפרמטרים של אותות אלו, כלומר שערוך התדר ההתחלתי וקצב שינוי התדר של הרכיב הבסיסי וכן שערוך מספר הרכיבים ההרמוניים בכל מסגרת זמן. הבעיה אותה אנו מנסים לפתור הינה תת־בעיה של בעיית שערוך פרמטרים של אותות מרובי רכיבים. כלומר אותות בעלי מספר רכיבים כאשר לכל אחד תדר שונה המשתנה בזמן ולא מניחים קשר בין התדרים של הרכיבים. ניתן כמובן לפתור את הבעיה הנוכחית בעזרת משערכי פרמטרים לאותות מרובי רכיבים אולם ניצול הקשר בין הרכיבים משפר את תוצאות השערוך. מעבר לכך, עבור המקרה הנוכחי, התדר הרגעי של כל הרכיבים ניתן לייצוג על ידי שני הפרמטרים של הרכיב הבסיסי בלבד ואין צורך לשערך פרמטרים עבור כל אחד מהרכיבים בנפרד, כפי שמבוצע כיום במשערכי פרמטרים של אותות מרובי רכיבים. שיטות שערוך של אותות הרמוניים לא סטציונריים טרם הוצגו בספרות, דבר אשר היווה את המוטיבציה למחקר הנוכחי.

העבודה נחלקת לשני חלקים. בחלק הראשון של העבודה, אנו מניחים מודל בו האמפליטודה של כל רכיב קבועה בכל מסגרת זמן. אנו מתחילים בהצגת קריטריונים סטטיסטים לבחירת סדר המודל,

תודות

המחקר נעשה בהנחיית ד"ר אלון עמר ופרופ' ישראל כהן מהפקולטה להנדסת חשמל. ברצוני להודות לשניהם על ההנחיה, ההדרכה והתמיכה בכל שלבי המחקר.

ברצוני להודות לאישתי יעל, עבור האהבה, העידוד והתמיכה הבלתי פוסקים.

ניתוח תדר של אותות לא סטציונריים בעלי רכיבים הרמוניים

חיבור על מחקר

לשם מילוי חלקי של הדרישות לקבלת התואר
מגיסטר למדעים בהנדסת חשמל

ירון דואק

הוגש לסנט הטכניון — מכון טכנולוגי לישראל
כסלו תשע"ו חיפה נובמבר 2015

ניתוח תדר של אותות לא סטציונריים בעלי רכיבים הרמוניים

ירון דואק